Research on types and sources of ice nucleating particles in boreal forests

Master's Thesis in Meteorology and Climate Physics
by

Dominik Spannagel

September 2024

INSTITUTE FOR METEOROLOGY AND CLIMATE RESEARCH
KARLSRUHE INSTITUTE OF TECHNOLOGY (KIT)

Advisor:	Prof. Dr. Thomas Leisner
Coadvisor:	Prof. Dr. Corinna Hoose
Supervisor:	Dr. Ottmar Möhler, Alexander Böhmländer

Ich versichere wahrheitsgemäß, die Arbeit selbstständig angefertigt, alle benutzten Hilfsmittel vollständig und genau angegeben und alles kenntlich gemacht zu haben, was aus Arbeiten anderer unverändert oder mit Änderungen entnommen wurde.

PLACE, DATE

. . . . . .

(Dominik Spannagel)

Abstract

Clouds and precipitation are a fundamental part of everyday life and climate. They reflect solar and terrestrial radiation and transport fresh water through the atmosphere. The formation of clouds and precipitation are influenced by the presence of aerosol particles. Ice-nucleating particles (INPs) are a minor subset of atmospheric aerosol particles, that lead to primary ice formation in clouds containing liquid water droplets above 238 K. Due to their impact on primary ice formation, they affect the radiative budget of the cloud as well as its precipitation and lifetime. Aerosols and INPs originate from a variety of sources including ocean, desert, and forest areas.

The Hyytiälä Ice Nucleation Experiment 2023 (HyICE23) in southern Finland aimed at investigating the sources and types of INPs in the boreal forest. During this campaign, which lasted from October 18th, 2023 to April 30th, 2024, INP measurements were done using the PINE (Portable Ice Nucleation Experiment) instrument and the INSEKT (Ice Nucleation SpEctrometer of the Karlsruhe Institute of Technology) method. The PINE instrument covered a temperature range from about 242 K to 262 K at a temporal resolution of up to 6 minutes, while the INSEKT method covered a temperature range from about 255 K to 273 K with a time resolution between 4 h and 4 days.

The INP concentrations generally show a seasonal pattern, with high concentrations (at high 10^{-1} to 10^{2} stdl^{-1}, at low temperatures) in autumn and spring and lower concentrations (at high 10^{-4} to 10^{2} stdl^{-1}, at low temperatures) during winter time. This matches the results from the previous HyICE campaign in 2018.

In general, the observed INP concentrations are correlated to the ambient air temperature. The INP measurement during this campaign did agree well to the parameterization developed after the previous field campaign. Again, a dependence on the ambient temperatures as well as snow cover was found. During several days, an increase of the INP concentration was observed with increasing temperature and decreasing snow depth.

Observations using the high temporal resolution of the PINE instrument allowed observations of short term INP concentrations, for example an increase by more than 10^{1} stdl^{-1} during 1 h long local street works on April 19th and during short term aerosol concentration increases. During some observed precipitation events, an influence on the INP concentrations was observed. Also observed was the change in INP ranging over 10^{1} over a day during a case study on multiple days, this could not be concluded to be a diurnal cycle due to additional factors like a decrease in snow depth. A diurnal cycle could not be distinguished in general. The results shown in this thesis show the importance and versatility of INP measurement methods with high temporal resolution to increase knowledge on INPs in the boreal forest.

Kurzzusammenfassung

Wolken und Niederschläge sind ein wesentlicher Bestandteil des Alltagslebens und des Klimas. Sie reflektieren Sonnen- und Erdstrahlung und transportieren Süßwasser durch die Atmosphäre. Die Bildung von Wolken und Niederschlägen wird durch die Anwesenheit von Aerosolpartikeln beeinflusst. Eisnukleierende Partikel (INPs) sind eine kleine Untergruppe atmosphärischer Aerosolpartikel, die zur primären Eisbildung in Wolken führen, die flüssige Wassertröpfchen über 238 K enthalten. Aufgrund ihres Einflusses auf die primäre Eisbildung beeinflussen sie den Strahlungshaushalt der Wolke sowie deren Niederschlag und Lebensdauer. Aerosole und INPs stammen aus verschiedenen Quellen, darunter Ozean-, Wüsten- und Waldgebiete.
Das Hyytiälä Ice Nucleation Experiment 2023 (HyICE23) in Südfinnland zielte darauf ab, die Quellen und Arten von INPs im borealen Wald zu untersuchen. Während dieser Kampagne, die vom 18. Oktober 2023 bis zum 30. April 2024 dauerte, wurden INP-Messungen mit dem Instrument PINE (Portable Ice Nucleation Experiment) und der Methode INSEKT (Ice Nucleation SpEctrometer des Karlsruher Instituts für Technologie) durchgeführt. Das PINE-Instrument deckte einen Temperaturbereich von etwa 242 K bis 262 K mit einer zeitlichen Auflösung von bis zu 6 Minuten ab, während die INSEKT-Methode einen Temperaturbereich von etwa 255 K bis 273 K mit einer Zeitauflösung zwischen 4 h und 4 Tagen.
Die INP-Konzentrationen zeigen im Allgemeinen ein saisonales Muster mit hohen Konzentrationen (bei hohen 10^{-1} bis $10^{2}\,\mathrm{stdl}^{-1}$, bei niedrigen Temperaturen) im Herbst und Frühling und niedrigeren Konzentrationen (bei hohen 10^{-4} bis $10^{2}\,\mathrm{stdl}^{-1}$, bei niedrigen Temperaturen) im Winter. Dies entspricht den Ergebnissen der vorherigen HyICE-Kampagne im Jahr 2018.
Im Allgemeinen korrelieren die beobachteten INP-Konzentrationen mit der Umgebungslufttemperatur. Die INP-Messung während dieser Kampagne stimmte gut mit der nach der vorherigen Feldkampagne entwickelten Parametrisierung überein. Auch hier wurde eine Abhängigkeit von den Umgebungstemperaturen sowie der Schneedecke festgestellt. Über mehrere Tage hinweg konnte mit zunehmender Temperatur und abnehmender Schneehöhe ein Anstieg der INP-Konzentration beobachtet werden.
Beobachtungen mit der hohen zeitlichen Auflösung des PINE -Instruments ermöglichten die Beobachtung kurzfristiger INP-Konzentrationen, beispielsweise einen Anstieg um mehr als $10^{1}\,\mathrm{stdl}^{-1}$ während 1 h langer lokaler Messungen Straßenbauarbeiten am 19. April und kurzfristiger Anstieg der Aerosolkonzentration. Bei einigen beobachteten Niederschlagsereignissen wurde ein Einfluss auf die INP-Konzentrationen beobachtet. Außerdem wurde im Rahmen einer mehrtägigen Fallstudie eine Änderung des INP im Bereich von mehr als 10^{1} über einen Tag hinweg beobachtet. Dies konnte aufgrund zusätzlicher Faktoren wie einer Abnahme der Schneehöhe nicht auf einen Tageszyklus geschlossen werden. Ein Tagesgang konnte generell nicht unterschieden werden. Die in dieser Arbeit gezeigten Ergebnisse zeigen die Bedeutung und Vielseitigkeit von INP-Messmethoden mit hoher zeitlicher Auflösung, um das Wissen über INPs im borealen Wald zu erweitern.

Contents

List of Figures

List of Tables

Chapter 1.

Introduction

Clouds play a key role in climate and weather. They are aggregations of liquid cloud droplets (warm clouds), ice crystals (cold clouds) or both (mixed-phase clouds) (Knopf et al. 2018). Clouds mostly made up of liquid cloud droplets reflect incoming solar radiation back to space, which results in a cooling of the surface below (Lohmann et al. 2016; Mueller et al. 2011)). Ice clouds, clouds where the ice phase dominates, reflect long wave radiation from the planet back to the surface, resulting in a global net warming effect (Boucher 2015; Boucher et al. 2013). The net radiative effect of clouds on climate is depending on whether the ice or liquid phase is more dominant (McCoy et al. 2018; Murray et al. 2021; Sun and Shine 1994).
In addition, clouds play a key role in the water cycle of Earth by transporting fresh water through the atmosphere (Lynch et al. 2002). Ice crystals in mixed-phase clouds grow to large sizes at the expense of liquid droplets (Bergeron 1935; Findeisen 1938; Wegener 1911) and fall out as precipitation. Precipitation in liquid or solid form refills fresh water reservoirs around the globe, allowing life in many different environments. The impact of climate change may also be reflected by clouds in Earths atmosphere. An increase in annual temperatures leads to an increase in liquid water vapor, which in turn may influence the formation, lifetime of clouds and intensity of precipitation (Climate Change (IPCC) 2023). The formation of precipitation in clouds, especially in mixed-phase clouds, is depending on the presence of ice crystals (Mülmenstädt et al. 2015).
Aerosols play a major role in the formation of liquid droplets as well as ice crystals in the atmosphere (Pruppacher and Klett 2010). Aerosols are liquid or solid particles suspended in the atmosphere (Hinds 1999) with sizes ranging between 10^{-3} to $10^{2}\,\mu m$. They affect climate directly by interacting with radiation and indirectly via cloud interactions. Natural sources of aerosols include the ocean, desert, and forest areas. Anthropogenic sources include biomass burning, industry and traffic as major contributors (Seinfeld and Pandis 2016).
Aerosols which affect the formation of liquid cloud droplets are called Cloud Condensation Nuclei (CCN). The much more scarce aerosols affecting formation of ice crystals are called Ice Nucleating Particles (INPs) (Schaefer 1946). The INPs population only amounts to a small subset (about 1 in 10^5) of all aerosols, but INP are of major importance in understanding weather and climate (DeMott et al. 2010).
In the absence of INPs, water droplets can cool down below 273 K without freezing, below this temperature, they exist in a supercooled state (Rosenfeld and Woodley 2000). At about 235 K[1], the transition to the solid phase happens homogeneously (Koop et al. 2000). This process is called homogeneous freezing, while processes above 235 K involve INP and are called heterogeneous (Kanji et al. 2017). INPs can alter the net-radiative effect, precipitation and thus the lifetime of a cloud by affecting the amount of ice crystals present. Heterogeneous freezing

[1]The precise temperature is dependent on different factors, but for this work an estimated temperature is sufficient.

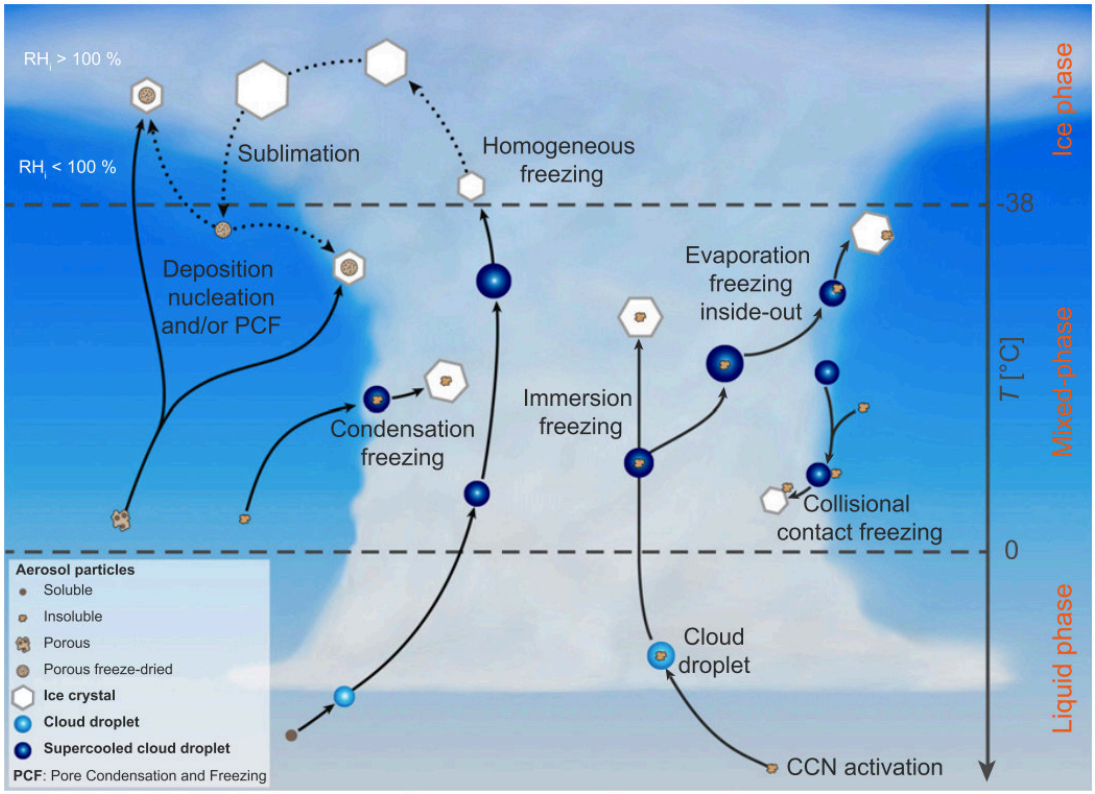

Figure 1.1.: Schematic adopted from Kanji et al. 2017 showing the possible primary ice nucleation pathways in the atmosphere.

processes can be categorized into four different modes:

Immersion freezing: An INP is already immersed in a droplet and starts the freezing process once the droplet cools down. This process is the most dominant process in mixed-phase clouds (Kanji et al. 2017; Burrows et al. 2022). The two methods used in this thesis, to measure the INP concentration, are mainly sensitive to immersion freezing.

Contact freezing: A super cooled droplet comes into contact with an INP. The INP initiates the freezing upon contact (Pruppacher and Klett 2010).

Condensation freezing: Water vapor condenses on the surface of an INP and freezes at the same time (Vali et al. 2015). This may happen in a very narrow temperature and saturation window.

Deposition Nucleation: Water vapor nucleates on the surface of an INP as ice directly under super saturation to ice, this mode is predominant in cirrus clouds (Cziczo et al. 2013).

The ice nucleation pathways possible in the atmosphere are depicted in figure 1.1, adopted from Kanji et al. 2017. In case the INP in question is not an ice crystal, these processes lead to the nucleation of primary ice crystals. Secondary ice production then leads to a multiplication of the number of ice crystals inside the cloud (Field et al. 2017; Keinert et al. 2020). Knowledge on processes in which INPs affect ice formation as well as types and sources of INPs can be used to further understand and predict our weather and climate (DeMott et al. 2010; Engström et al. 2015; Perlwitz et al. 2020; Storelvmo et al. 2011; Trueblood et al. 2020; Tucker et al. 2018). A variety of biogenic aerosols were found to have atmospherically relevant ice-nucleating abilities (Augustin et al. 2013; C.E. Morris et al. 2004; Creamean et al. 2013; Hader et al. 2014;

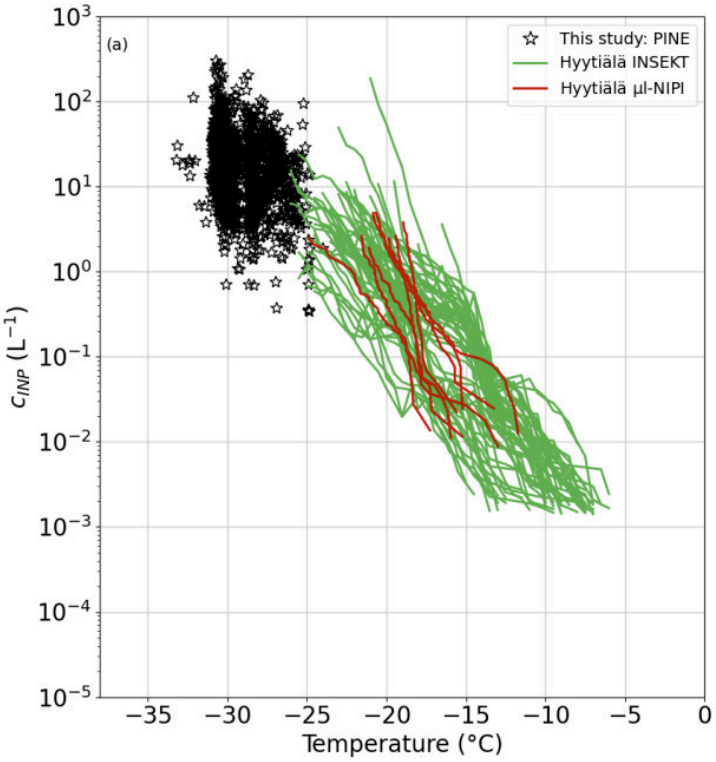

Figure 1.2.: Graph adopted from Vogel et al. 2024, showing a comparison of INP concentrations (c_{INP}) measured with PINE (black stars), INSEKT (green lines) and µl-NIPI (red lines) during HyICE-2018.

Möhler et al. 2007; O'Sullivan et al. 2015, 2018; Pratt et al. 2009; Schnell and Vali 1973), at temperatures above 258 K (Christner et al. 2008; Murray et al. 2012).
One of the natural sources of biogenic INPs are the boreal forests (Schneider et al. 2021). They include roughly 30% of the global forest area (Tunved et al. 2003). The knowledge on INP originating from the boreal forests is scarce. A study on boreal forests was the Hyytiälä Ice Nucleation Experiment 2018 (HyICE-2018), during which INP observations were done at the Station for Measuring Ecosystem-Atmosphere Relations II (SMEAR II) in Hyytiälä in the boreal forest of southern Finland (Brasseur et al. 2022). During the campaign, INP concentrations were measured by collecting ambient aerosols on filters and analyzing the samples using INSEKT (Schiebel 2017), as well as using the first prototype of the mobile cloud expansion chamber (Möhler et al. 2021), the PINE-1A. The working principles of both methods is discussed in section 2.1. The filter samples were taken over periods of 10 to 24 h from February 2018 to May 2019. PINE-1A measured at an approximate time resolution of 6 minutes in parallel from March to May 2018.
Figure 1.2 shows the observations on INPs done in HyICE-2018 for INSEKT measurements (green lines) ,PINE measurements (black stars) and µl-NIPI (red lines), another offline method (see Harrison et al. 2018) over the two months. The INSEKT measurements had been extended beyond the duration of the HyICE-2018 campaign. Schneider et al. 2021 found the boreal forest to be an important source of biogenic INP, generating concentrations comparable to other environments (Kanji et al. 2017). A seasonal cycle in INP concentrations and types was found for the year-long measurements with INSEKT. INP concentrations measured at around 257 K were found to be lowest during winter compared to measurements during spring (Kaufmann 2019). This seasonal trend was especially pronounced in INP concentrations between 255 K and

259 K. This cycle was concluded to be linked to the prevalence of biogenic aerosol particles by heat treatment (see section 2.1.2) of filter samples and comparison of INP concentrations at 257 K with Wideband Integrated Bioaerosol Sensor (WIBS) data, primarily emitted by the forest vegetation.
In this work, the parameterization of Schneider et al. 2021 was used to predict measured INP concentrations, showing a general good agreement for INSEKT and PINE data. Further measurements with a high time resolution were done to investigate possible relations to meteorological events like precipitation and frontal passages in more detail.
The PINE-1A measurements suggest that INPs in this boreal forest that are active below 249 K can be also biological (Vogel et al. 2024). Snow cover reduced potential local INP sources to only a few, including the tree dwelling lichens (Proske et al. 2024) which might emit INPs (Moffett et al. 2015). The lichen were found to be possible sources of biogenic aerosols under complex humidity conditions (Marshall 1996; Armstrong 1991; Proske et al. 2024). Proske et al. 2024 found INP derived from Lichen species sampled in this region to be ice active at 257 K and 255 K and in a size range where previous studies could detect them ($<2\,\mu m$)).
The successor campaign HYICE23 started on October 18th, 2023 and ended on April 30th, 2024. INSEKT filter samples and PINE data were collected during the whole duration, utilizing the high sensitivity of INSEKT to the INP concentration and the high temporal resolution of the PINE instrument. INSEKT is sensitive to nucleation temperatures above ≈ 255 K, while PINE measured between 262 K and 242 K. INSEKT measurements were used to observe INP concentrations of particles ice active above 247 K at intervals reaching from 4 hours to 4 days. The PINE instrument measured INP concentrations at ground level in a container. In parallel, filter samples for INSEKT were taken in the container as well as on a 35 m high tower, to compare ground level to above canopy observations. An Aerodynamic Particle Sizer (APS) was deployed to measure the aerosol particle size distribution during the whole campaign. Later on during the campaign, measurements of fluorescing particles using WIBS were added.

Chapter 2.

Experimental Methods

Multiple characteristics of Aerosols in the boreal forest of southern Finland were measured during the HyICE23 campaign. Two different methods were used to measure INP concentrations (c_{INP}), the Portable Ice Nucleation Experiment (PINE) and the Ice-Nucleation SpEctrometer of the Karlsruhe institute of Technologie (INSEKT). Size distributions of aerosols were measured with the Aerodynamic Particle Sizer (APS) over the whole campaign. For shorter time periods, the size distribution was also measured with Promo-2000 and welas-2500 sensor setups. Fluorescing particles of biological origin were measured with a Wideband Integrated Bioaerosol Sensor (WIBS). The following section will describe the different instruments and measuring methods used in the HyICE23 campaign in more detail.

2.1. Ice-Nucleating Particle Concentrations

2.1.1. Portable Ice Nucleation Experiment (PINE)

The Portable Ice Nucleation Experiment, in short PINE, is an expansion-type cloud chamber designed after the AIDA cloud chamber at IMK-AAF (see Möhler et al. 2021). The working principle is the same, but the size was reduced to enable mobile measurements in the field. The instrument used for this thesis was built by Bilfinger Nuclear & Energy Transition GmbH as a commercial version of the fourth instrument generation labeled PINE-04-01. Over an inlet system, air is sampled into a chamber. Directly below the chamber an optical particle counter (fidas-pine, Palas GmbH, Karlsruhe, Germany) is located in the flow tube connecting the chamber with the pump system.
As depicted in figure 2.1 on the left side, the PINE instrument is composed of five major components, namely the inlet system (I), the cloud expansion chamber (II), the cooling system (III), the particle detection (IV) and the control system (V). The right side shows the PINE instrument located in the PINE container.
In the inlet system, the sampled air first flows through a diffusion dryer, controlling the frost point temperature of the incoming air. A semipermeable membrane (Nafion$^{\mathrm{TM}}$) allows diffusion of water vapor from the incoming sample air flow into an outgoing air flow at lower pressure. The pressure gradient between the two air flows drives the diffusion transport of water vapor across the membrane. The pressure gradient up to 800 mbar is maintained with a pressure controller (Wagner Mess- und Regeltechnik GmbH, type P-702). Reducing the frost point temperature in the sampled air is important to avoid the accumulation of ice and frost layers inside the chamber. The control system sets various valves so that the sampled air flows either directly through the

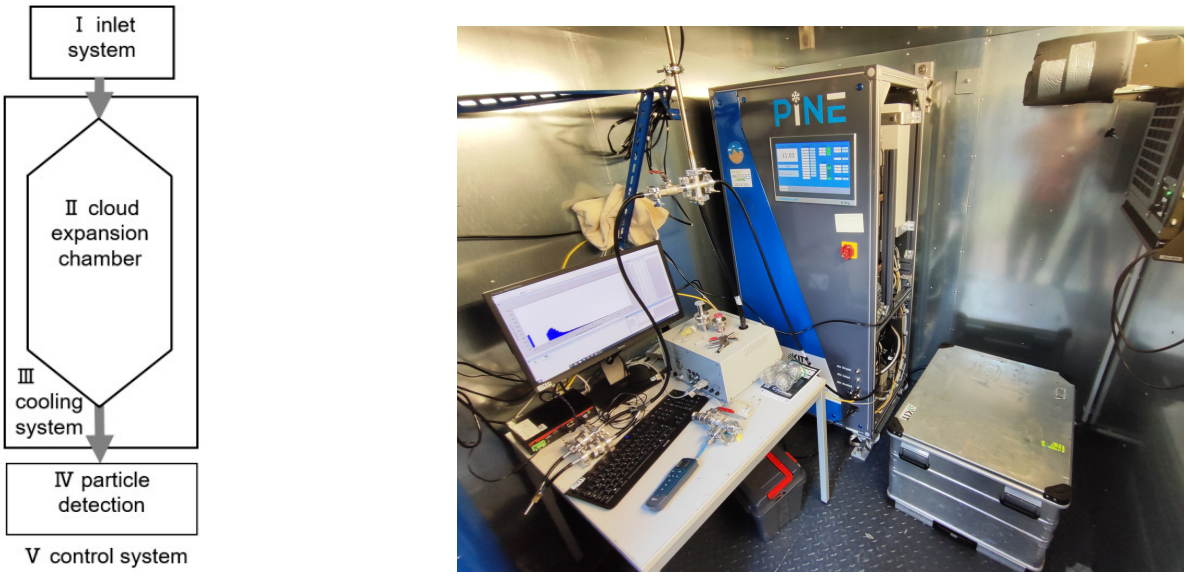

Figure 2.1.: Schematic of the Portable Ice Nucleation Experiment (PINE) on the left, from Möhler et al. 2021 and a picture of the Instrument which was located inside a measurement container (PINE container) during the HyICE23 Campaign.

chamber, around said chamber (”bypass” mode), or through an aerosol particle filter (HEPA filter). The filter removes any aerosols particles and is used to clean the chamber and check the background of measurements.
The cloud expansion chamber with a volume of 10 l resides within a vacuum chamber for thermal insulation. A cooling system (Stirling type, Thales, LPT9310) and heating elements are attached to the outer wall of the cloud expansion chamber. These allow for reducing or increasing the temperature of the air inside the expansion chamber. The gas temperature is measured with five sensors located inside the cloud chamber. The wall temperature is measures with three sensors attached to the chamber walls, and one additional sensor is used for temperature control. The temperatures and other important instrument parameters like the pressure and the dew point temperature are recorded automatically as part of the measurement.

The PINE instrument is controlled by a custom-made LabView software. Measurements are performed in operations which are composed of pre-defined runs. Each run includes the three modes ”flush”, ”expansion” and ”refill”, as shown in figure 2.2. In the software, a run setup can be defined with the duration of the flush, the flow rates for each mode as well as the minimum pressure which needs to be reached at the end of the expansion. A temperature program can be set, independent of the run setup. It consists of a series of set temperatures and a duration for each of them. The heating elements automatically activate as soon as the set temperature is 3 K higher than the temperature measured by the control temperature sensor.
In figure 2.3, a schematic of a typical run of the PINE instrument is shown. The graph in panel (a) shows the temperature and pressure measurements in the chamber, showing the rapid decrease during ”expansion”. The graph in panel (b) shows the supersaturation S_W in the chamber. For this graph, several conditions were assumed. The saturation of water vapor was close to 100% and all water in the chamber was still in the gas phase, at the start of the expansion. The water vapor mixing ration was assumed to be constant over the duration of the expansion, as there are no additional sources or sinks assumed to be in the chamber. As such, the condensation of

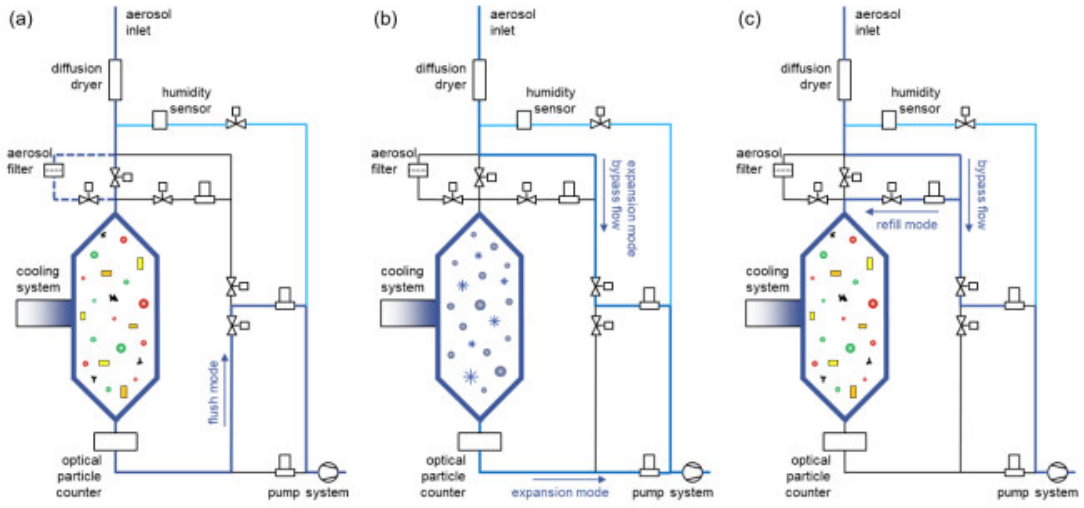

Figure 2.2.: Scheme adopted from Möhler et al. 2021 showing the run modes "flush" (a), "expansion" (b) and refill (c).

water droplets is assumed to balance the saturation ratio to 1, which is why the line is dotted when supersaturation conditions are met. The graph in panel (c) shows the time series of the optical diameter of single particles detected with the optical particle counter. Roughly 10 s after the start of the expansion, S_W is calculated to rise above 1. At this point, water droplets form. These are visible as a cluster or cloud of dots with diameters roughly smaller than 10 µm. A smaller number of particles are shown to be of larger diameters than the 'cloud' droplets. These are identified as ice crystals formed during the expansion. These droplets and ice crystals evaporate soon after the refill mode is initiated. Once the chamber is refilled to the pressure at the start, the flush mode will be enabled to start the next run.
During the "flush" mode, ambient air is passed through the chamber for about 5 minutes at 2 $Lmin^{-1}$ in order to replace residual aerosols in the chamber. The flow rate is controlled by a mass flow controller. At the end of the flush period, the valve at the top of the chamber is closed while the outflow stays open. The flow rate during "expansion" was set to 3 l min^{-1}. The pumping of air out of the chamber leads to a pressure decrease and thereby also a decrease of the gas temperature. This causes an increase of the relative humidity and, after some time of expansion, water supersaturated conditions are reached in the chamber volume.
Once supersaturation is reached, the available CCN lead to the formation of liquid water droplets. At temperatures lower than 0 °C, ice formation may occur via immersion freezing, if INPs are present.
During the "expansion" as well as the "refill" time, the sample flow is set to "bypass" mode, which allows for a constant air flow through the inlet system of the instrument. After the pressure within the chamber reaches 860 hPa, the valve at the top is reopened to "refill" the chamber. During the refill, the flow rate was set to be 2 l min^{-1}. Once the pressure within the chamber reaches ambient pressure, the instrument will restart with a "flush", enabling repeated measurements roughly every 6 minutes.
The fidas-pine optical particle counter below the chamber measures the optical size of individual particles leaving the chamber. The OPC is sensitive to large aerosol particles, droplets and ice crystals. Particles above a certain size threshold are identified as INP, as ice crystals grow non spherically and are visible in the OPC data as particles larger than liquid droplets, see figure 2.3 left side. Each particle, identified as ice crystal, counts as a single INP.

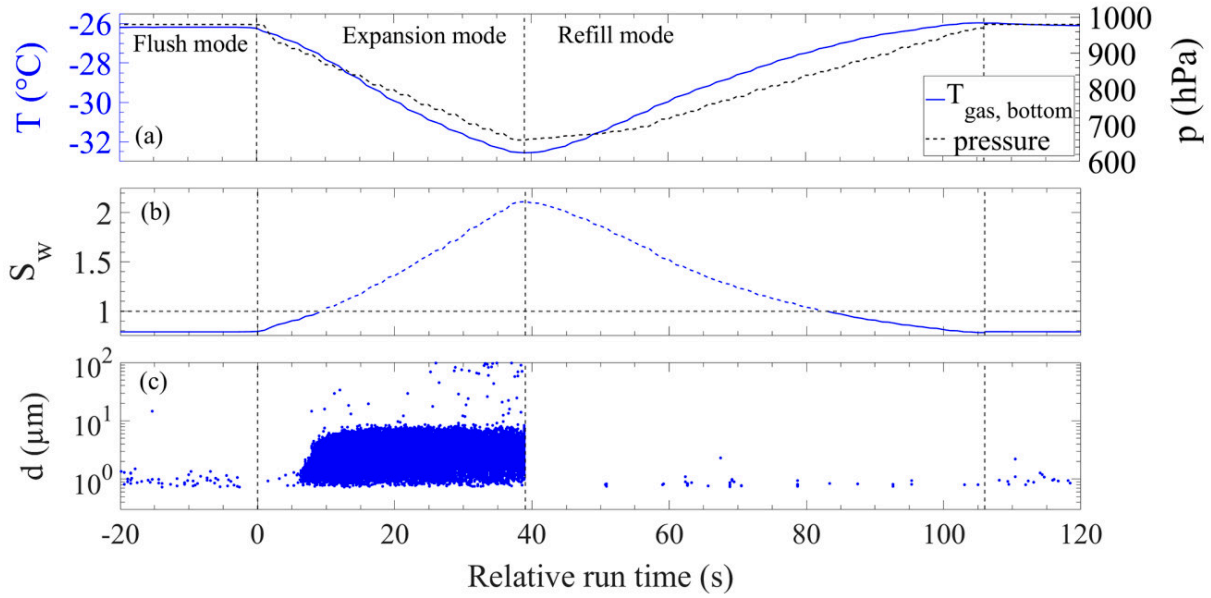

Figure 2.3.: Time series of a typical run of the PINE instrument with the "flush", "expansion" and "refill" modes indicated. The gas temperature and pressure are shown in panel (a), the corresponding supersaturation in the chamber in panel (b), and the optical diameters of individual particles detected with the optical particle counter in panel (c).

Calculation of the concentration of ice-nucleating particles

The concentration of INPs, c_{INP}, for each run "i" of the PINE instrument operation is calculated as the ratio of the total number of ice particles, N_{i} detected during the run, and the volume of air $V_{\mathrm{air,i}}$ that passed the OPC during the ice particle detection time. $\mathrm{N_i}$ is determined by counting all particles above a run-dependent size threshold in the OPC data. The threshold is calculated by a Python program[1], which also calculates the INP concentrations. $v_{\mathrm{air,i}}$ is calculated by multiplying the flow rate during the expansion (F_{exp}) with the duration of the expansion during run "i" ($t_{\mathrm{exp,i}}$). The $c_{\mathrm{INP,i}}$ can then be calculated using:

$$c_{\mathrm{INP,i}} = \frac{N_{\mathrm{i}}}{V_{\mathrm{air,i}}} = \frac{N_{\mathrm{i}}}{F_{\mathrm{exp}} \times (t_{\mathrm{exp,i}})}. \tag{2.1}$$

Each $c_{\mathrm{INP,i}}$ can be assigned a temperature T_{i} which is the minimum value measured by the gas temperature closest to the OPC. This leads to a $c_{\mathrm{INP,i}}(T)$ with a temperature uncertainty of $\pm$ 1 K. Considering this uncertainty, the $c_{\mathrm{INP,i}}$ data is analyzed and discussed in 2 K temperature bins.
With ($t_{\mathrm{exp,i}}$) ranging from 30 to 35 seconds and (F_{exp}) set to 3 stdl $\mathrm{min^{-1}}$ the volume of air flowing through the fidas-pine during each expansion is around 1.5 to 1.75 stdl which results in a $c_{\mathrm{INP,i}}$ single run detection limit of about 0.6 $\mathrm{stdl^{-1}}$. A lower detection limit can be achieved by averaging over multiple consecutive runs. This reduces the time resolution for the INP measurements. A new temperature ramp was designed for this campaign to optimize the measurements of PINE at a high temporal resolution as well as over a wide temperature range. The validation of the temperature ramp is shown in the following.

[1] Available at: `https://codebase.helmholtz.cloud/pine` (last accessed: August 29th, 2024)

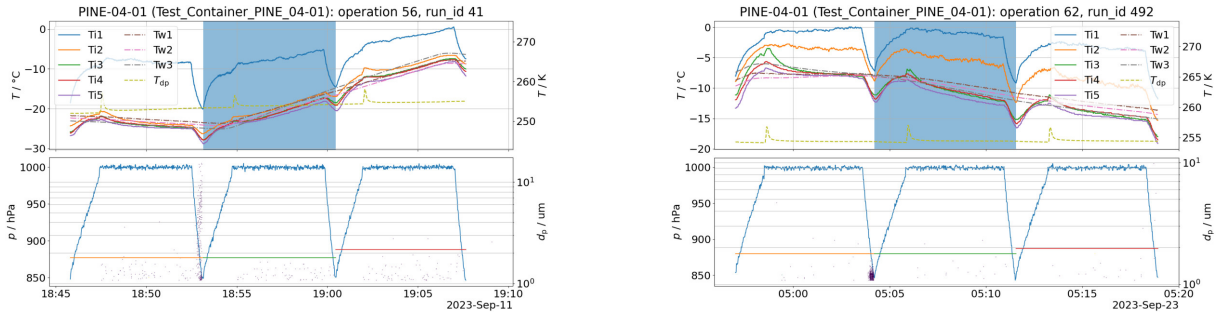

Figure 2.4.: Example of INP data loss due to heating / cooling during test measurements at KIT Campus North. The respective top graphs show the temperatures measured during a set of runs coinciding with a heating (left) or cooling (right) phase. Below are graphs showing the pressure and detected particles, the respective runs with loss of measurements are highlighted in blue.

Validation of PINE Temperature Programs

Various tests were done at KIT Campus North prior to the HyICE23 campaign. The focus of these were the various possibilities of the temperature program used for PINE operation. In addition to the temperature steps at which measurements should be done, two further factors need to be included. The limit of the dryer and the heating and cooling rates between temperature steps.

The drying efficiency of the Nafion membranes is limited. The dew point temperature may be above the temperature at which measurements are done, depending on ambient conditions. In this case, water will accumulate inside the chamber by freezing on the interior. This accumulation may lead to interference with the valve used to close the top of the chamber. This can be detected by observing the pressure gradient during the refill. During normal refill the pressure increase is linear, with an iced valve, the increase will show irregularities. Expansions, where this is detected, may be unusable for INP concentration measurements. The Python program[1] used to calculate INP concentrations detects these automatically and flags the run, which may have to be removed from the measurement by a quality control afterwards.

To balance the deposition of water inside the chamber, the temperature of the chamber needs to be above the dew point for a certain amount of time. This way, accumulated ice will evaporate, and the chamber will effectively be dried. This 'dry phase' needs to be long enough to balance out the water deposition into the chamber, but short enough to keep the humidity inside the chamber at close to 100% at the start of each expansion. Expansions during which no supersaturation is reached, will not result in formation of droplets or ice crystals and lead to loss in measurements.

The issue of heating and cooling rates is connected to the above rather closely. To ensure measurements with high time resolution at different temperatures, the heating and cooling phases could be adjusted to the limitations of the heating and cooling system. The observed maximum cooling rate was at $0.6\,\mathrm{K\,min^{-1}}$, as mentioned in Möhler et al. 2021. The maximum heating rate was observed to be $1.4\,\mathrm{K\,min^{-1}}$. This heating rate is for active heating elements. The difference between set and measured temperature at which the heating elements activate can be set manually, but for this campaign it was kept at 3 K.

During the tests, as well as during various campaigns, problems with the measurements during heating phases were observed. Similar problems were observed during cooling phases at maximum cooling rate during the tests. When an expansion happens during these phases, no, or close to no, formation of droplets or ice crystals can be observed. This might be related to the

evaporation of cloud droplets before reaching the OPC. Examples of these missing measurements are depicted in figure 2.4. The respective top graphs show temperature measurements in the chamber, on the walls, as well as the dew point. The lower graphs show the measured pressure in the chamber (blue line) as well as single particles detected by the OPC and the threshold set by the Python program[1]. The respective blue colored areas depict the runs, where the INP concentration measurement was lost.
For temperature differences between set and measured temperature below 3 K, heating is done passively with the sample air. Phases of passive heating showed no loss of measurements. For HyICE23, the PINE instrument was operated using only passive heating. By trial and error, a temperature program was found which results in a cooling rate of $0.17\,\mathrm{K\,min^{-1}}$ and a heating rate of $0.14\,\mathrm{K\,min^{-1}}$. These rates allow measurements at roughly 1 K intervals during the cooling. During test measurements (with ambient air), as well as measurements in the field, the INP concentration measured during a heating phase was less than 10% larger than during the cooling phase, which hints to residual particles from previous runs at lower temperature having an effect, but the effect is negligible. For a proper evaluation, further tests with a constant aerosol need to be done in the lab. In figure 2.5 a comparison of measurements during heating and cooling phases (up and down ramps) is shown. The boxes stand for the INP concentrations measured within the different temperature bins, while the different colors stand for heating, cooling or constant temperature respectively (for comparison of all measurements done with PINE during the campaign, see Appendix fig. A.1).
The temperature program mostly used during the campaign is shown in figure 2.6, showing the temperature measured at the chamber wall at middle height. The program is shown with a two-hour period of measurements at high temperatures of around 257 K and a temperature scan down to around 243 K. The period of measurements at high temperature allow for higher sensitivity by calculating a mean over the roughly 20 expansions during this period. On the left is a slightly changed version with only temperature scans. The duration of a cycle of temperatures is around 5 hours 30 minutes. This graph also shows slight variability in the length of each temperature cycle, which is mostly due to ambient temperature differences affecting the heating rate slightly. For the program, a maximum difference of 15 minutes could be observed. A short temperature scan was used without the 2 h period at high temperatures, shortening the scan to 3 hours 30 minutes and a maximum variation of 6 minutes (see Appendix fig. A.2)

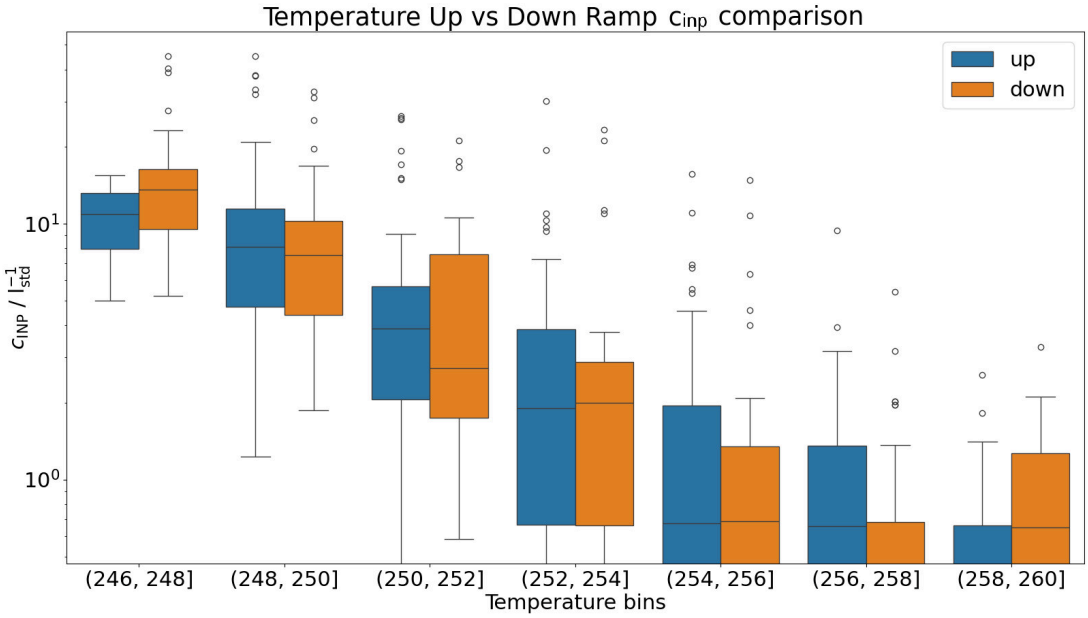

Figure 2.5.: Comparison of PINE data created during the cooling (down ramp) and heating (up ramp). The graph shows a comparison of PINE measurements during cooling (blue) and heating (orange) phases.

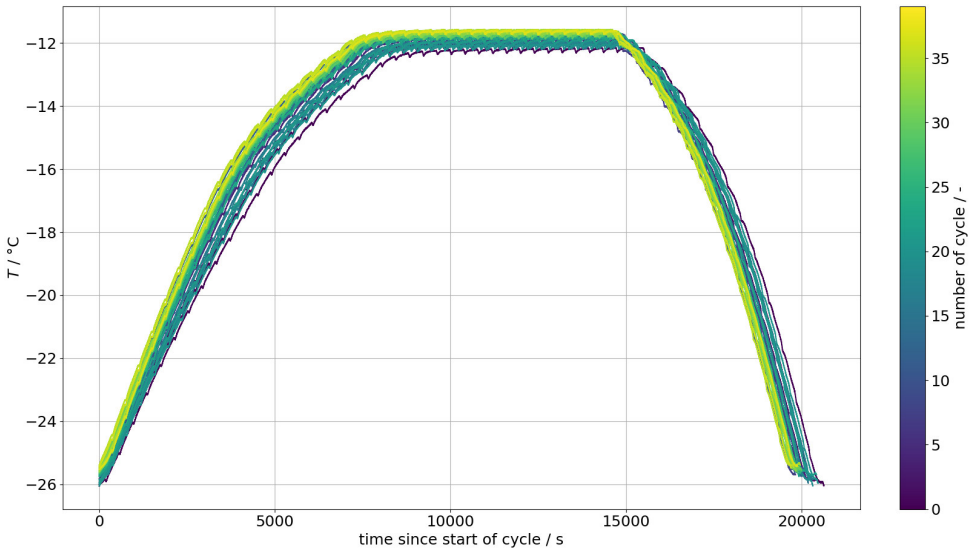

Figure 2.6.: PINE Temperature program cycle for long temperature scan. Shown is the temperature measured at the wall at middle height of the chamber. The graph shows cycles of a 2 h period at 257 K and a scan to 243 K over a period of 5.5 h.

2.1.2. Ice Nucleation SpEctrometer of the Karlsruhe institute of Technologie (INSEKT)

INSEKT is a freezing essay (Schiebel 2017) used to observe immersion freezing of aerosol samples, based on the Colorado State University Ice Spectrometer (CSU-IS) (Hill et al. 2016). Aerosols are collected using a filter from a sample flow of ambient air in the field. The particles gathered on the filter are washed off in a laboratory using water of high purity. The suspension of aerosol particles is then analyzed with INSEKT. This way, immersion freezing capabilities of the gathered aerosols can be analyzed for temperatures above 247 K (for a general look, see Schneider et al. 2021; Böhmländer et al. 2024).
The filters used are 47 mm diameter poly carbon filters with pores of 0.2 µm size (Whatman Nuclepore®track-etched). The filters are prepared in a flow box which provides a clean environment, to avoid contamination. Tweezers used to handle the filters are cleaned the same way as the filters. The filters are cleaned by submersion in a solution of 10% hydrogen peroxide, rinsed with deionized water (about 0.057 μScm^{-1}) and dried in the flow box. The filters and tweezers are then packaged in aluminium foil after drying in the flow box. The aluminium foil used has been cleaned and sanitized by heating in an oven at 300 °C for about 20 minutes. To further keep polluting factors to a minimum, the holders in which the filters are inlaid, are cleaned using a disinfectant (Bacillulol or 2-Propanol) and wiped every time the filters are changed, as shown in figure 2.8. For storage, the samples are put in sterile petri dishes, further packaged in aluminium foil and kept in a freezer at −18 °C until analysis.

The filter holder mounted with a clean filter is installed in a filter setup described in 3.2.1, where a pump creates a sample air flow through the filter. A critical orifice (CO) is used to keep the air flow during sampling on a constant level. Pressure measurements between filter and CO are used to monitor the change in flow rates caused by accumulation of particles on the filter. During this campaign, the accumulation of particles on the filter showed no significant effect on the measured pressure compared to changes in ambient pressure. For the HyICE23 campaign, four filter samples were taken in parallel at two different locations. The corresponding flow rates of the CO (F_{CO}) and their uncertainty are listed in table 2.1. The flow rates were validated by measuring the flow with a flow meter (Defender™ 530H). The measured flow rates showed a deviation of less than 1% from the expected flow rates for the intact filter holders. One of the 12 filter holders used was found to be defect. The flow rate measured through this filter holder was up to 25% lower than the expected flow rate. A comparison of parallel aerosols sampling with the defect and an intact filter holder showed no significant bias within the INSEKT measurement uncertainty (see Leonhard 2024). The defect filter holder was replaced later during the campaign.

Figure 2.7.: INSEKT Filters (left) and filter holders (right) used during the HyICE23 campaign.

Figure 2.8.: Process of filter change in facilities of Hyytiälä (Flow box - Lamair), here done by Tobias Leonhard. On the left is the transfer of a sample from a filter holder to a petri dish. In the middle is a part of the cleaning process of the filter holder. The transfer of a new filter from an aluminium package in to the filter holder is on the right.

Table 2.1.: Flow rates F_{CO} of the different filter lines at normal conditions and errors (1%).

Filter line / Critical Orifice	F_{CO} [stdl min^{-1}]	uncertainty of F_{CO} [stdl min^{-1}]
A	4.3834	0.043834
B	4.2365	0.042365
C	4.29	0.0429
D	4.2419	0.042419

To include pollution from handling of filters during transport and the procedure of each change, blank filters were taken additionally. The blank filters differ from normal filters only in the fact that no air flow was enabled once the filter holders holding them were installed. The analysis of the samples is done in a Laboratory. Preparation of sample suspensions are done in a flow box. As preparation, Nanopure™ (from now on NP) water is filtered using a 0.1 µm syringe filter. The filtered NP water is used to clean 50 mL centrifuge tubes (CELLSTAR® polypropylene tubes). The tubes are then filled with 6 mL of filtered nano pure water using a pipette[2].
The filter to be analyzed is moved into the tube using a pre-clean plastic tweezer. The tube is then placed into a rotator at 60 rpm for 20 min. Afterwards, 3 µL of the suspension are transferred to a new cleaned tube for heat treatment (see the following subsection), using a pipette. The heat treated as well as the non-heated suspension are then handled the same way. The suspensions are diluted with 5- and 25-, or 10- and 100-fold volumes of filtered NP water, to extend the INSEKT detection range to lower temperatures. The original suspension and the two diluted suspensions are distributed into two 96-well Polymeraze Chain Reaktion plates (PCR) plates (Brand, Cat. No. 781368), together with the filtered NP water as a background. The NP water background typically freezes around 250 K, limiting the experimental temperature ranges observable with this method. The 192 well can be divided into different partitions. For higher diluted suspensions, more wells are filled to increase the precision of measurements for low concentrations of particles in the suspension. Each well is filled with 50 µL using an electrical pipette. The PCR-plates are then set into the freezing array INSEKT consisting of aluminium blocks which are cooled by a cryostat (Lauda®, ProLine RP 855 for INSEKT1, Pro RP 245 E for INSEKT2[3]. A plastic pane covers the PCR plates to reduce contamination during the experiment. Eight Pt100 sensors measure the temperature inside the cooling block, the mean temperature is taken as a reference temperature for the calculation of the frozen fraction. Compressed air is flowing below and above the glass cover to prevent condensation. Above the setup, a camera captures the PCR plates as well as the state of the suspension within the wells. If a suspension within a well freezes, the brightness of this well reduces. This change can

[2]A list of the used pipettes can be found in Kaufmann 2019, as these were also used for this thesis.
[3]At the IMK-AAF, two INSEKT freezing arrays are used, both featuring the same setup and components, except for the used chiller.

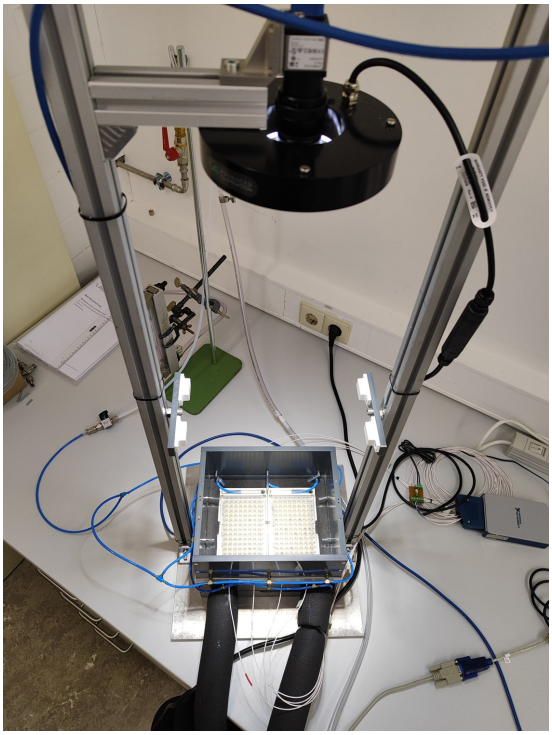

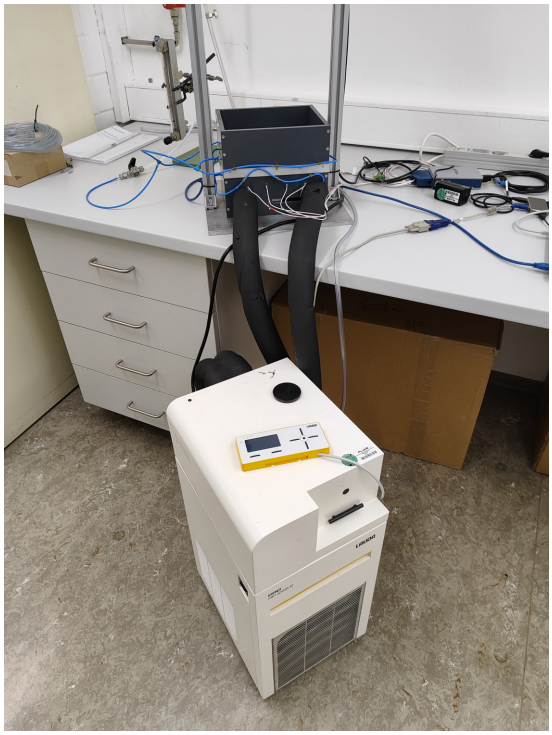

Figure 2.9.: INSEKT PCR-plates installed in aluminium blocks and camera above (left) and cooler connected to aluminium blocks (right).

be detected with the camera. During the analysis, the aluminium blocks are cooled down at 0.33 K per minute starting from 274 K. During the cooling, brightness changes are detected and noted down automatically using a LabView program on a laptop which also sets the cryostat temperature.
By comparing the frozen (dark) wells with non-frozen wells (bright) of the same dilution, a frozen fraction can be calculated. Using these frozen fractions, INP concentrations can be calculated for a spectrum of temperatures ranging from 268 to 248 K.

Calculation of the concentration of ice-nucleating particles

The calculation of c_{INP} for INSEKT is done by calculating the frozen fraction, dilution factors, solvent volume and the volume of sampled air. The volume of sampled air is calculated with the duration of each filter and the flow rate of ambient air through the filter. The flow rates of each critical orifice are determined at standard conditions (293.15 K, 1013 hPa). To calculate the INP concentration in stdl^{-1} the flow rates of each CO is used. Using these informations, the frozen fractions can be translated into c_{INP} following the relations developed by Vali 1971. With the INP concentration of each well of the PCR-plate $c_{\mathrm{INP,V}}$:

$$c\mathrm{INP,V} = -\frac{d}{V\mathrm{well}} \times ln\left(\frac{N\mathrm{l}(T)}{N\mathrm{all}}\right), \tag{2.2}$$

where $N_{\mathrm{l}}(T)$ equals subtracting the frozen fraction from 1. d corresponds to the dilution factor, V_{well} the volume of liquid in each well and V_{all} the total number of wells filled with the dilution. By factoring in the volume of filtered nano pure water used to wash the filter V_{wash} the actual

c_{INP} can be calculated with:

$$c_{\mathrm{INP}} = \frac{V_{\mathrm{wash}}}{V_{\mathrm{air}}} \times c_{\mathrm{INP,V}}. \tag{2.3}$$

The error estimation used in this thesis follows a combination of systematic and statistic uncertainties which have been investigated in depth in the Master Thesis 2018 of Julia Schneider (formerly Kaufmann) (Kaufmann 2019). The c_{INP} is calculated with a Python Program[4].

Heating of sample during processing with INSEKT

For the heat treatment, the suspension is put into a measuring beaker filled with boiling water for 20 min. During the treatment, heat-sensitive INPs will become deactivated (e.g. Barry et al. 2021; Hill et al. 2013; Hill et al. 2016; Schneider et al. 2021). This test can be an indicator for the presence of biogenic INPs, when compared to the original non-heated sample. The INP concentration over the temperature spectrum will be reduced compared to the non heat treated sample, unless no biogenic or other heat sensitive components were caught on the filter.

[4] Available at: `https://codebase.helmholtz.cloud/insekt/py_raw_insekt` (last accessed: August 29th, 2024)

2.2. Measurement of Particle Properties

2.2.1. Particle Concentration and Size Distribution

Aerodynamic Particle Sizer (APS)

The Aerodynamic Particle Sizer (APS) detects the aerodynamic size of particles by detecting the velocity distribution after acceleration of particles through a rapid increase in flow rate. The sample air flow containing the aerosol particles is embedded in a particle free sheath flow and directed through an accelerating orifice nozzle. The sheath flow is cleaned through a particle filter before combining with the sample flow. The nozzle accelerates the air flow and directs it and the containing aerosols into a pair of polarized laser beams, see figure 2.10. After acceleration, larger particles have a slower velocity than smaller particles. The particles scatter the light of the two beams at different times and create detectable signals. Each particle creates a pair of signals, the time difference between can be used to determine the aerodynamic diameter of the particle (see fig. 2.10). The shape of a particle can not be determined this way as the effective air drag coefficient is dependent on multiple variables including particle size, shape, material and density. These variables are combined into the aerodynamic diameter. Particles of the same aerodynamic diameter behave similarly when a change in surrounding air velocity or direction happens. The APS detects particles with an aerodynamic diameter between 0.54 µm and 20 µm. Particles between 0.48 µm and 0.54 µm are still counted, but not differentiated in size. Sample times used during the campaign were 300 and 120 seconds.

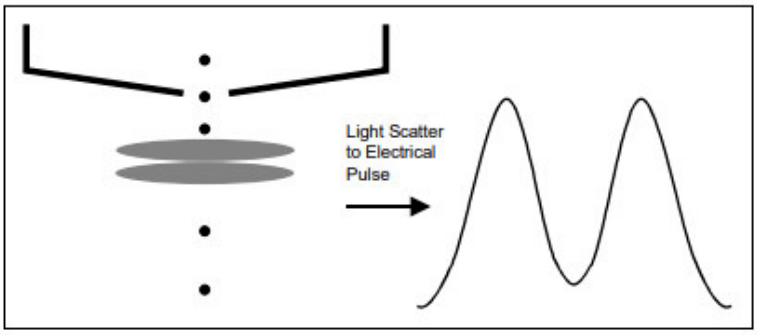

Figure 2.10.: Schematic of the APS working principle (Aerodynamic Particle Sizer® Spectrometer Model 3321 - User Manual).

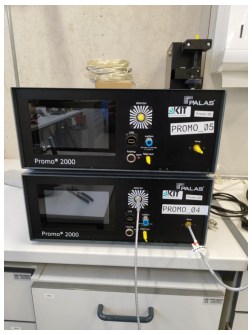

Figure 2.11.: Pictures of a welas sensor (left) and the Promo devices used in the HyICE23 campaign (right)

White Light Aerosol Spectrometer (welas) and Promo

The White Light Aerosol Spectrometer (welas) and Promo are a set of devices of a sensor and a device that emits a light beam and detects light signals. A beam of white light emitted by the Promo is transferred to the sensor via an optical fiber. There it is focused on a small window inlaid in a tube through which sample air flows. Aerosols within the sample air flow scatter the light when they flow through the detection volume, see figure 2.12. The shape of the window allows elimination of particles which are only detected at the edges of the light beam. A second window in a 90° angle connects to a detector over a second optical fiber. The intensity of the reflected light is converted into a voltage signal and allocated to a channel. A calibration table with size ranges for each channel allows a transformation of the light signal into a particle diameter. A size range between 0.3 µm and 17 µm was used for the measurements. A LabView program is used to store the data as single particle data. The OPC used in the PINE instrument is a special version called fidas-pine. This version observes the whole sample flow to better detect large ice particles.

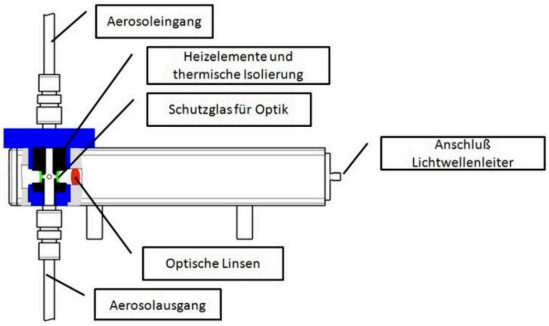

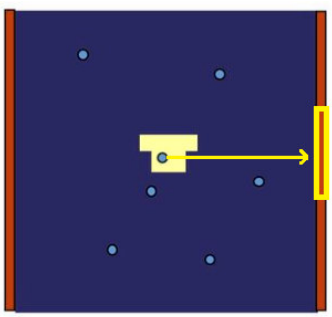

Figure 2.12.: welas sensor, schematic of structure of the sensor (left) and schematic working principle (right)

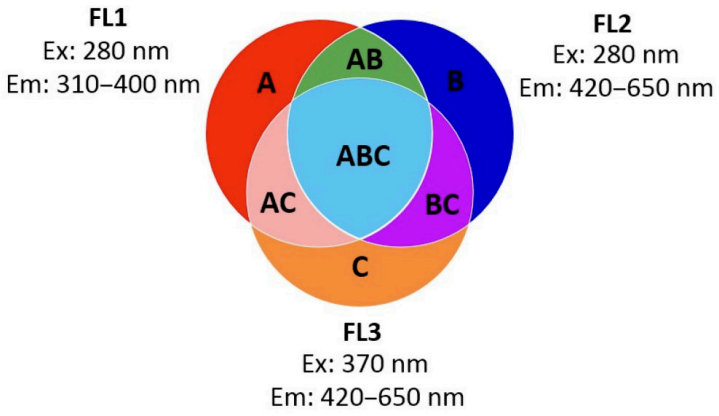

Figure 2.13.: Particle type classification with WIBS by Perring et al. 2015. The three modes (FL1, FL2 and FL3) correspond to the Aerosol particle type classification based on the fluorescence measurements by WIBS by Perring et al. 2015, leading to seven categories to which fluorescent particles can be associated. Figure adopted from Savage et al. 2017.

2.2.2. Measurement of fluorescent particles

The Aerosols Wideband Integrated Bioaerosol Sensor (WIBS) is an instrument for online measurement of fluorescence of single particles of diameter between 0.5 and 30 µm (see Gratzl et al. 2023). First, size and asphericity are measured with a laser using the forward scattering properties. Two neon lamps are then used to excite the particles using different wavelengths, 280 nm and 370 nm. The excited particles will lose the excess energy by emitting one or more photons of different wavelengths. Two detectors detect emitted photons in the two wavelength bands 310 nm to 400 nm and 420 nm to 650 nm. This allows categorizing the fluorescent particles into 7 categories (Perring et al. 2015; Savage et al. 2017), see figure 2.13.

Chapter 3.

Field campaign HyICE23

The Hyytiälä Ice Nucleation Experiment 2023 (HyICE23) is an international measurement campaign aiming at increasing the knowledge on sources and types of aerosols in the boreal forests of southern Finland. In a previous campaign at the same location, HyICE2018, studies of these aerosols have already been done in a similar way, see Brasseur et al. 2022. During this campaign, an increase of the INP concentration at around 257 K was observed during the snow melting period at the beginning of April 2018. This increase was less pronounced at lower temperatures. Another part of this campaign is producing new data on seasonal variability and influence of air mass origin on INPs.
The campaign started on the October 18th, 2023 and ended on the April 29th, 2024. The campaign was split into three phases, two of them with more intensive measurements, and a longer one in between with less intensive measurements. The first intensive measurement period (phase 1) began on October 18th, 2023 and ended on the November 7th, 2023. The longer but less intensive period (phase 2) ranged from the end of phase 1 until March 22nd, 2024. This was the beginning of the second intensive measurement period (phase 3) which ended on April 29th, 2024 (see tab. 3.2).
Aerosol filter sampling for INSEKT as well as microscopic analysis were done during all phases, between 10 and 14 h in phase 1; 3 to 4 days in phase 2 and 4 to 24 h in phase 3. Durations of the filter measurements as well as sampling rates of the different instruments during the three phases can be found in table 3.2. Measurements of the INP concentrations as well as particle properties mentioned in section 2.2 were performed inside a measurement container (from now on PINE container) and on a 35 m high tower (from now on Tower container). A list of the relevant instruments and measured properties is in table 3.1. Results and correlations between the different data will be presented in chapter 4. A more in-depth description of the field site and experimental setups is described in the following sections.

Table 3.1.: Used instruments and measurement methods as well as measured properties.

Instruments/Measurement Method	Measured Properties
PINE	INP concentration
INSEKT	INP concentration
APS	aerodynamic particle size distributions
welas & Promo	optical particle size distribution
WIBS	fluorescence of aerosols
Sample collection	snow depth
SMEAR II instrumentation	meteorological data

Table 3.2.: Sample rate of Instruments and Methods used in the HyICE23 campaign.

	Phase 1 10/17/2023– 11/07/2023	Phase 2 11/07/2023– 03/22/2024	Phase 3 03/22/2024– 04/29/2024
PINE	6 minutes	6 minutes	6 minutes
INSEKT (PINE container)	10–14 hours	3–4 days	4–24 hours
INSEKT (Tower container)	10–14 hours	3–4 days	10–24 hours
APS	5 minutes	5 minutes	2 minutes
welas & Promo	-	-	2 minutes
WIBS[1] (PINE container)	-	2 minutes Start 01/05/2024	2 minutes
WIBS[2] (Tower container)	-	-	2 minutes Start 04/05/2024

3.1. The SMEAR II field site

The HyICE23 campaign was conducted at the Station for Measuring Ecosystem-Atmosphere Relations SMEAR II (led by University of Helsinki (Junninen et al. 2009), which is located in southern Finland in Hyytiälä 60 km northeast of Tampere (Sogacheva et al. 2008) and 220 km north of Helsinki (Hari and Kulmala 2005) (see map in fig. 3.1). The direct anthropogenic influence at this remote site is low because the closest settlements have a population of less than 2500 inhabitants. Therefore, the aerosols at SMEAR II mostly originate from the natural environment or from long range transport. Figure 3.2 shows a picture of the PINE container and the 35m high tower, where some measurements were performed (see tab. 3.2). These are the locations used for the instruments and measurement methods described in chapter 2.
A 120 m high measurement mast was used for ambient air temperature measurements and snow depth was measured on the GPM-Field. The map in figure 3.3 shows the different locations of the measurement sites at the SMEAR II Hyytiälä forest station. The proximity (less than 1 km) allows for correlations between measured properties with low influence of changes due to distance. The snow depth measurements in the open field do not cover the snow accumulation within the forest area.
The site had a closed snow cover from November 13th 2023 until April 15th 2024. The transition from winter (with snow cover) to spring (without snow cover) was different compared to the more steady and smooth transition during the HyICE-2018 campaign. During HyICE23, the temperatures varied close to 0 °C for two months from February 21st until April 23rd, while during HyICE-2018, the transition from temperatures below 0 °C to above 0 °C happened during 3 weeks from March 25th 2018 to April 15th 2018.

[1]Provided by Hinrich Grothe et al. from TU Wien
[2]Provided by Jorma Keskinen et al. from University Tampere

Figure 3.1.: Map[3] showing the location of the SMEAR II Station in Finland.

[3] Available at `https://www.helsinki.fi/en/research-stations/hyytiala-forest-station` (last accessed: 2nd September 2024

Figure 3.2.: Picture of the PINE container and the 35 m tower of SMEAR II. On top of the PINE container on the left, the PM 10 inlet (Comde-Derenda) is visible. The same inlet was used for the filter-based measurements on the tower.

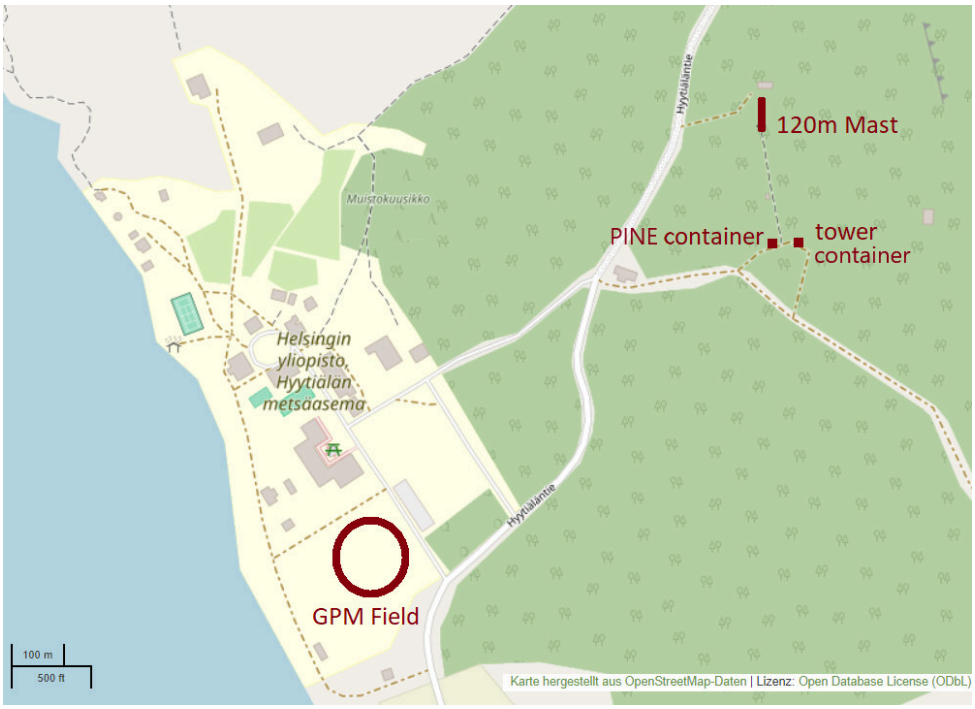

Figure 3.3.: Map (OpenStreetMap contributors 2017) showing the sampling locations at the SMEAR II Station.

3.2. Measurement setup at the measurement locations

3.2.1. The PINE container

Ground-based measurements were performed in a container (PINE container) during the HyICE23 campaign. The setup used during the different phases is shown in figure 3.4. It includes the PINE instrument for measurement of INP concentrations at high temporal resolution a setup for filter sampling for INP measurements over longer periods and an APS for particle size distribution measurements during phase 1 and 2 (right).

The air flow to the instruments inside the PINE container first passes a PM10 inlet (Comde-Derenda) which removes particles with a diameter larger than 10 µm. The incoming air is split into three branches to the different instruments.
The setup used during phase 1 and 2 is shown in figure 3.4 on the left. The sample line to the right connected to the PINE, which was operated with a sample flow rate of 2.2 to 2.5 l min^{-1}. The vertical sampling tube is connected to the APS. The APS was operated with a flow rate of 5 l min^{-1}, the WIBS with a flow rate of 0.3 l min^{-1}. The sample line to the left was used for the filter based aerosol sampling setup. A valve before the filters allow disconnecting the sampling flow to this branch during filter changes (see section 2.7). The valve between the filter setup and the pump was used to stop the air flow through the filters during filter changes. The filter sampling setup was used with flow rates between 3.4 l min^{-1} and 3.8 l min^{-1} during the whole campaign.
The changes to the setup in phase three are shown in figure 3.4 on the right. At the beginning of January 2024, a WIBS from TU Wien was connected to the vertical branch. A second pressure meter was added to the filter setup on the left branch. Two welas-2500 sensors were added to the setup at different positions, see figure3.4 (left) and figure 3.5. One was mounted to the vertical main sampling line before the line splits into the different branches, in order to measure the size distribution of incoming particles in the total sampling flow. The total flow rate at that position is 14.5 to 15.2 l min^{-1}. The second sensor was mounted to the vertical sampling tube directly above the cloud chamber of the PINE instrument (see fig. 3.5 left side). The welas sensors at the start and end of the sampling line can be used to observe particle loss due to the setup, by comparing the measured size distributions. This needs further evaluation, not part of this thesis.

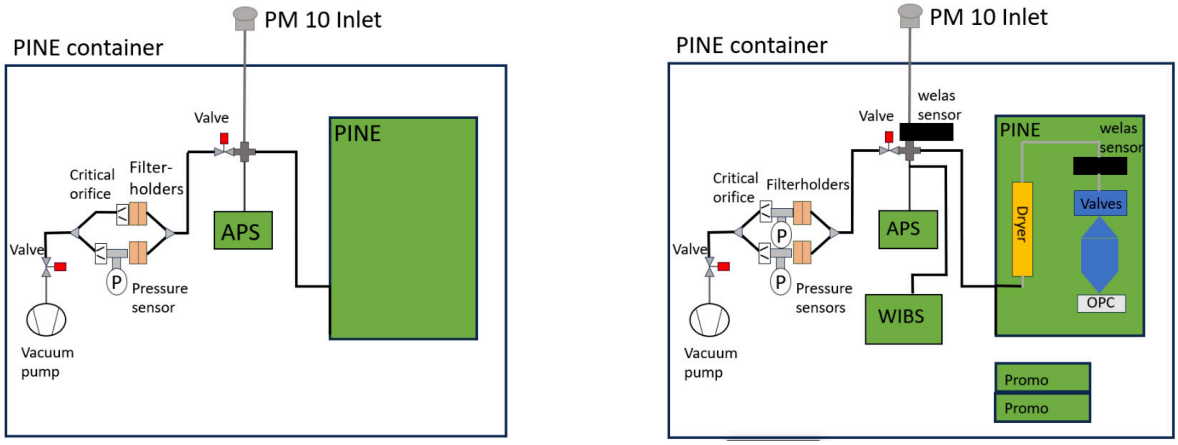

Figure 3.4.: Scheme of the PINE container setup during phase 1 and 2 (left) and phase 3 (right).

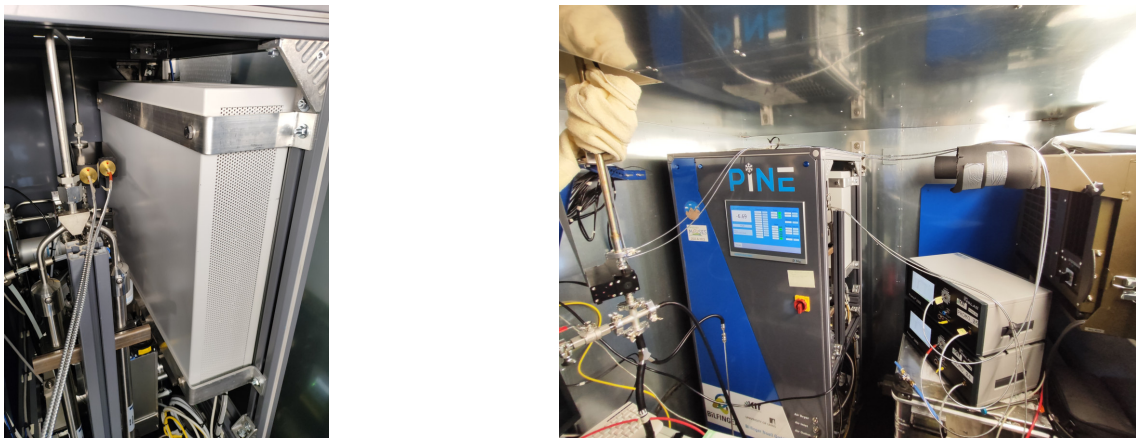

Figure 3.5.: Pictures of the additional welas-2500 sensors and Promo-2000 devices added during phase 3. A picture showing a welas sensor built into the PINE instrument (left). The welas sensor built in before the split of the sampling line and the Promo devices are shown on the right.

3.2.2. The tower container

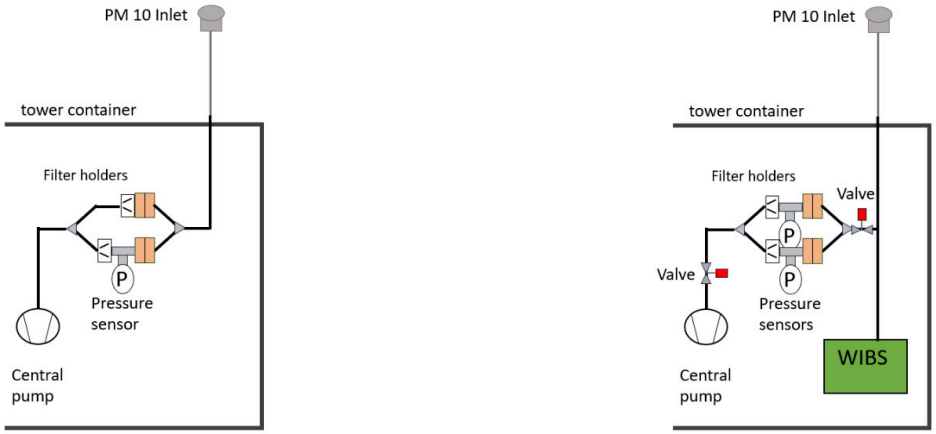

Figure 3.6.: Scheme of tower container measurement setup during phase 1 and 2 (left) and phase 3 (right).

A container (tower container) located on a 35 m high tower was used for aerosol and INP measurements above the canopy level. The sample flow for these measurements was passed through a PM10 inlet. On the inside of the tower container, a setup for taking filter samples was installed. Similar to the setup in the PINE container, the main sample flow was split into several flows for the parallel sampling of aerosols on two filters with flow rates between about 3.4 l min^{-1} and 3.8 l min^{-1}. The sample line was connected to the central pump system of the tower container. The aerosol filter setup was in operation during all three campaign phases.
At the start of April, a WIBS from the University of Tampere was connected to the sample line. Prior to installation in the tower container, a comparison between the two WIBS instruments was done in the PINE container. The comparison was repeated at the end of the measurement period. Valves and a second pressure meter were added to the filter setup. The valves allowed continuous measurement of the WIBS instrument even during filter changes.

Chapter 4.

Results

This chapter includes a presentation and discussion of results obtained during the HyICE23 campaign. The data time series are shown in section 4.1 and a case study of the period between April 18th and 25th, 2024, is shown in section 4.2.

4.1. Long Term Measurements

This chapter gives an overview of the measurements done during the HyICE23 campaign. Presented are measurements of INP concentrations over the whole campaign using PINE in section 4.1.1 and INSEKT in 4.1.2. A comparison between the two INP measurement methods is shown in section 4.1.3. Detailed data time series for each month of the campaign are shown in section 4.1.4. A comparison of the INP measurements with ambient conditions and the aerosol particle size distribution are shown in Sections 4.1.6 and 4.1.5.

4.1.1. PINE measurements

An overview of the PINE data measured during the HyICE23 campaign is presented in figure 4.1. The INP concentrations measured at higher time resolution are shown here as daily means for temperatures between 242 K and 260 K. Concentrations are plotted with the color code at the right side, with dark blue colors for the lowest concentrations and yellow colors for the highest concentrations. The INP concentrations were averaged for 2 K temperature intervals. PINE measurements were performed between mid-October and mid-November at different temperature ranges in order to obtain an overview for the range of the local INP population. The PINE instrument was then operated in repeating periods of constant temperature at 257 K and temperature ramps to 243 K from mid-November to mid-March. The PINE instrument was operated at different temperature settings from mid-March to end April.
The measurements at high temperatures (around 257 K) showed INP concentrations around $1\,\mathrm{stdl}^{-1}$ to $10^{-2}\,\mathrm{stdl}^{-1}$. INP concentrations at low temperatures (around 247 K) varied between $1\,\mathrm{stdl}^{-1}$ and $10^{2}\,\mathrm{stdl}^{-1}$.

Figure 4.2 shows time series of the INP concentrations at the selected temperatures 247 K (blue), 251 K (orange), and 257 K (green). Again, the INP concentrations are shown as daily means. The day to day INP concentrations varies for all temperatures. For the PINE measurements at the lowest two temperatures, the day to day variability can be as high as one order of magnitude, in some cases a change of two orders of magnitude could be observed. No significant seasonal

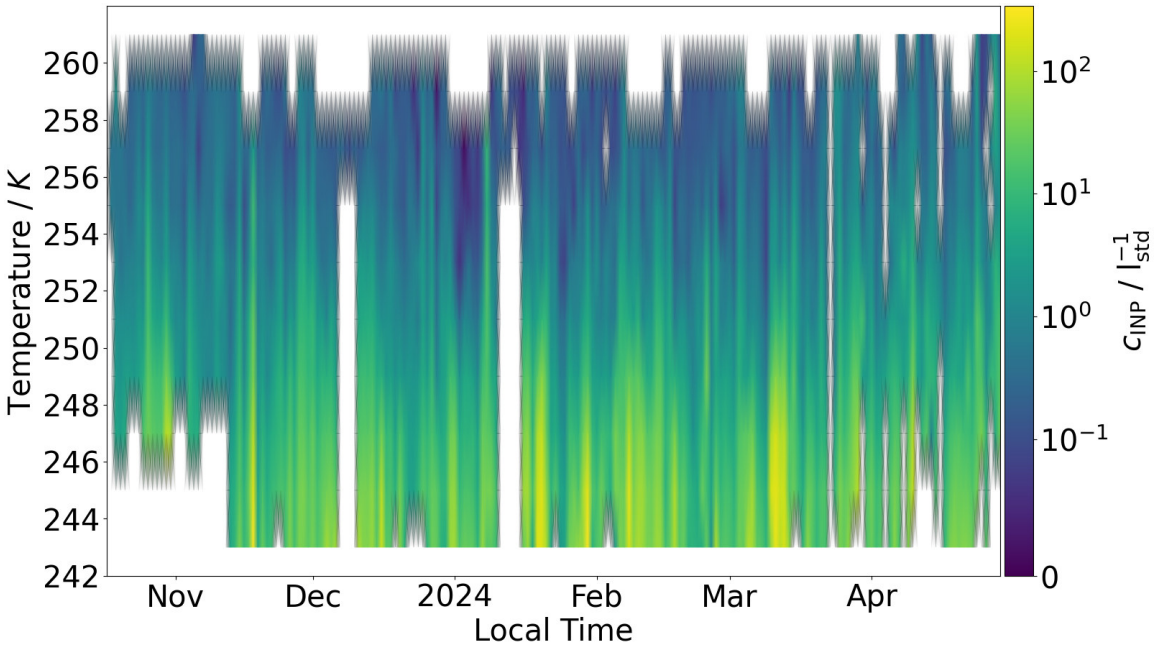

Figure 4.1.: Overview of the PINE data set for the whole campaign period. The INP concentration (color code) is shown as time series with daily mean values and for the temperatures from 242 K to 262 K. During two separate periods in December and January, the measurements were done at a constant temperature.

variation of the INP concentrations was observed at these low temperatures. The measurements at 251 K show a slight seasonal trend with decreasing INP concentrations from October to January and increasing concentrations from February to May. The day to day variability of INP concentrations at the highest temperatures is within about one order of magnitude. For March and April, an increasing variability of the INP concentration can be seen at the highest temperature.
Figure 4.3 shows the monthly mean INP concentrations for the temperatures 247 K, 249 K, 255 K and 257 K. The boxes are calculated using the daily mean values of the PINE INP measurements at each temperature. This representation confirms the conclusion from the time series plots above with not clear seasonal trend for the INP concentration at temperatures below about 249 K, but a more clear trend at temperatures above about 255 K. At 257 K, the mean values decreased from about 0.44 $stdl^{-1}$ in October to 0.14 $stdl^{-1}$ in January in mid-winter. The INP concentrations then increased from about 0.25 $stdl^{-1}$ in February to 0.57 $stdl^{-1}$ in April. This result confirms a trend for the INP concentration in Hyytiälä already observed by Schneider et al. 2020 for temperatures above about 255 K.

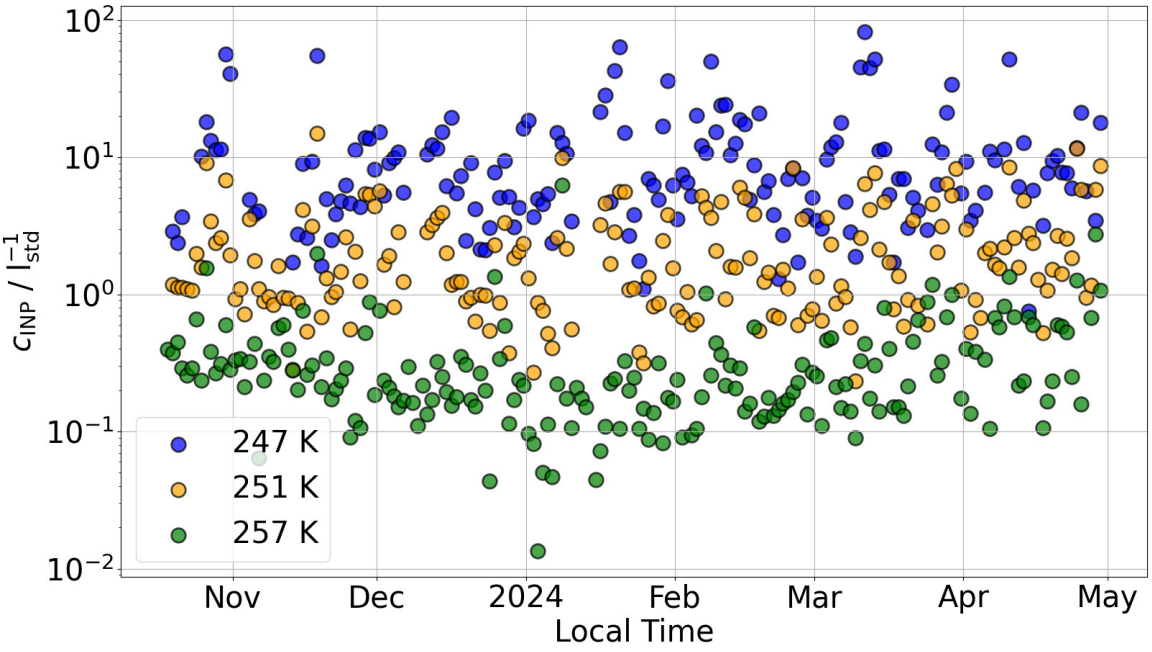

Figure 4.2.: PINE INP concentration time series for three different temperatures. The INP concentration is shown as daily means at 247 K (blue), 251 K (orange) and 257 K (green).

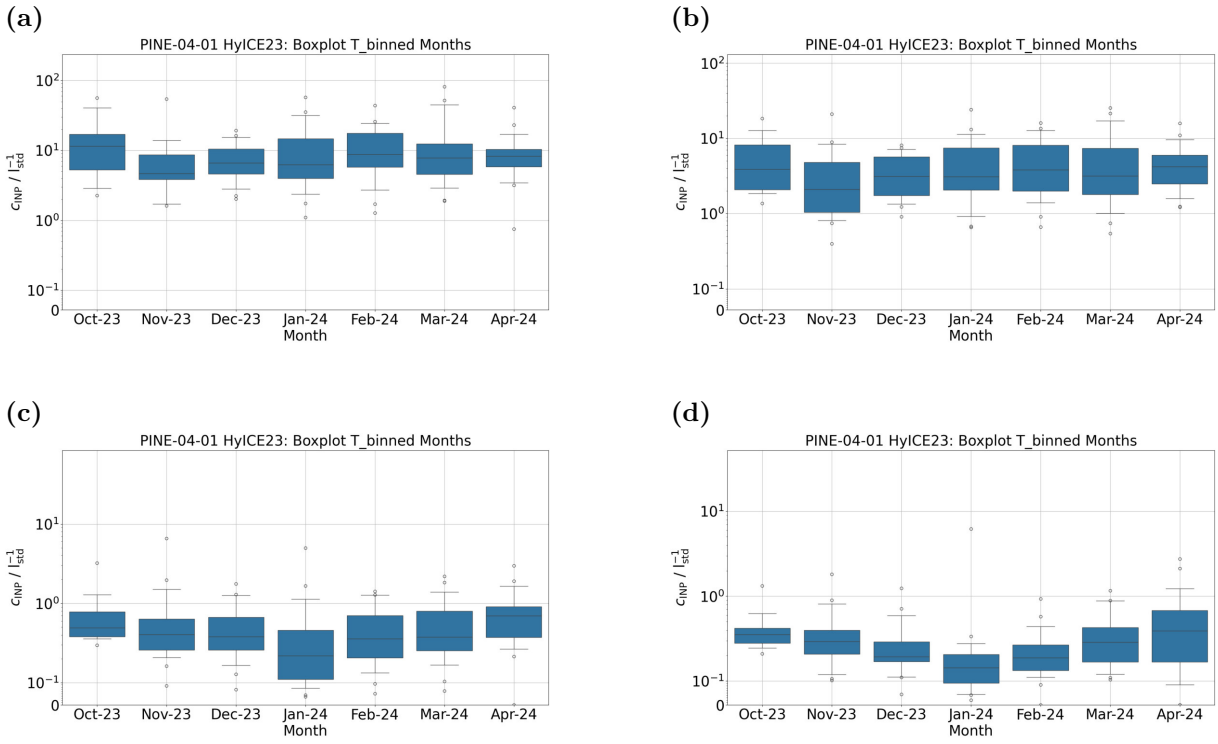

Figure 4.3.: Monthly mean INP concentrations measured with PINE. The boxes are calculated by using daily mean INP concentrations for temperatures of 247 K (a), 249 K (b), 255 K (c) and 257 K (d). Each box represents one month, from October 2023 to April 2024. The frame of each box represents the quartiles, the line within the box depicts the median. The whiskers stand for the area of 5 and 95% of all measurements. Outliers are shown as singular dots.

4.1.2. INSEKT measurements

In addition to the PINE measurements, aerosol filter samples were taken during the whole campaign period for offline INP analysis with the INSEKT method. For this thesis, samples between October and December 2023 and during spring 2024 have been analyzed. Samples have been taken in two locations, the PINE container, for ground based measurements and the tower container for measurements above the canopy (see sections 3.2). Figure 4.4 shows the INP concentrations measured with INSEKT from samples taken in the PINE container. Figure 4.5 shows the INP concentrations measured with INSEKT from samples taken in the tower container. For both locations, the INP concentrations between 246 K and 268 K are shown as color-filled circles. The measurements were divided into temperature bins of 0.5 K, the color shows the time, when the sample was taken.
The INP concentrations at high temperatures (around 260 K) were usually around 10^{-3} stdl^{-1} to 10^{-1} stdl^{-1}. At low temperatures (around 252 K), the INP concentrations varied between 10^{-1} stdl^{-1} and 10^{1} stdl^{-1}. Samples taken during spring 2024 (March and April, light green and yellow colors) show variability over all measured INP concentrations. A few samples from this season show enhanced INP concentrations at temperatures around 259 K to 255 K. This can be seen at both locations.
Figure 4.6 shows the monthly distribution of INP concentrations measured with INSEKT (PINE container, non-heated). The data in each panel is depicted in the same way as in figure 4.4, but here only the data of the respective month is color-coded, while all the other measurements are shown in gray in each panel. They show the samples taken in October (a), December (b), March (c) and April (d). Samples taken in both, March and April show the spread mentioned above. Samples taken in December show lower INP concentrations compared to all measurements. Additional analysis of the samples using heat treatment was performed for the samples taken during the winter to spring transition.
Figure 4.7 shows a comparison of the INP concentrations measured in the PINE container and the INP concentrations measured in the tower container. The INP concentrations measured in the tower container are around 4.6% higher compared to the INP concentrations measured in the PINE container. Figure 4.8 shows a comparison of the INP concentrations of samples taken during daytime and nighttime, the deviations are shown to be rather small. A comparison between the INP measurements of non-heated and heated samples is presented in figure 4.9. The dots are calculated by comparing the INP concentration measured at different temperatures before and after heat treatment. The color shows the time when the sample was taken. For low concentrations, the non-heated samples show a concentration almost 10 times larger than the heated samples. Figure 4.10 shows the same comparison, but as a quotient, between the different INP concentrations for different temperatures. The color in this graph also shows the time, when the sample was taken. The INP concentrations observed between 260 K and 251 K are roughly 10 times larger for non-heated compared to heated samples. The ratio for this deviation slightly decreases for lower temperatures. This can be explained by a change of prevalent INP particle types with temperature, from biogenic at high temperatures to dust or sea salt at lower temperatures, which are less affected by the heat treatment.
Figure 4.11 shows a monthly comparison of INP concentrations of the heated samples. The graph is built up similarly to Fig 4.6, with measurements of heated samples from the PINE container. Heated samples during different months showed a similar variety in INP concentrations to the non-heated measurements. Samples taken in December show lower values, while samples from March and April show a large spread.

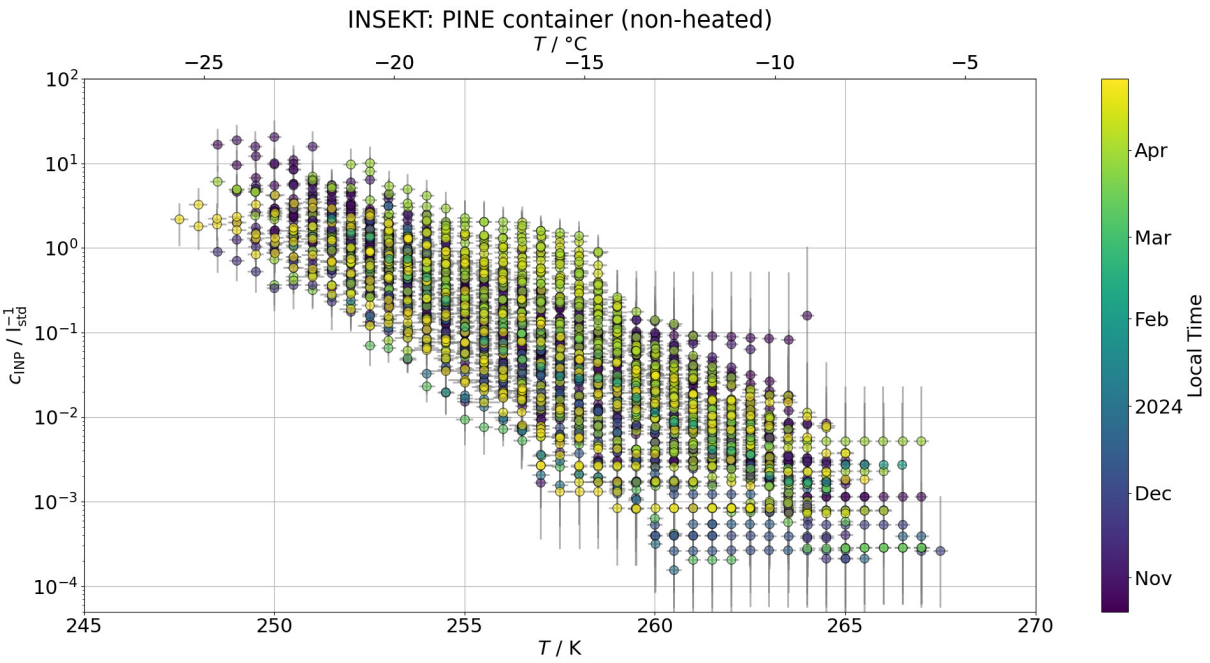

Figure 4.4.: INSEKT INP measurements from the PINE container aerosol samples (non-heated). The graph shows the INP concentrations for the whole temperature in 0.5 K steps. The colored circles represent the measured INP concentrations, while the whiskers stand for the measurement uncertainty for the INP concentration. The color code indicates the aerosol sampling time.

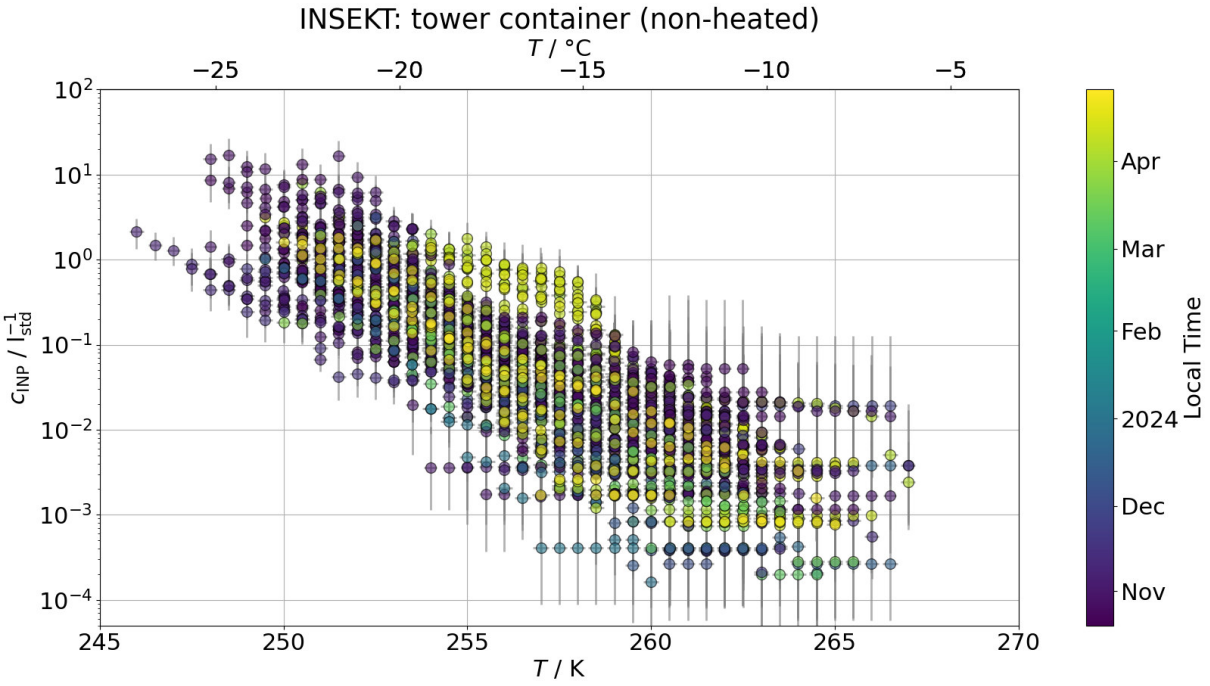

Figure 4.5.: INSEKT INP measurements from the tower container aerosol samples (non-heated). The colored circles represent the measured INP concentrations, while the whiskers stand for the measurement uncertainty for the INP concentration. The color code indicates the aerosol sampling time.

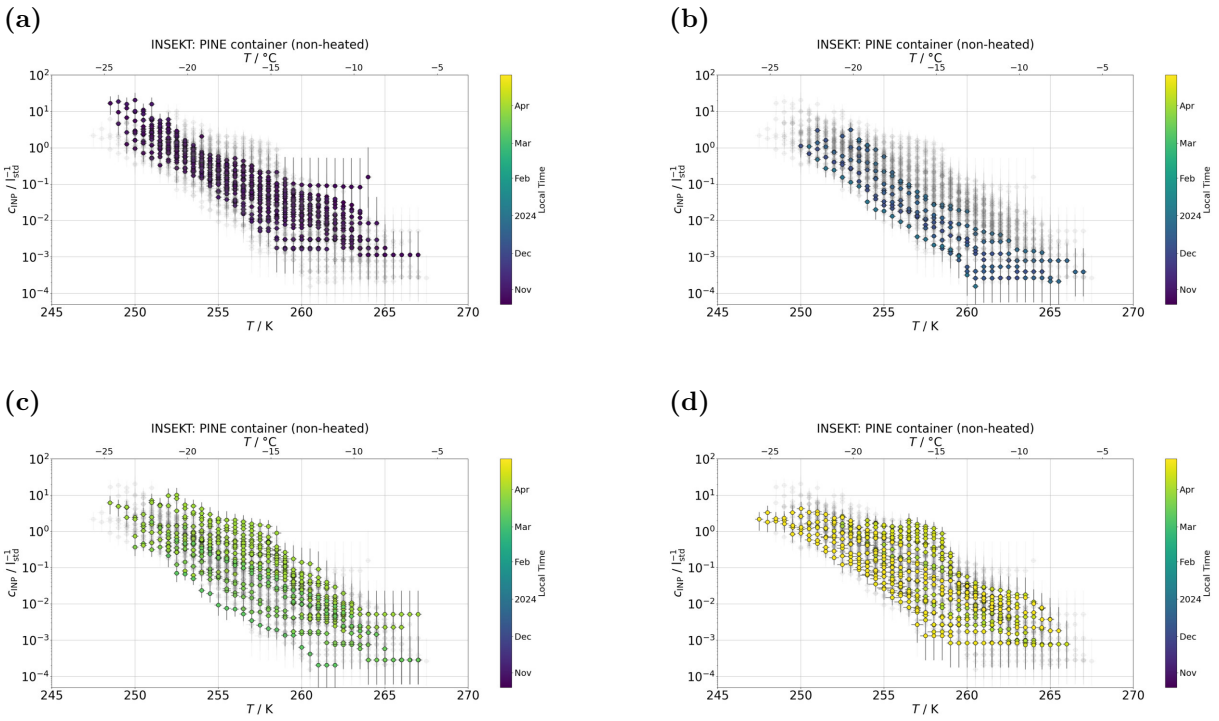

Figure 4.6.: Monthly INP concentrations measured with INSEKT for the PINE container. The four panels show the INP spectra for the four months October, December, March and April. The INP concentrations represent a mean value over the time when each sample was taken at different temperatures, divided into 0.5 K bins. Every panel includes the INP spectra of all samples taken in the PINE container displayed in gray, whereas the spectra of the particular months are highlighted with colors. The color represents the time when the sample was taken.

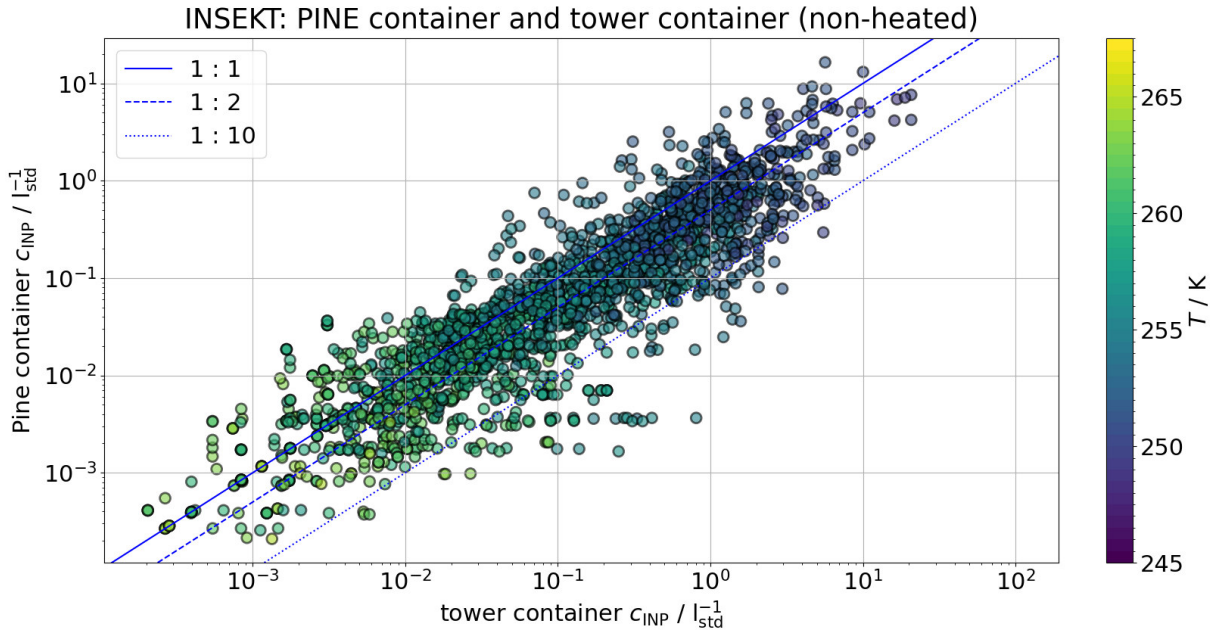

Figure 4.7.: Comparison of INSEKT INP concentrations measured in the PINE container and the tower container. The solid blue line indicates the 1:1 ratio, the dashed line a 1:2 ratio, and the dotted line a 1:10 ratio. The INP concentrations measured in the tower container are around 4.6% higher compared to the INP concentrations measured in the PINE container.

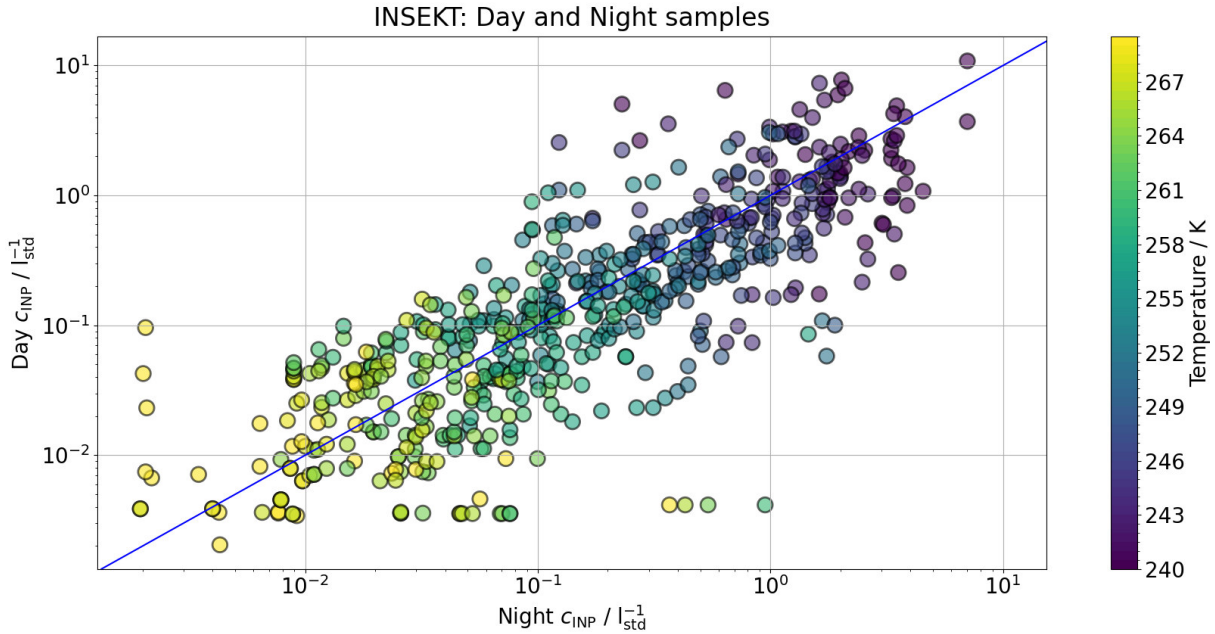

Figure 4.8.: Comparison of the INP concentrations from day and night samples for the PINE and the tower container taken during the first phase.

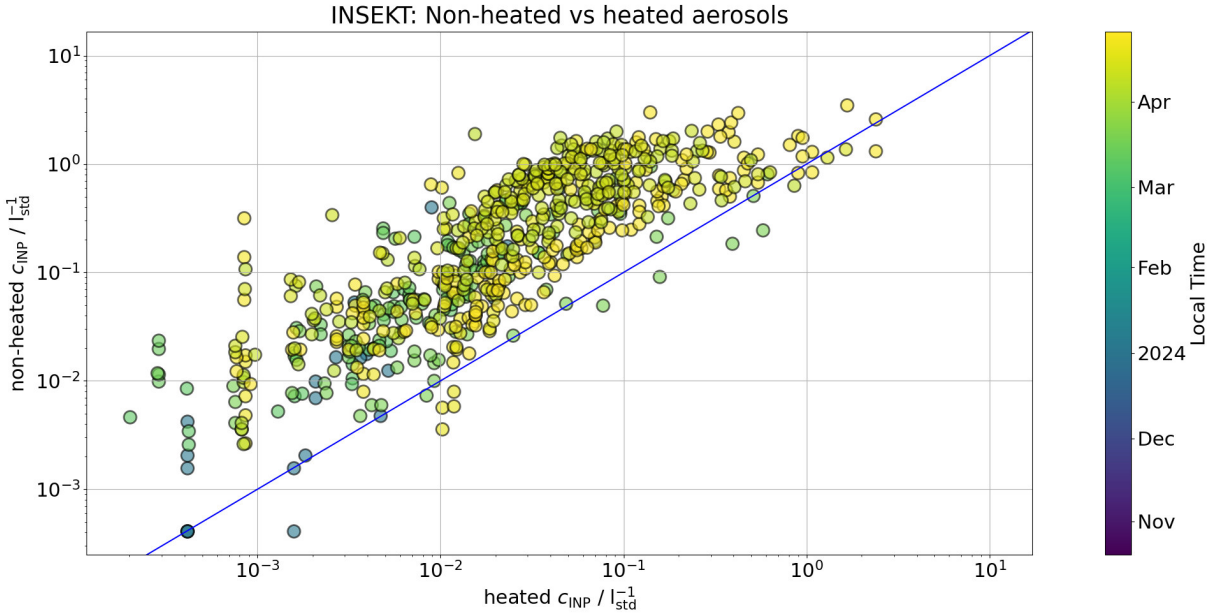

Figure 4.9.: Comparison of INSEKT INP measurements from heated and non-heated aerosol samples from the PINE container and the tower container. The color shows the time when the filter was taken.

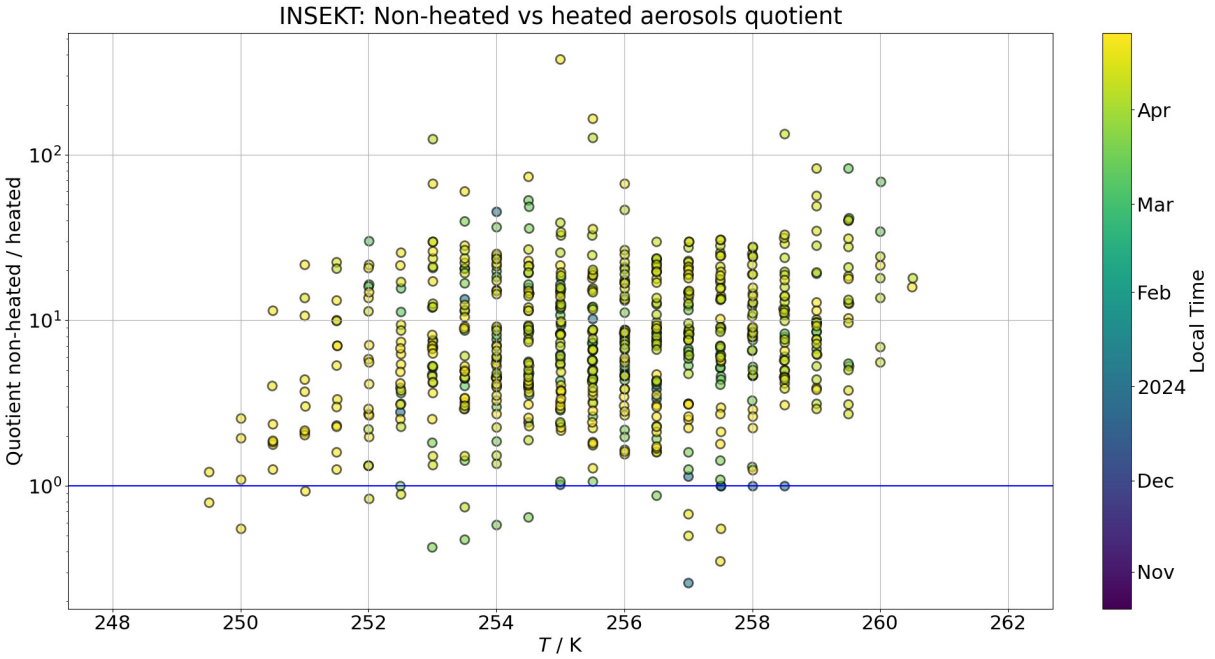

Figure 4.10.: Ratio of the INSEKT INP concentrations from the non-heated and the heated aerosol samples from the PINE container (same data as shown in fig. 4.9). The color shows the time when the filter was taken.

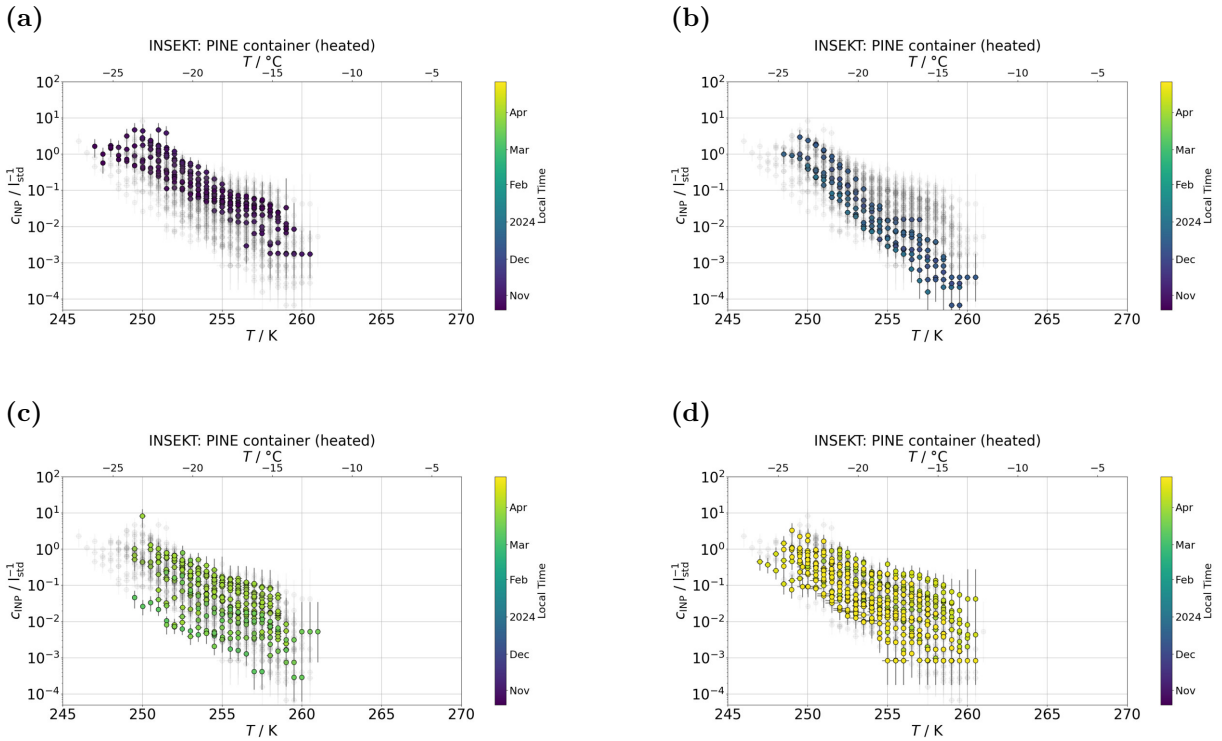

Figure 4.11.: Monthly INSEKT INP concentrations from heated samples. The panels show the INP concentrations for the four months October, December, March and April as shown in figure 4.6 for samples after heat treatment.

4.1.3. Comparison of PINE and INSEKT

A comparison of INP concentrations measured with the PINE instrument (triangles) and the INSEKT method (circles) is presented in figure 4.12 for samples taken in the PINE container, and in figure 4.13 for samples taken in the tower container. The INP concentrations measured by PINE were averaged over the times when each aerosol sample for INSEKT analysis was taken. The INP temperature spectra of PINE and INSEKT are analyzed and plotted in steps of 2 K and 0.5 K, respectively. In general, the INP concentrations measured with PINE and INSEKT agree well to each other. Only towards higher temperatures, the PINE data seems to show a high bias compared to the INSEKT data, but overall the two instruments complement each other very well.
A selection of four examples for the comparison of PINE data to a single INSEKT sample is shown in figure 4.14. During one sample (light green), the PINE was operated at a constant temperature, the mean value of which is shown as a single triangle. For all examples, the overlap of PINE and INSEKT is very good for temperatures below 255 K, above this temperature, the PINE instrument may measure slightly higher INP concentrations as shown in the yellow graph. For two examples (purple) PINE and INSEKT show very good agreement over the whole temperature spectrum. As such, during times of high INP concentrations at temperatures above 255 K, PINE measurements do not overestimate the real INP concentration.

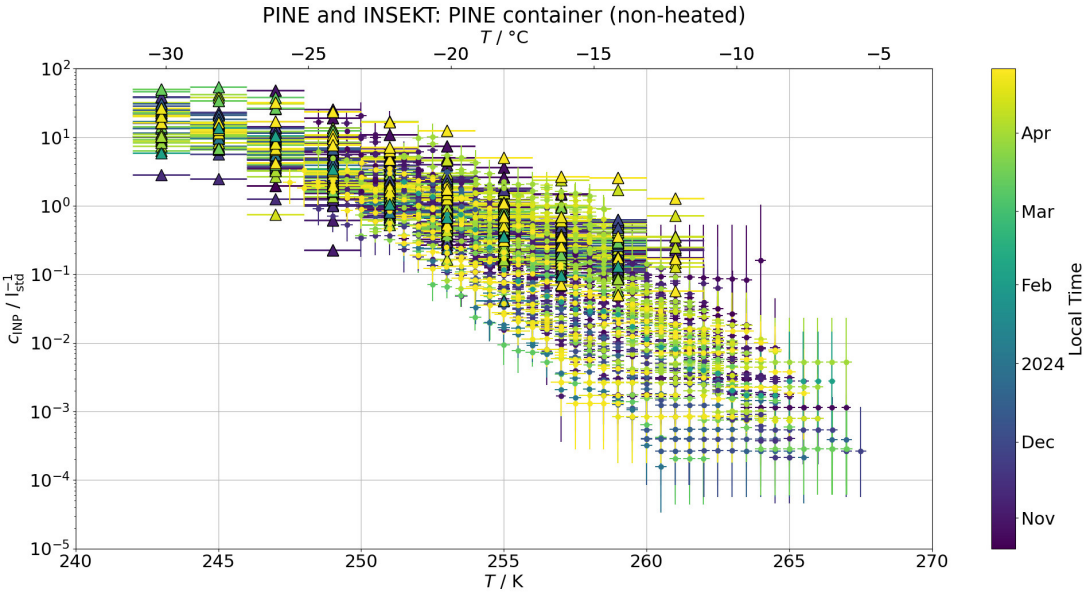

Figure 4.12.: INP concentrations measured with the PINE instrument (triangles) and with INSEKT for non-heated aerosol samples from the PINE container (dots) over a temperature spectrum between 242 K and 268 K. The PINE measurements were averaged over the sampling time of each INSEKT sample. For PINE, the temperatures are binned into 2 K intervals and for INSEKT into 0.5 K intervals. The color shows the time of each measurement.

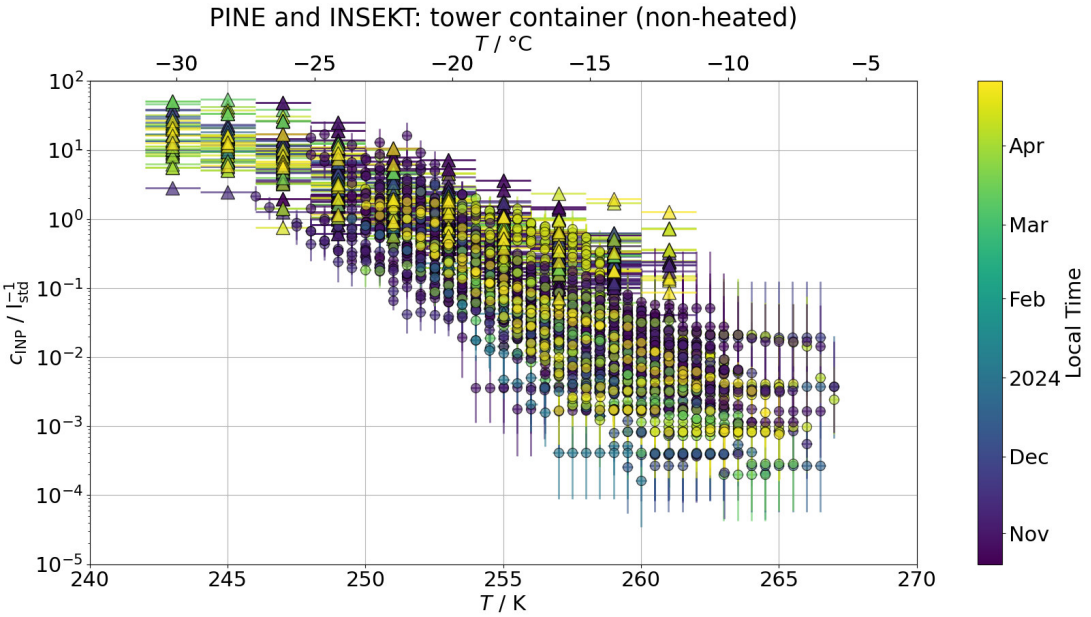

Figure 4.13.: INP concentrations measured with the PINE instrument (triangles) and with INSEKT for non-heated aerosol samples from the tower container (dots) over a temperature spectrum between 242 K and 268 K. The PINE measurements were averaged over the sampling time of each INSEKT sample. For PINE, the temperatures are binned into 2 K intervals and for INSEKT into 0.5 K intervals. The color shows the time of each measurement.

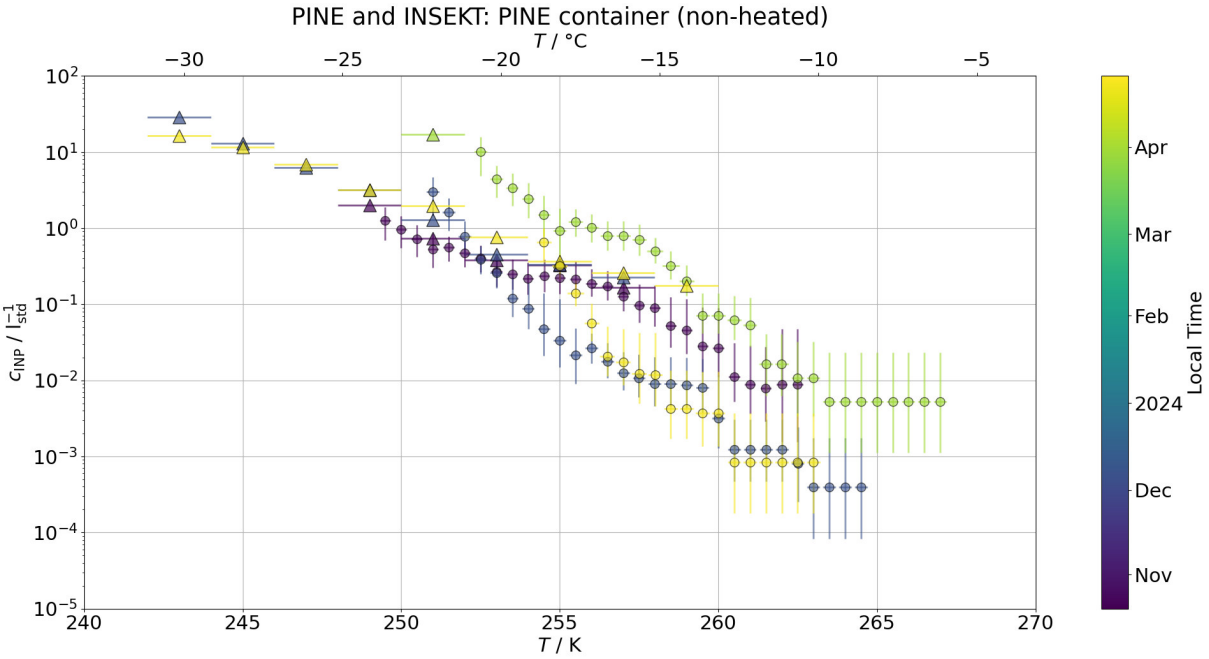

Figure 4.14.: Comparison of INP concentrations from PINE and INSEKT measurements in the PINE container for selected single INSEKT sampling periods.

4.1.4. Monthly data time series

In this section, detailed data time series are shown and discussed subsequently for each month of the campaign time period. The aim here is to provide an overview of the INP and other important data as well as their variation and correlation for the full campaign period.
The INP concentrations measured with PINE and INSEKT are shown in figures 4.15 to 4.21 together with aerosol and meteorological data[1].

The top panel of these figures shows the INP concentrations measured with PINE together with precipitation. The INP concentrations (circles) at temperatures 249 K (blue) and 257 K (green) were averaged over 12 to 24 h periods (phase 1 and 3, and phase 2). The precipitation is shown as 6 h accumulative liquid water equivalent (blue shaded areas) measured at the GPM-field (OTT Pluvio2 weighing rain gauge). The averaging was done, to show and compare the PINE data for a time resolution similar to the INSEKT measurements. The 12 h averaging of the PINE data starts from 06:00 local time, while the 24 h averaging starts from 12:00 local time.
The second panel shows INSEKT INP measurements (circles) and relative humidity (blue line). The INP concentrations at temperatures 254 K (blue) and 257 K (orange) from PINE container (non-heated) samples are shown for 12 h daytime and nighttime samples during phase 1 and 3 and 3 to 4-day periods for phase 2. The relative humidity measured at 1.5 m above ground (Rotronic MP102H RH/T sensor) is shown as 12 h running mean for autumn and spring and a one-day running mean for winter.
The third panel shows the air temperature (red line) and snow depth (black line). The air temperature is measured at 1.5 m above ground (Rotronic MP102H RH/T sensor), it is shown as a 12 h (autumn and spring) and 24 h (winter) running mean, to better fit the averaging of INP concentrations. The snow depth is measured at the GPM-field (Jenoptik SHM30) and shown with no averaging (still zero until end of October).
The fourth panel shows the number concentration of aerosol particles measured with APS in the PINE container. The measured concentration of particles larger than 0.5 µm (blue line) and the concentration of particles larger than 2.5 µm(black line) is shown as 12 h (autumn and spring) and 24 h (winter) running mean.
The lowest panel shows the wind direction Wd (red line) and wind speed Ws (black line) also using a running mean of 12 (autumn and spring) and 24 h (winter). The wind direction is measured at 120 m (Metek 3D ultrasonic anemometer) and the wind speed at 8.4 m (Thies 2D Ultrasonic anemometer) above ground.
The changes in wind direction coincide often with changes in ambient temperature, but to differentiate the actual origin of the air mass, modelling of back trajectories with HYSPLIT (Stein et al. 2015) is more reliable (see section 4.2).

October: The INP concentrations varied until October 23rd, where INSEKT measurements show a decrease in INP concentrations at 257 K after a precipitation (snow) event that day. A change in wind direction from north-east to south east on this day may hint to a change in air masses. During the night to 24th and the following days ambient temperatures stayed close to 0 °C. During daytime of the 23rd INP concentrations measured with PINE at 249 K were by close to 10^{-1} lower compared to the days prior and after. The INP concentrations at 257 K measured with PINE could be observed to decrease during a decrease in ambient temperatures from October 24th to 26th. The INP concentrations at 249 K showed a slight increase during this time. Measurements with INSEKT also showed decreasing INP concentrations at 254 K

[1]Available at: `https://avaa.tdata.fi/web/smart` (last accessed: September 2nd, 2024)

and 257 K in the same period. The concentration of particles larger than 0.5 µm, as well as concentration of bigger particles (larger than 2.5 µm) measured with APS, showed no systematic change. An increase in INP concentrations was observed on the 26th, with increasing ambient temperature with PINE and INSEKT, while particle concentrations showed no change. INP concentrations at 249 K measured with PINE increased with no visible connection to changes in ambient temperature, except on the 26th. Decreases in INP concentrations showed no visible connection to changes in temperature or particle concentration. A change in wind direction from north-east to south-west could be observed during the 29th, the INP concentrations showed no change connected to this. At the end of the month, decreasing INP concentrations at all temperatures were observed during a precipitation event. During this event, the 6 h accumulative precipitation was observed to be above 5 mm liquid water equivalent over a duration of 18 h. Ambient temperatures were close to 0 °C and showed no particular change. The measured particle concentrations decreased during this time by about one order of magnitude, and slightly more for particles larger than 2.5 µm.

November: At the start of November, INP concentrations decreased with decreasing ambient temperature until around the 3rd. From this day, an increase in ambient air temperature as well as increasing INP concentrations can be observed. During this time, a decrease in snow depth was observed. Particle concentrations increased by around 10^1. Decreases in INP concentrations at 257 K could be observed during high ambient temperatures from November 5 to 6. The measured particle concentration of large particles showed a decrease by 10^1 at the same time. The concentration of particles larger than 0.5 µm showed no particular change during this time. The INP concentration could be observed to decreases during precipitation events on two occasions of long (more than 12 h) snow fall during November 11 and 12. This decrease was observed at all temperatures measured with PINE. INSEKT samples during this time spanned multiple days and showed a decrease of less slightly than 10^1. INP concentrations measured with INSEKT showed a decrease in conjunction with decreasing ambient temperature over most of November. This seems to be the inverse of the winter to spring transition, considering the closed snow cover after November 13th. A steady decrease in INP concentrations from 1 to 10^{-2} stdl^{-1} over a period of two weeks can be observed during this transition. During a period where ambient temperatures increased by 10^1 K to around 0 °C around November 23, no significant change in INP concentrations was observed. At this time, the concentration of particles larger than 0.5 µm measured with APS decreased by 10^1. On this occasion, the decrease in concentration of particles larger than 0.5 µm and the increase in the INP concentrations possibly caused by increasing temperatures may have balanced out to the observed indifference of observed INP concentrations. During a second event (November 27th to 29th) of ambient temperature increase by more than 10^1 K, no significant change in particle concentration was measured. INP concentrations measured with PINE at high temperatures increased simultaneously to the change in ambient temperature at this event. The INP concentrations at low temperatures show similar behavior to INP concentrations at high temperatures for most of November. Changes of wind direction over the month could not be connected to changes in the INP concentrations, more so to changes in ambient temperature, hinting to changing air mass origin over the month.

December: The INP concentrations at high temperatures were low during December compared to the previous months. Around mid-December, INP concentrations measured with INSEKT increased together with an increase in ambient temperature from around 10^{-2} to 10^{-1} stdl^{-1} at 257 K while at 254 K a increase from around 1 to 10^1 stdl^{-1} could be observed. Fluctuations due to precipitation could not be observed to reflect on INP concentrations measured

with INSEKT during this increase due to long measurement periods. The INP concentrations at low temperatures measured with PINE in December varied. During the period of warmer temperatures (December 16th to 23rd), the INP concentrations measured at low temperatures with PINE showed a decrease from 10^1 to 1 stdl^{-1}. The PINE measurements showed a decrease in the INP concentrations during multiple precipitation events in December. Measurements at high temperatures showed fluctuations similar to the INSEKT measurements but seem to be more affected by precipitation events. During one specific increase in INP concentrations (on 17th), a short dry phase at ambient temperatures close to 0 °C could be observed. The particle concentrations measured with APS showed a decrease during these events, especially particles larger than 2.5 µm. Changes in the particle concentrations during this month showed mostly no parallels to changes in the measured INP concentrations, except during precipitation events. In late December, the INP concentrations measured with PINE at low temperatures increased with decreasing ambient temperature. During this time, the INP concentrations measured with INSEKT decreased by around 10^{-2} for the observed temperatures. Measurements with INSEKT at high temperatures showed a decrease from 10^{-1} to 10^{-3} stdl^{-1}. Wind direction during this month could be connected to periods of increasing ambient temperature during west-wind and decreasing ambient temperature during periods of east-wind until 21st December.

January: The INP concentrations measured with PINE decreased at the start of January, while ambient temperature stayed low (<−20 °C). The INP measurements at temperatures above ambient temperature were possible due to relative humidity being below 80%. The INP ice active above ambient temperature were not activated due to low ambient water vapor pressure. An increase in INP concentrations at low temperature with PINE from 1 to 10^1 stdl^{-1} could be observed during increasing ambient temperatures on January 7th. On January 8th (12:00 to 14:00 UTC), INP concentrations measured with PINE at high temperatures rose to 10^1 stdl^{-1} due to local concentration of particles being high during a four-hour-long event. Low temperature measurements were done directly before and after the event and may have missed the changes in INP concentrations connected with it. INSEKT samples have only been analyzed until before this event. The long period of INSEKT measurements may make this event invisible compared to possible increase in INP due to increasing temperature. Further measurements with PINE at high temperatures showed variations, most likely connected to changes in ambient temperature. Decreases in the particle concentration measured with APS coincided with INP concentration decreases twice during this month (10th and 24th). During both, the INP concentrations measured at low temperatures showed a decrease. During a precipitation event on January 22nd, the INP concentrations at low temperature decreased, while at high temperatures no change was observed. From mid of the month, INP concentrations at low temperatures showed inverse development compared to ambient temperature, showing increases during decreasing ambient temperature and vise versa. Wind direction varied more over this month compared to December, which may have affected the INP concentrations, but specific back trajectories may give more reliable information.

February: An increase in the INP concentrations at low temperatures was observed during decreasing ambient temperature at the beginning of February, a change in wind direction from north-west to north-northeast could be observed at the start of the decreasing trends. From mid to late February, INP concentrations at low temperatures decreased while ambient temperatures rose. During this month, the INP concentrations at high temperatures varied only a few times from around 10^{-1} stdl^{-1} On February 7th (08:00 to 11:00 UTC), a short term increase in the INP concentrations from 10^{-1} to 1 stdl^{-1} was measured with PINE at high temperatures. During

this event, no changes in aerosols were measured with APS or most station measurements. The DMPS showed an increase from 750 to 1200 cm^{-3}, a connection to the INP increase is not yet possible. At around mid of the month, the INP concentrations at low temperatures decreased, while the INP concentrations at high temperatures showed an increase. Ambient temperature rose to around 273 K. APS measurements showed a decrease of particle concentrations by around 1 around the 17th, while a precipitation event was observed. During this event, the INP concentrations also showed a decrease at all temperatures. In the night prior to the 17th a change in wind direction from south to north could be observed. A decrease in the INP concentrations at high temperatures could be observed during the following days, while ambient temperature decreased. A peak in INP concentrations at low temperatures on 24th was observed, but could not be connected to changes in any other measurement part of this thesis. Wind direction during this month was observed to be mostly south during periods of increasing, or ambient temperature close to 0 °C and mostly north during periods of decreasing temperature.

March: At the start of March, the INP concentrations measured with PINE decreased and increased with changes in particle concentrations measured with APS. The ambient air temperature stayed close to 0 °C (between −10 °C and 10 °C) for most of the month. INP concentrations at high temperatures followed increases and decreases in ambient temperature, except during a precipitation event on March 16th. The INSEKT measurements showed increases of INP concentration at high temperatures by 10^2 during increasing ambient temperature and decreasing snow depth. The PINE measurements also follow this trend for measurements at high temperatures. During a precipitation event on 22nd, the INP concentration at high temperatures decreased by 10^1. The INP concentrations at low temperatures increased from 1 to 10^2 $stdl^{-1}$ from 8th to 10th March. The INP concentrations at high temperatures showed an increase of less than 10^1 on 10th March. The ambient temperature showed a decrease during this time (March 8th to 10th). A decrease of the INP concentration at high temperatures from 1 to 10^{-1} $stdl^{-1}$ was observed during a precipitation event around 15-16th. The PINE Measurements of INP concentrations at low temperatures showed no changes connected to ambient temperature, except during decreasing snow depth. INP measurements with INSEKT at high temperatures were around 10^{-2} $stdl^{-1}$ around 20th March. Measurements at the end of March showed INP concentrations at around 10^{-1} $stdl^{-1}$ to 1 $stdl^{-1}$. Measurements in between have not been analyzed yet. The wind direction during this month varied more compared to February, still, mostly south-wind was observed during warm periods and wind from northern directions during cool periods.

April: The INP concentrations measured with PINE at high temperatures decreased for measurements with PINE and INSEKT at the start of April and slowly increased by about 10^1 until April 7th. The INP concentrations at low temperatures followed this trend. Ambient temperature decreased from around 5 °C to −8 °C on the 4th and increased to 5 °C by 7th. At around April 7th to 8th, a precipitation event was observed with decreasing INP concentrations at low temperatures. The INP concentrations at high temperatures seem less affected, which may be due to increasing ambient temperature during the event. The INP concentrations measured with INSEKT at high temperatures showed a decrease from 10^{-1} to 10^{-2} $stdl^{-1}$ from the beginning of April until 7th, after the precipitation event, an increase to 1 $stdl^{-1}$ was observed. Until April 12th, PINE and INSEKT measurements show increasing INP concentrations at all temperatures, while ambient temperature stayed above 0 °C even during the night. The particle concentrations measured with APS varied, but showed no correlation to changes in INPs until mid-April. From around 12th, the INP concentrations at all Temperatures decreased over the next 2 days and varied until 16th. Around this time, the measured particle concentrations

showed similar changes and may be connected. From 16th to 18th, INP concentrations were observed to decrease with decreasing ambient temperature. Afterward, day-to-day changes are shown in the case study in section 4.2. A general trend of the INP concentrations changing with changes in ambient temperature was observed 18-25th. After 25th, the INP concentrations show dependence on ambient temperature as well as particle concentration measured with APS. Wind direction during this month could be connected to periods of increasing ambient temperature during west-wind and decreasing ambient temperature during periods of north-east-wind until April 25th.

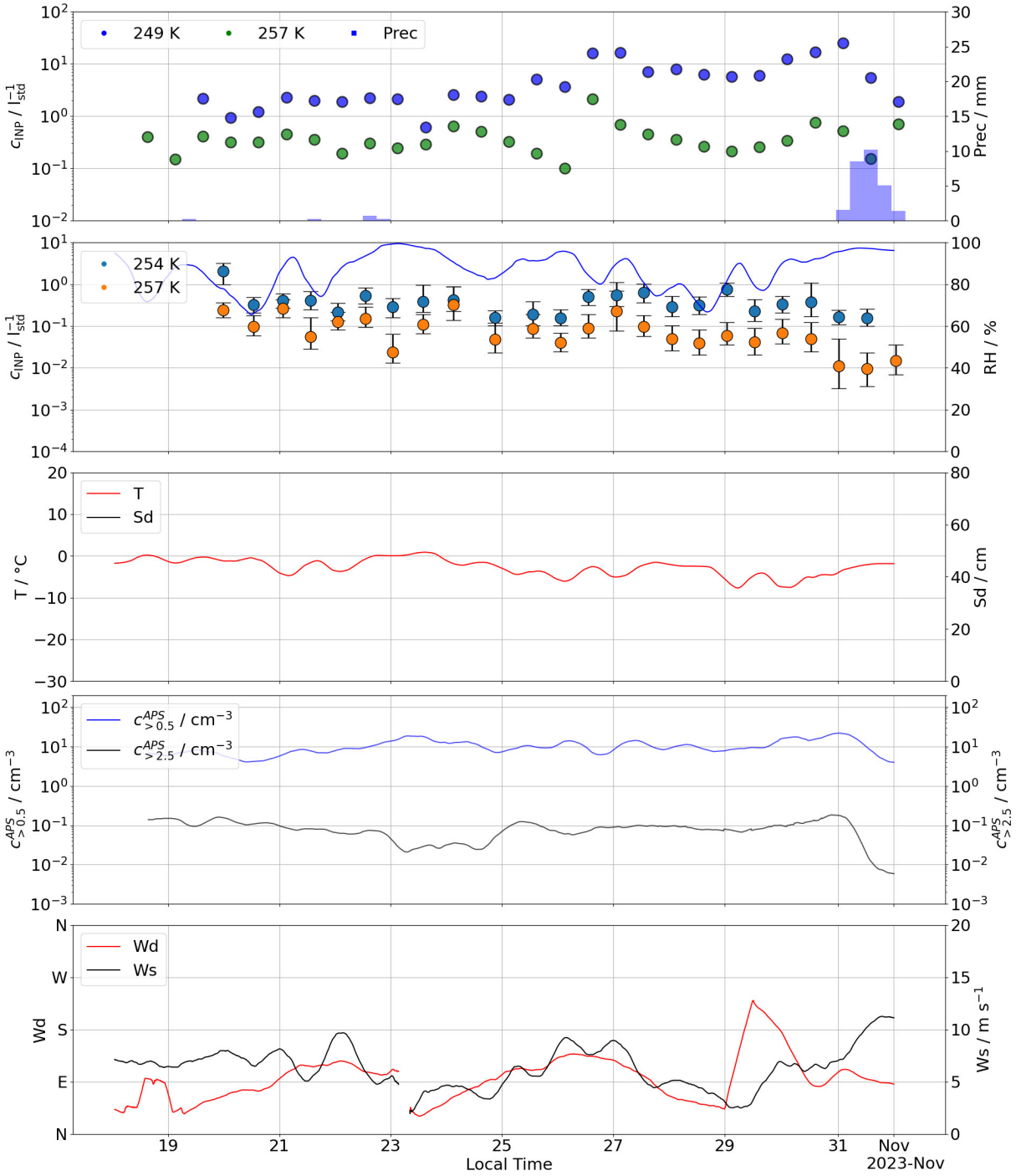

Figure 4.15.: Data time series for the first campaign month October 2023. The top panel shows 12 h daytime and nighttime means of the INP concentrations measured with PINE at temperatures of 249 K (blue circles) and 257 K (green circles), as well as 6 h accumulative precipitation amounts (liquid water equivalent, blue shaded areas). The second panel shows INSEKT INP measurements at temperatures of 254 K (blue circles) and 257 K (orange circles) from 12 h daytime and nighttime aerosol filter samples (non-heated) in the PINE container, as well as the one-day running mean of the ambient relative humidity. The third panel shows the one-day running mean of the air temperature (red line) and the snow depth (black line, still zero during October). The fourth panel shows the number concentrations of aerosol particles larger than 0.5 µm (blue line) and larger than 2.5 µm (yellow line), both measured with the APS in the PINE container. The lowest panel shows the wind direction Wd (red line) and the wind speed Ws (blue line).

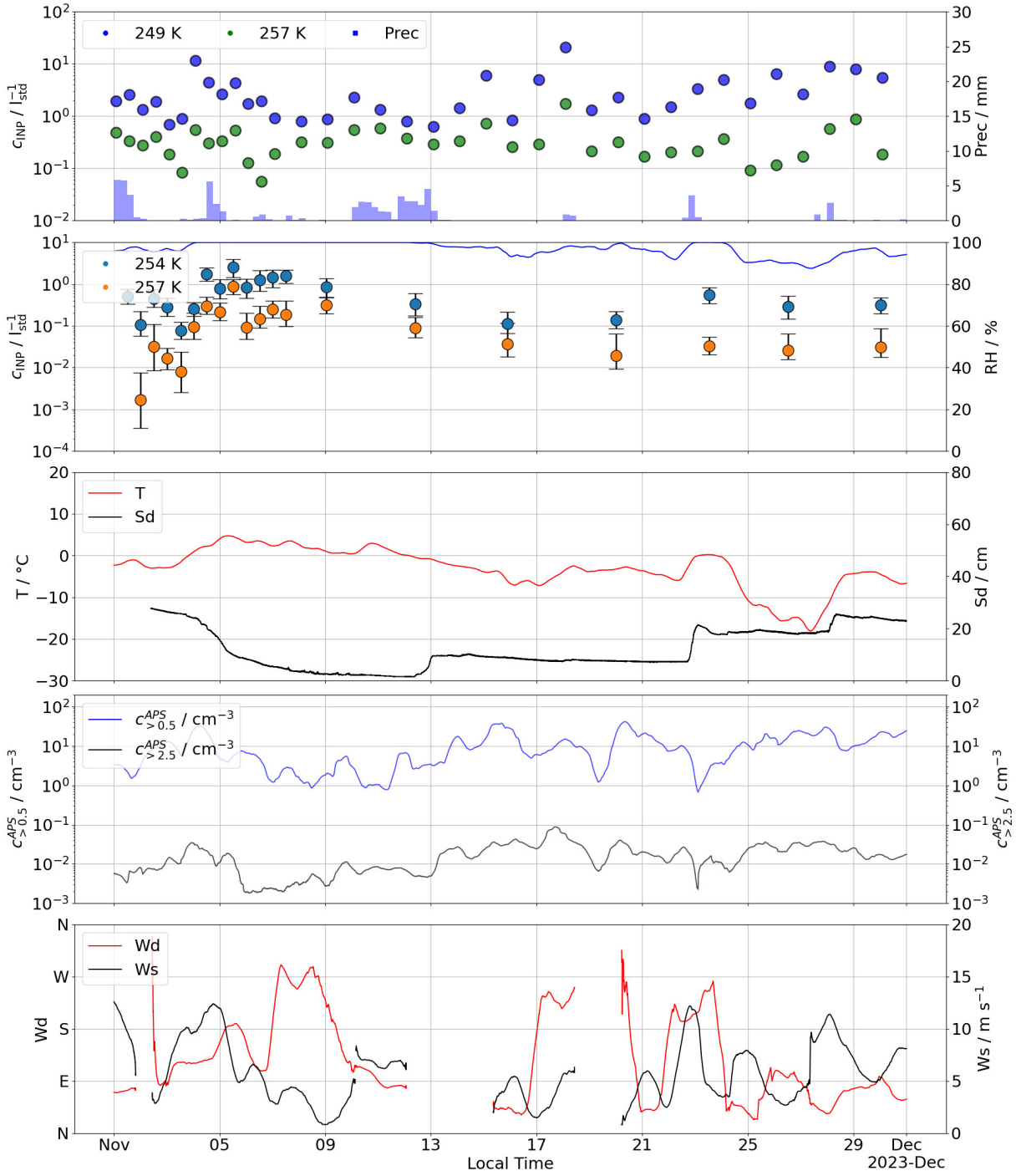

Figure 4.16.: Data time series for the campaign month November 2023. The same panels and data are the same as in fig. 4.15, only the time period for the INSEKT aerosol samples did vary during the month.

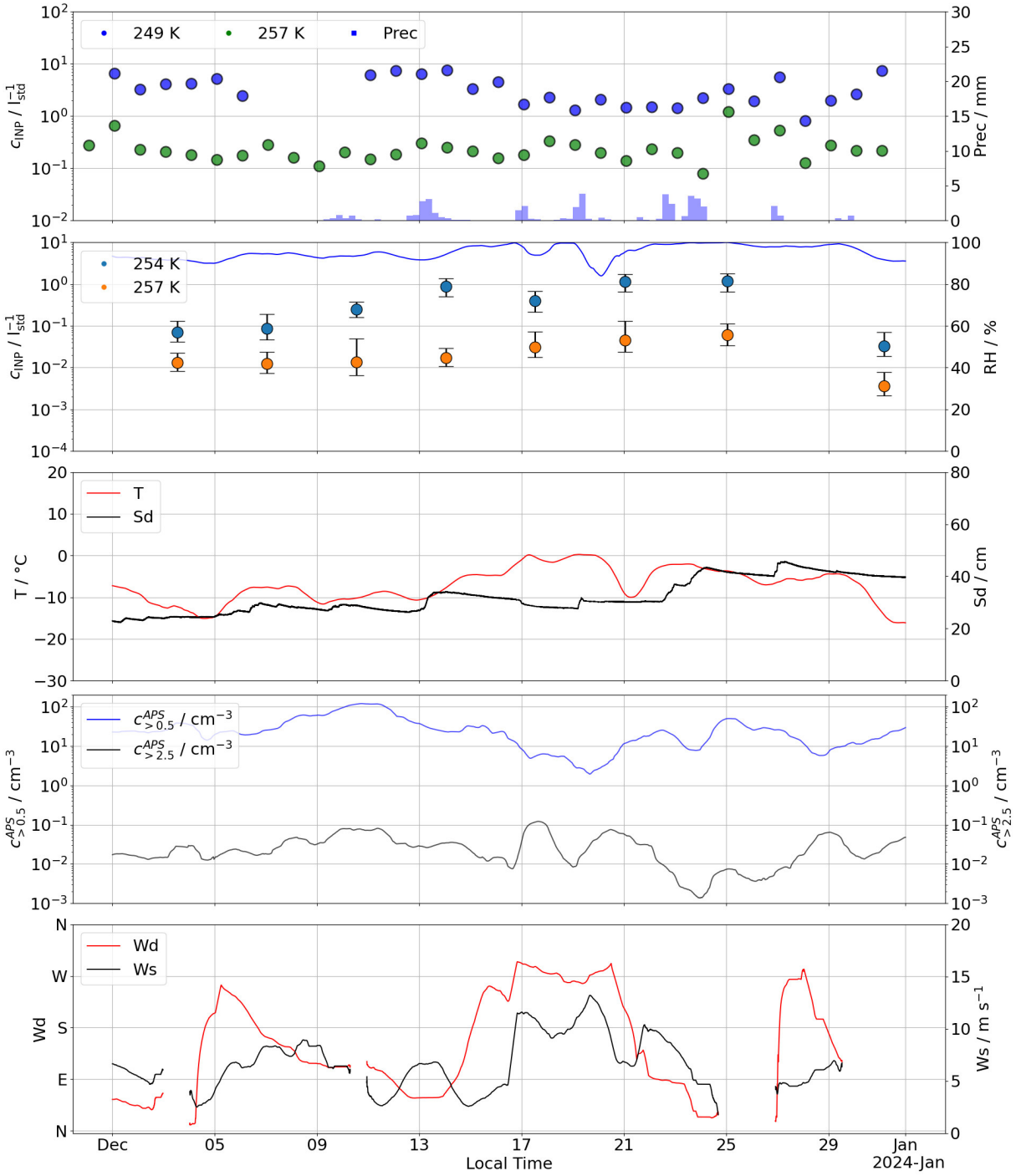

Figure 4.17.: Data time series for the campaign month December 2023. The same panels and data are the same as in fig. 4.15, only the 12 h running mean of meteorological and APS data was changed to a one-day running mean.

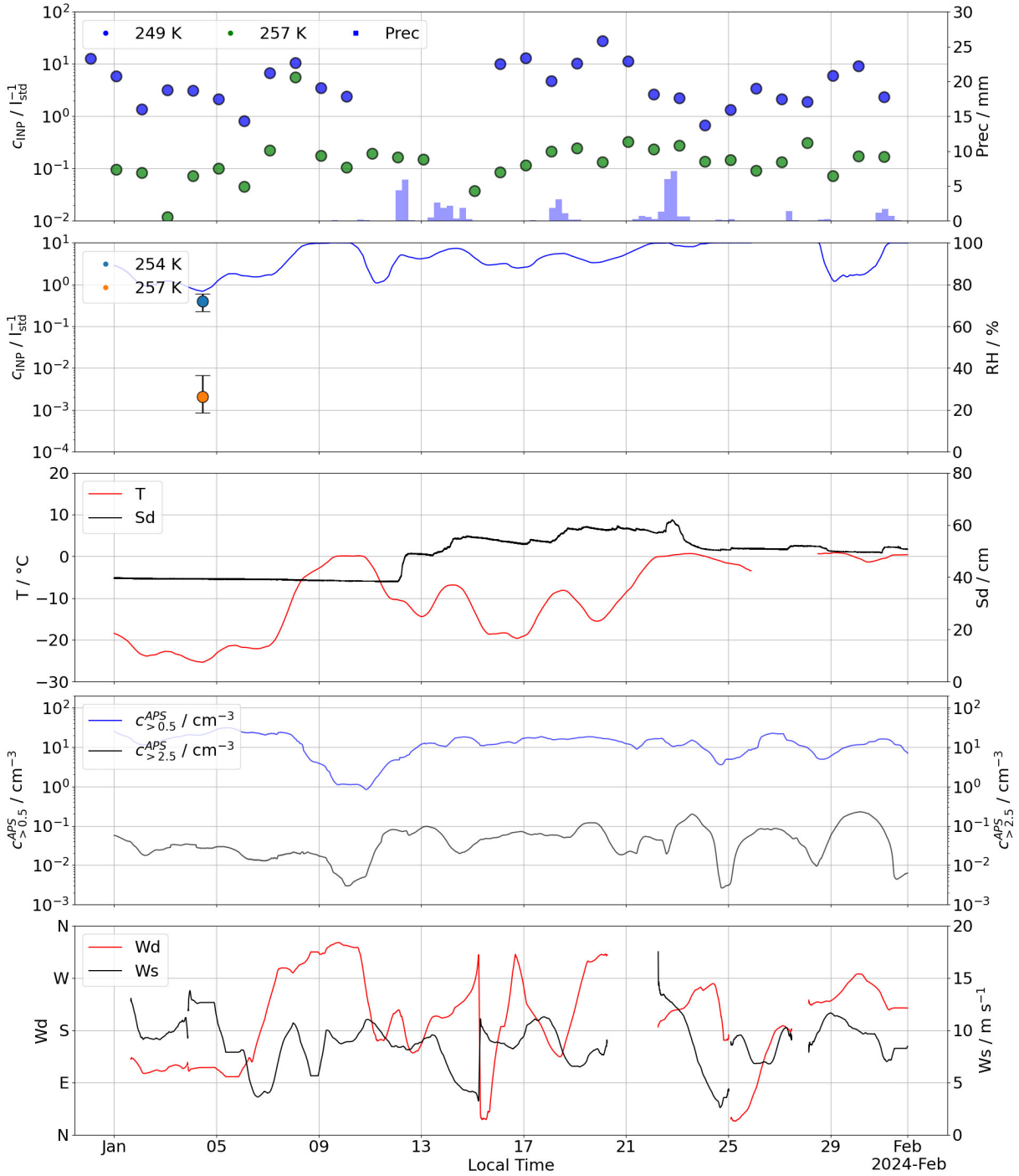

Figure 4.18.: Data time series for the campaign month January 2024. The same panels and data are the same as in fig. 4.15, only one INSEKT analysis was done selectively and the 12 h running mean of meteorological and APS data was changed to a one-day running mean.

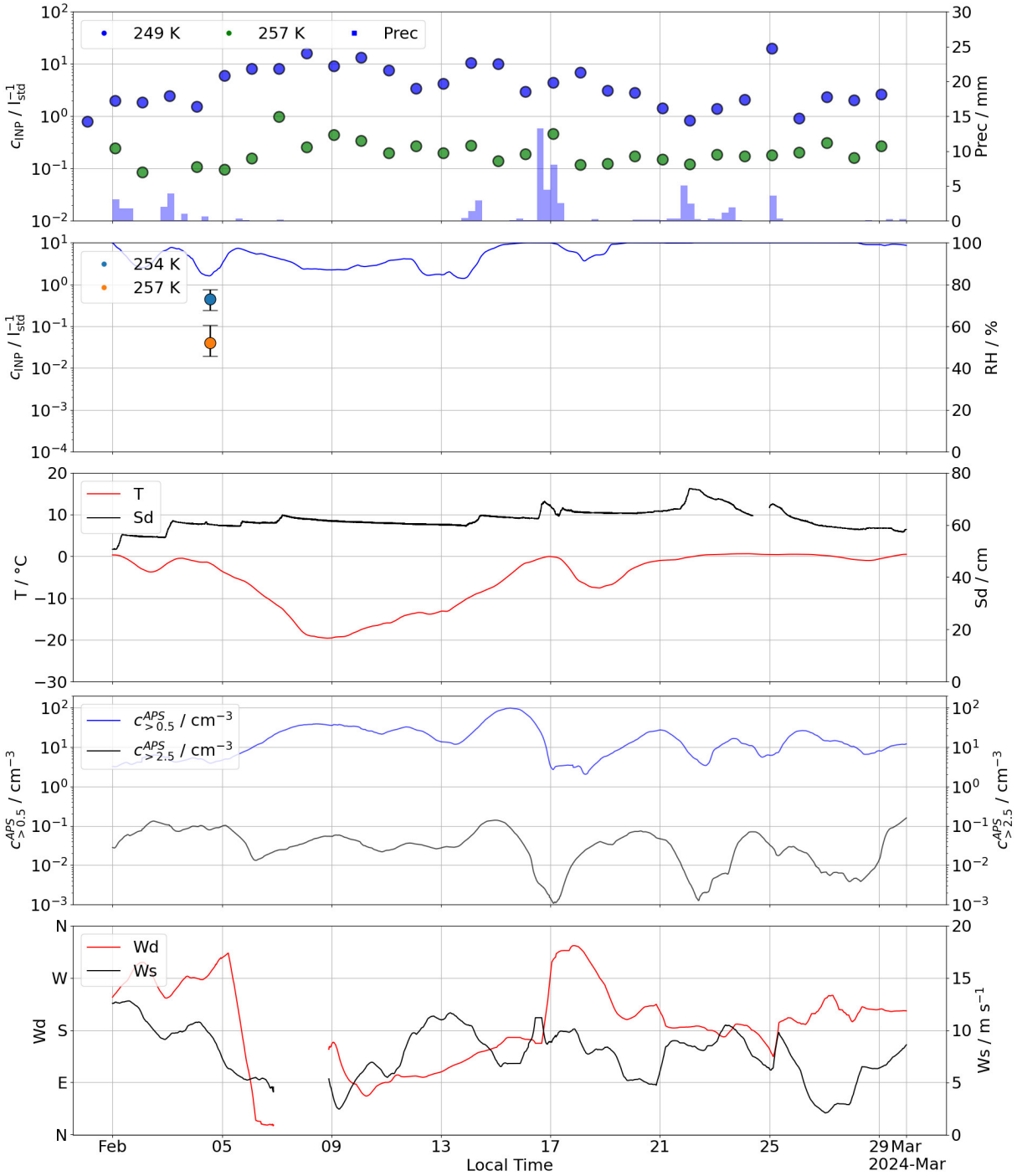

Figure 4.19.: Data time series for the campaign month February 2024. The same panels and data are the same as in fig. 4.15, only one INSEKT analysis was done selectively and the 12 h running mean of meteorological and APS data was changed to a one-day running mean..

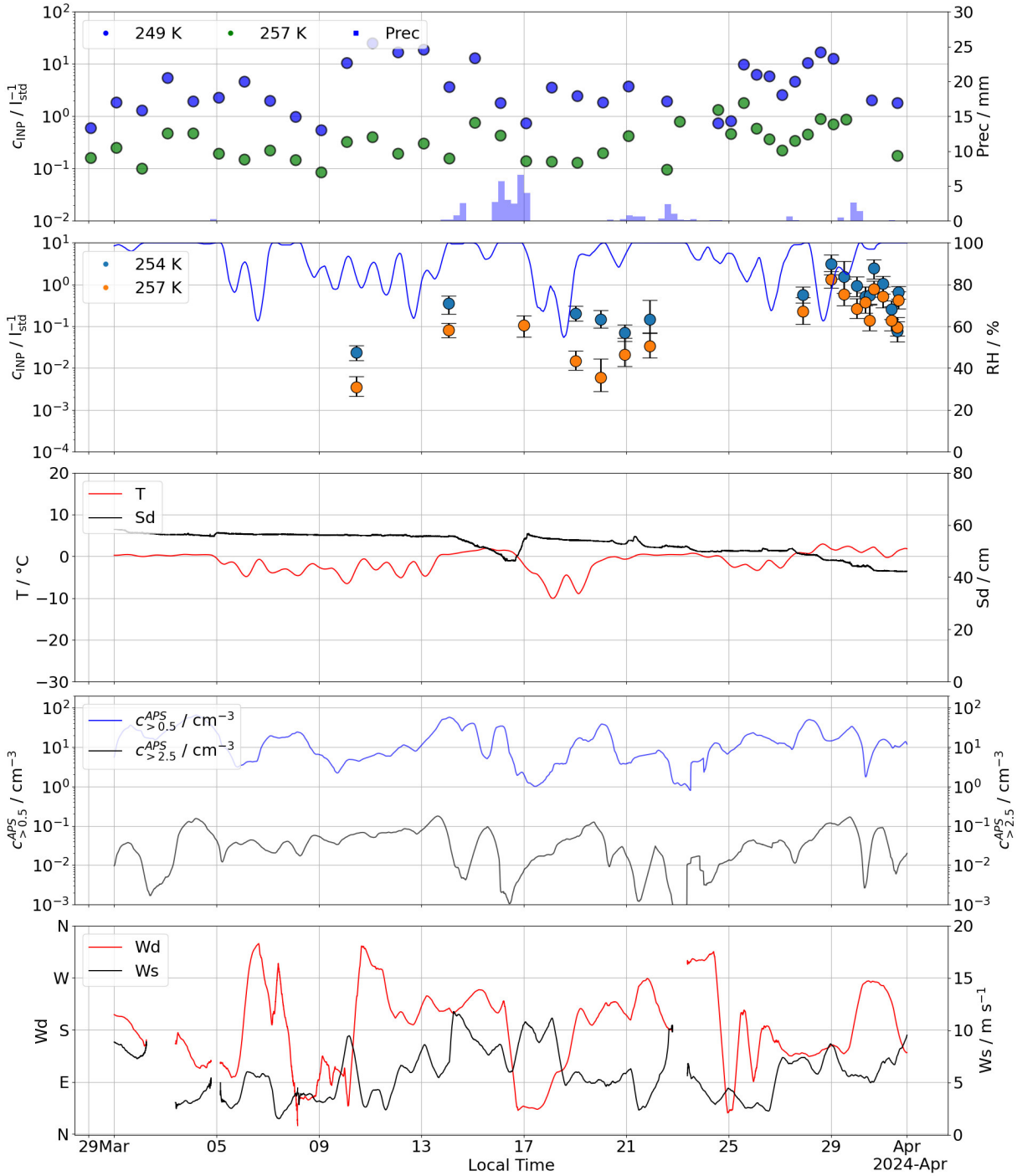

Figure 4.20.: Data time series for the campaign month March 2024. The same panels and data are the same as in fig. 4.15, only the time period for the INSEKT aerosol samples did vary during the month and INSEKT analysis was done selectively around periods of decreasing snow cover.

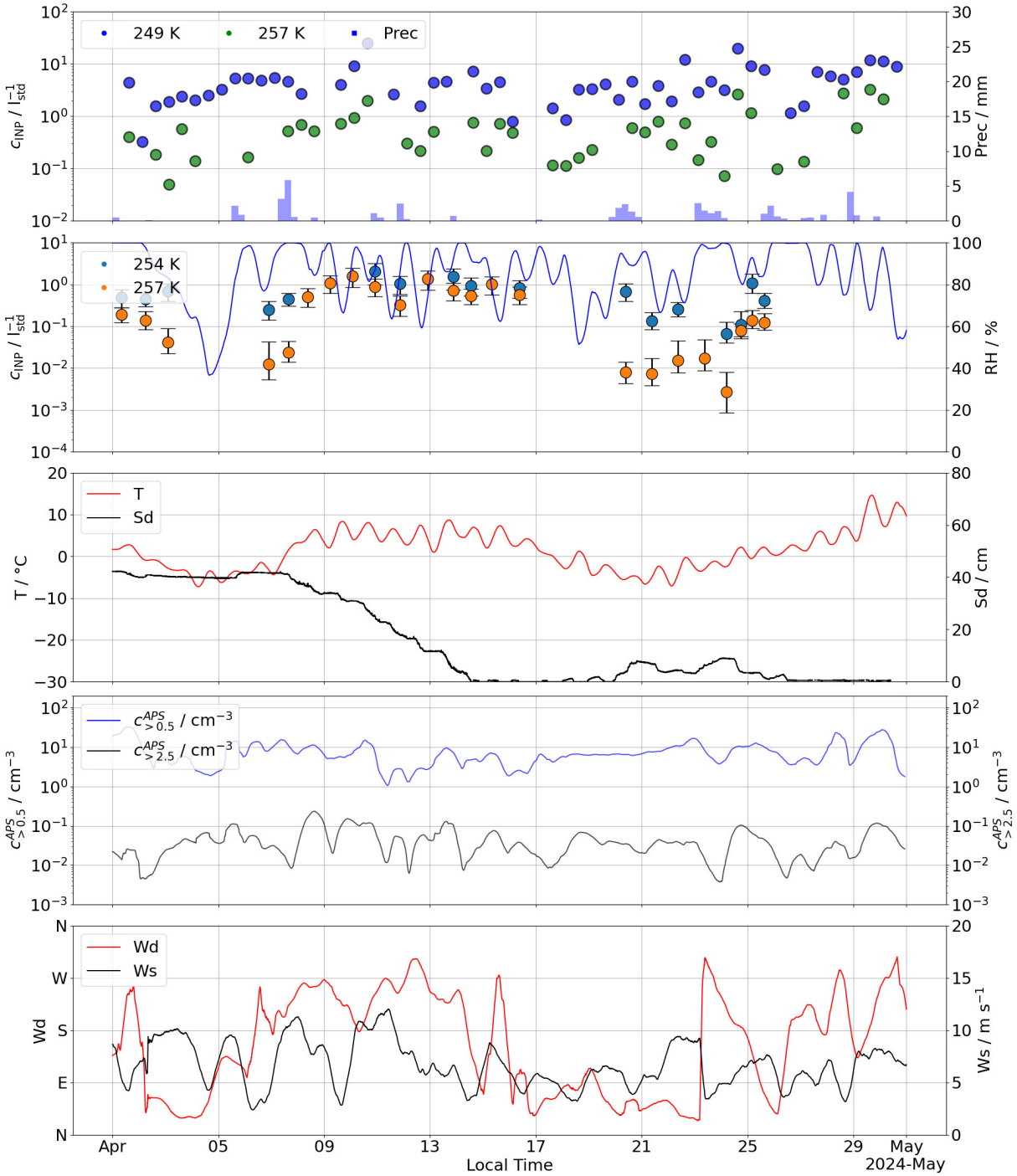

Figure 4.21.: Data time series for the campaign month April 2024. The same panels and data are the same as in figure 4.15, only the time period for the INSEKT aerosol samples did vary during the month and INSEKT analysis was done selectively around periods of decreasing snow cover.

4.1.5. INP correlation to aerosol number concentrations

Parallel to the INP measurements, particle number concentrations and size distributions were measured with an APS instrument (see section 2.2) over the whole duration of the campaign. For a general comparison of INPs and particle properties, the Spearman correlation coefficients were calculated for the INP measurements and the particle size distribution of particles larger than 0.5 µm as well as the particle size distribution of particles larger than 2.5 µm (see Kaufmann 2019) measured with the APS. Figure 4.22 shows the calculated correlation coefficients for comparison between APS and INSEKT (PINE container, non-heated) (a) and APS and PINE (b). The correlations are calculated by using a mean of the size distributions measured over the time of measurements of PINE and INSEKT respectively.
The correlation between INP concentration measured with INSEKT and concentration of particles larger than 0.5 µm measured with APS are low for all temperatures and above 254 K, slightly negative. The correlation between INP concentration measured with INSEKT and concentration of particles larger than 2.5 µm measured with APS are higher for temperatures between 255 K and 262 K. The INP concentrations measured with PINE show a slight correlation to the aerosol concentration for temperatures below 251 K. The increase in the correlation coefficient by looking only at particles larger than 2.5 µm can still be observed, but is much less pronounced compared to the comparison to INSEKT measurements. A more in depth comparison of INP measurements and APS data is shown in sections 4.1.4 and 4.2.

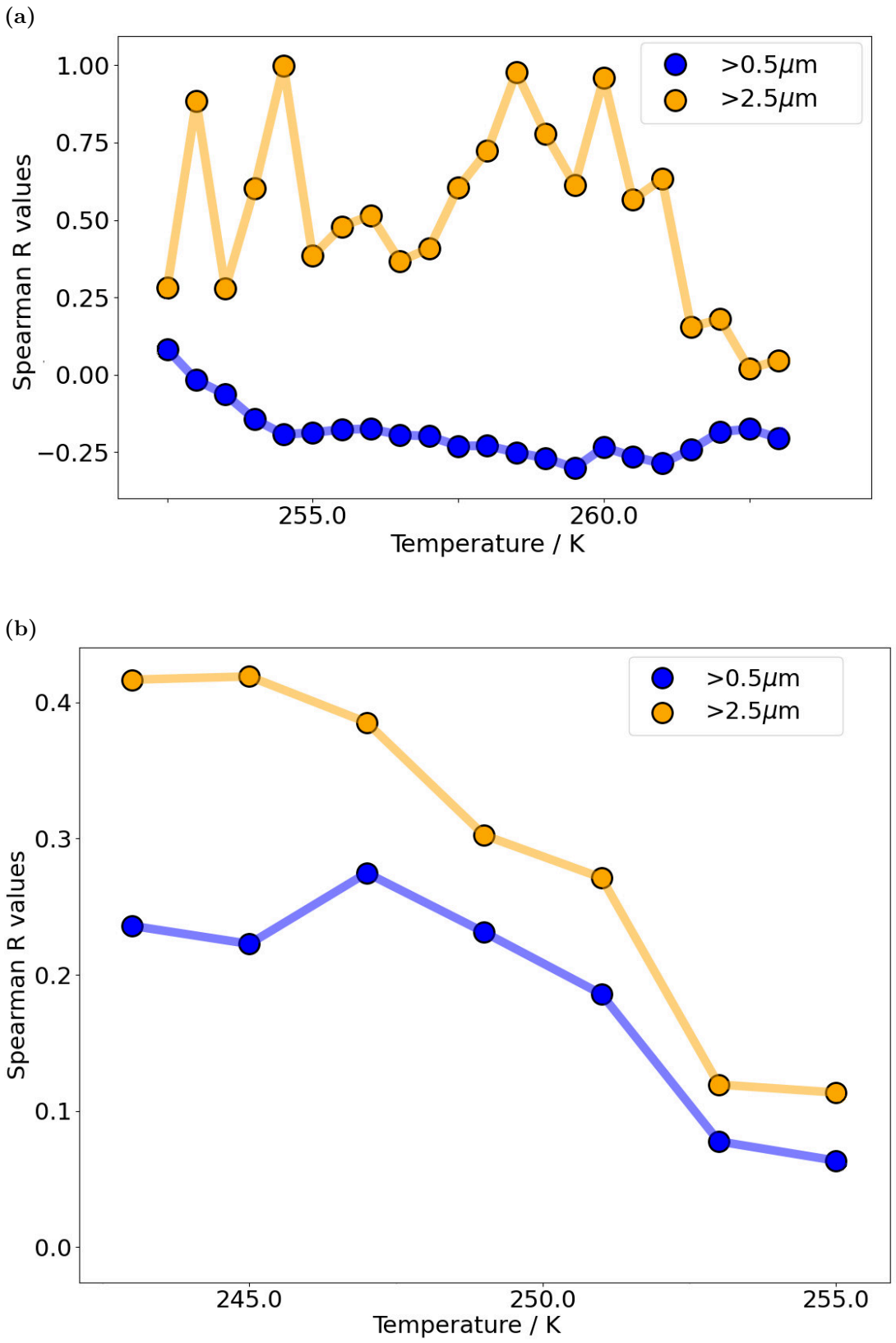

Figure 4.22.: Spearman correlation coefficient between INSEKT measurements (a) and PINE measurements (b) to the APS aerosol concentration measurements. The orange graphs show the correlation of INP concentration to concentration of particles larger than 2.5 µm while the blue graphs show the correlation to the particle concentration of particles larger than 0.5 µm.

4.1.6. INP correlation to meteorological conditions

Correlating the INP concentrations to meteorological data may provide insight into possible sources. For the measurements in Hyytiälä, local and regional sources may play an important role. As these mostly produce biogenic particles, the meteorological factors may also impact the prevalent type of measured INPs. However, neither wind direction, wind speed nor precipitation showed significant correlation with the INP concentrations measured with either PINE or INSEKT on long term. The highest correlation was found to be in regard to the ambient temperature. The Spearman correlation coefficients for INSEKT INP concentration and ambient temperature at 1.5 m (Rotronik MP102H RH/T) were calculated at different nucleation temperatures. The correlation coefficients for samples taken in the PINE container are presented in figure 4.23. The coefficients are calculated by using a mean of the temperature measured during the duration when the sample was taken. Figure 4.24 shows the difference in correlation coefficients for the two locations, Pine container and tower container, compared to temperature at 1.5 m was used. A difference in the correlation was observed for the two locations. The INP measurements with INSEKT in the PINE container showed higher correlations compared to the measurements done on the tower container. This may be due to the sources, which react to the temperature changes, being closer to the ground than above the canopy, while above the canopy the INP from further away sources influence the measurement more.

Figure 4.25 shows the correlation made for INSEKT measurements during the different phases. During autumn (phase 1), temperatures varied only slightly, while INP concentrations at high temperatures varied by up to 10^3. Decreases in INP concentration were observed during precipitation (snow) events. INP concentrations increased after these events, while temperature changes were different to these events. Due to generally low ambient temperature in winter (phase 2) a correlation to low INP concentrations is acceptable, but INP concentration decreases were observed to reach a lower limit around $10^{-3}\,\mathrm{stdl}^{-1}$. These concentrations were reached during ambient temperatures above $-10\,^{\circ}\mathrm{C}$, during winter ambient temperatures were observed below $-10\,^{\circ}\mathrm{C}$. During spring (phase 3), changes in INP concentrations could be observed to be largely influenced by ambient temperature.

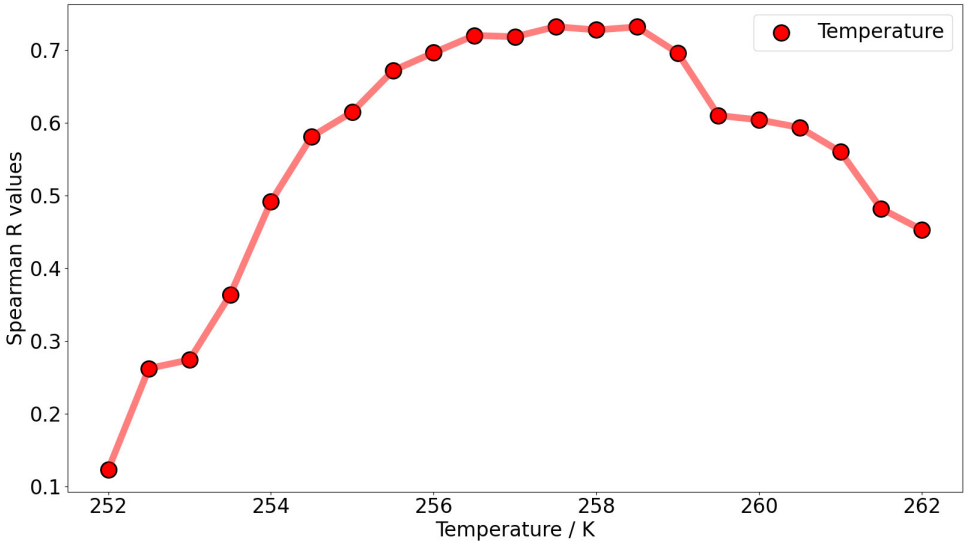

Figure 4.23.: Spearman correlation coefficient R between INSEKT INP measurements (PINE container, non-heated, whole campaign period) and the ambient temperature.

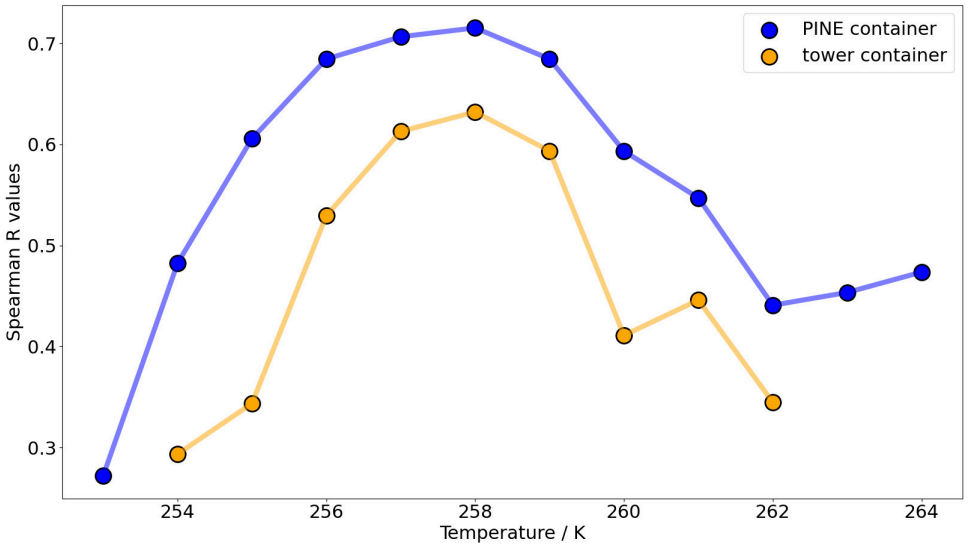

Figure 4.24.: Spearman correlation coefficient R between INSEKT INP measurements (non-heated, whole campaign period) and the ambient temperature. The blue graph shows the correlation for the PINE container measurements, the yellow graph shows the correlation for the tower container measurements.

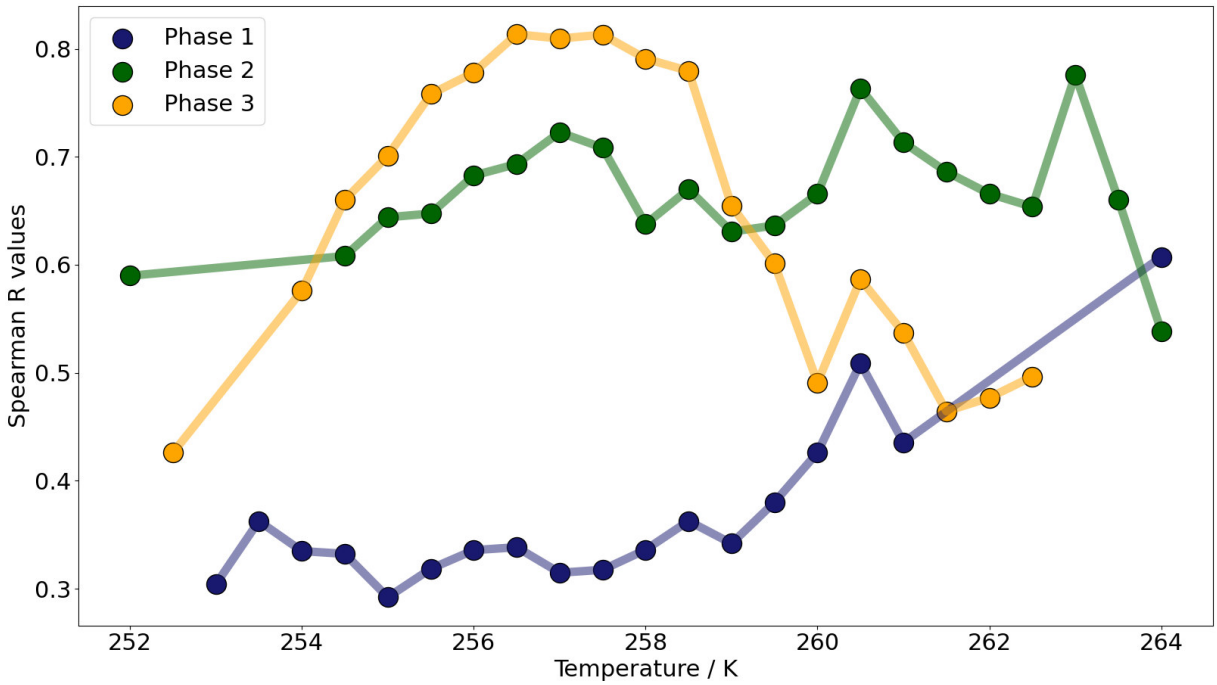

Figure 4.25.: Correlation coefficient between INSEKT measurements and the ambient temperature at each phase. The graph shows the Spearman correlation coefficient R of INP concentration (non-heated) measured in the PINE container and ambient temperature at 1.5 m above ground for the first phase (blue), second phase (green) and third phase (yellow).

4.1.7. Comparison to parametrization

A parametrization describing the INP concentration in the boreal forest was proposed in Schneider et al. 2021. The predicted INP concentrations, at ice active temperature T, $c_{\mathrm{INP}}(T)$ are calculated using the ambient temperature T_{amb} as follows:

$$c_{\mathrm{INP}}(T) = 0.1 \times exp(a_1 \times T_{\mathrm{ab}} - a_2) \times exp(b_1 \times T - b_2), \tag{4.1}$$

with $a_1 = 0.074 \pm 0.006\,\mathrm{K}^{-1}$, a_2 = -18 ± 2, b_1 = -0.504 ± 0.005 K^{-1} and $b_2 = 127 \pm 1$. A comparison of the predicted INP concentrations $c_{\mathrm{INP,pred}}$ and the measured INP concentrations $c_{\mathrm{INP,obs}}$, during this campaign, is shown in figure 4.26 for daily mean values of PINE measurements and in figure 4.27 for INSEKT measurements. The comparison of predicted INP concentrations show a good agreement with the measurements using INSEKT. The comparison to PINE measurements show only few deviations.

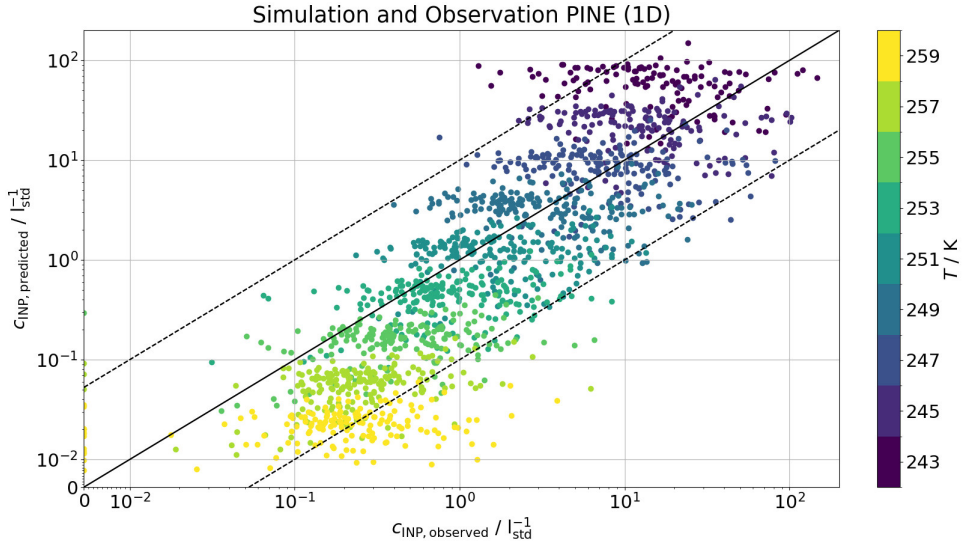

Figure 4.26.: Comparison of the daily mean INP concentrations $c_{\mathrm{INP,obs}}$ measured with the PINE instrument and predicted concentrations $c_{\mathrm{INP,pred}}$ using the parametrization proposed in Schneider et al. 2021.

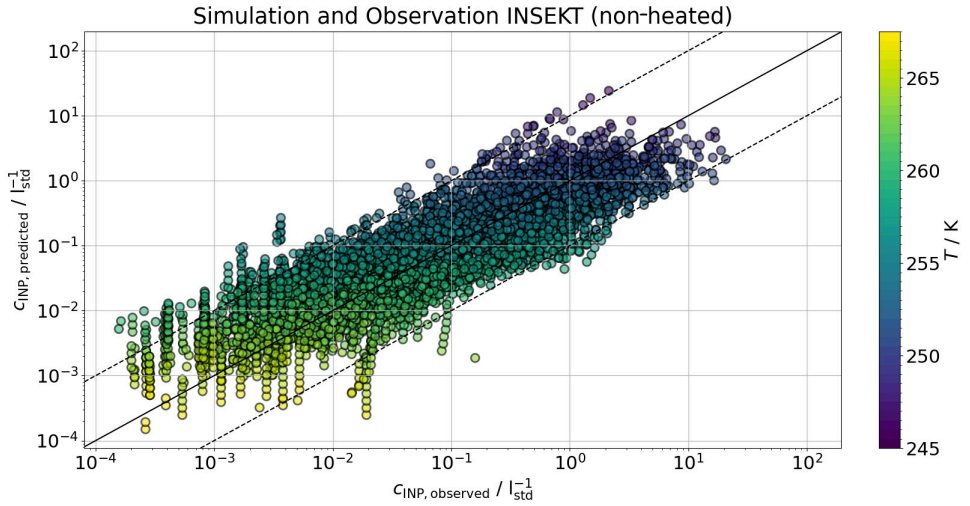

Figure 4.27.: Comparison of INP concentrations $c_{\mathrm{INP,obs}}$ measured with INSEKT and predicted concentrations $c_{\mathrm{INP,pred}}$ using the parametrization proposed in Schneider et al. 2021.

4.2. Case Study for the week from April 18th to 25th, 2024

In this chapter, a period of 8 days from April 18th to 25th, 2024, is discussed in more detail. INP measurements with PINE and INSEKT were compared to short term changes in aerosol parameters and meteorological conditions. INSEKT measurements were obtained for 10 to 24 h periods. These allow insight into the changes from day to day. The PINE instrument was operated at constant temperatures of 249 K or 250 K during some periods, and with temperature ramps from 257 K to 242 K in between. Figure 4.28 shows a time series of the PINE measurements at 249 K and 250 K compared with snow depth and temperature measured at 1.5 m above ground. The INP measurements were calculated using a running mean over a 1 h period. The ambient temperature and snow depth in this figure are depicted as 1 min mean values.
Figure4.1.4 shows an overview of the meteorological changes during the 8-day period in the same way as for monthly graphs. INP concentrations measured with INSEKT for heated (circles) and non-heated (triangles) aerosol samples at temperatures of 254 K and 257 K are shown in the top panel. A 1 h running mean was applied to the meteorological data (except precipitation). The APS data was averaged with a running mean of 1 h. The INP concentrations at 257 K measured with INSEKT were in the range from 10^{-3} $stdl^{-1}$ to 10^{-2} $stdl^{-1}$ until April 24th, then increased to values around 10^{-1} $stdl^{-1}$. The INP concentrations at 254 K showed some variation before 24th but then also steadily increased to about 10^{1}.
The INP concentrations were observed to correlate with temperature and the presence of snow. INP concentrations increased with increasing temperature, in particular during phases where the snow depth decreased. The INP concentrations then also decreased with decreasing temperature. During the period under discussion here, this happened mostly in the evening hours, and at the same time precipitation in the form of snow was observed. A peak in INP concentrations on April 19th could be connected to a local source of particles.
Following the overview given in the previous paragraphs, several graphs are now shown comparing the changes in INP concentration with various other data. These include the air temperature and the snow depth, aerosol concentrations from APS measurements, as well as biological particles measured with WIBS. The INP measurements and aerosol concentrations were calculated using a running mean over a 1 h period. The ambient temperature and snow depth in this figure are depicted as 1 min mean values.

April 18th (fig. 4.30): During this day, the INP concentrations at 249 K increased from around 1 to roughly 3 $stdl^{-1}$. The ambient temperature first increased from about −3 °C to 3 °C, then decreased again to about −3 °C, while INP concentration stayed almost constant. The snow depth was observed to decrease and was observed to be zero after 10:30 (UTC+3). However, pictures from a webcam show snow inside the forest area (see fig. 4.31). The INP concentrations at 249 K decreased to 1 $stdl^{-1}$ during the night. The air temperature was observed to decrease and the snow coverage increased during the night.

April 19th (fig. 4.32): The INP concentrations on this day followed a similar trend as on the day before, while the temperatures stayed below 0 °C and the snow cover decreased to zero by 11:00 (UTC+3). The INP concentrations at 249 K increased by a factor of 10^{1} for around one hour at around 14:00 (UTC+3). Figure 4.36 shows the INP measurements on 19th in comparison to APS measurements of the same day. An increase in the particle concentration of particles larger than 0.5 µm (blue line) occurred shortly before the peak in the INP concentrations, while the concentration measured for particles larger than 2.5 µm (black line) showed almost no increase. The sudden increase of the aerosol could be traced back to a

local source of dust due to other observations. Figure 4.34, panel (a) shows a picture of a close by road covered in grit on April 13th. On the 19th, the grit was removed, panel (b) shows the road on the evening of this day. The removal process involves use of heavy machinery (panel (c)), which produced large dust clouds at the dry conditions. Panel (d) shows a map with the location of the street close (<500 m) to the PINE container. The overview for the week revealed relative humidity at around 60% at the time of the peak in INP. The INP concentrations were observed to decrease during the evening hours, while the air temperature decreased and the snow cover started to increase.

April 20th (fig. 4.35): The PINE instrument was disconnected for routing cleaning and background procedures during late night to morning of this day, so that the measurements only started around midday. The INP concentrations at lower temperatures were observed to have increased when measurements were restarted. The air temperature stayed below 0 °C, but increased slightly until 13:00 (UTC+3). The INP concentrations decreased starting from 10:00 (UTC+3) over the rest of the day. The snow cover increased between 08:00 (UTC+3) and 10:00 (UTC+3) from around 4 to around 7 cm, with further increasing to about 8 cm until the evening. The precipitation on this day could not be observed to influence PINE INP measurements. It should be noted, however, that the highest intensity precipitation happened during the cleaning of the PINE instrument. The INP concentration at 257 K measured with INSEKT (see fig. 4.29) on this day, was observed to be 10^{-3} lower compared to the last analyzed sample on 16th April (see fig. 4.21), while the INP concentration at 254 K showed no obvious change.

April 21st (fig. 4.37): During this day, an increase of the INP concentrations was observed along with increasing ambient temperatures in the morning. The INP concentrations then levelled off during a period of increasing temperature and decreasing snow depth from 07:00 to 12:00 (UTC+3). Measurements with the APS (fig. 4.38) showed changes in the particle concentration, which are aligned quite well with the changes of the INP concentration. The concentration of particles larger than 0.5 µm varied only slightly during the whole day, while the concentration of particles larger than 2.5 µm showed an increase with the increasing INP concentration from around 1.5×10^{-2} on 07:00 (UTC +3) to 5×10^{-2} cm^{-1} on 11:00 (UTC +3). The INP concentrations increased from around 1.5 to 6 $stdl^{-1}$ during this period. This may indicate that the INP concentration was more influenced by larger aerosol particles on this day.
The WIBS data of this day shows an increase in fluorescing particles (fig. 4.39), in parallel to increasing INP concentrations. While the INP concentrations decreased, concentration of fluorescing particles stayed level. A further in-depth look at different categories of fluorescing particles (see section 2.2, Savage et al. 2017) reveals a good correlation between INP concentrations and particles of category A on this day (fig. 4.40). The concentrations of fluorescing particles (A, B) are similar to the INP concentrations. A comparison of the concentrations of particles larger than 0.5 µm measured with APS and WIBS shows that WIBS measures a factor of 10^1 lower particles, probably because the WIBS has a higher detection threshold for the particle diameter. The INP concentrations decreased during the evening with decreasing ambient temperature during the night.

April 22nd (fig. 4.41): The INP concentration at 249 K on this day followed the trend of the ambient temperature. From 03:00 (UTC+3) to 12:00 (UTC+3), the INP concentration measured at 249 K increased from around 0.1 to around 20 $stdl^{-1}$. The ambient air temperature increased from 03:00 (UTC+3) to 11:00 (UTC+3) from around −9 to 1 °C. The increase in

INP concentration showed a more rapid development (0.5 $stdl^{-1}$ to 2 $stdl^{-1}$) during a period of decreasing snow depth between 12:00 (UTC +3) and 15:00 (UTC +3). Until the evening, the INP concentration dropped with decreasing ambient temperature from 2 $stdl^{-1}$ to about 0.2 $stdl^{-1}$. Particle concentrations measured with APS (fig. 4.42) showed no change until the evening and seem to be not connected to the changes in INP concentration during this day. The same was observed for fluorescing particles measured with the WIBS (fig. 4.43) in the PINE container. The pictures in figure 4.44 show the absence of snow on the tree crowns during the measurements on 22nd April.

April 23rd (fig. 4.45): During this day, INP measurements showed a similar trend as during the 20th April, with a slight increase until midday and a decrease for the rest of the day. The ambient air temperature stayed below 0 °C, but increased during the day. The snow depth increased over the whole day with an almost constant rate. The particle concentrations were observed to decrease over the whole day (see fig. 4.46).

April 24th (fig. 4.47): The INP concentrations at 251 K on this day were observed to increase from 0.1 $stdl^{-1}$ at 09:00 (UTC +3) to 2 $stdl^{-1}$ at 12:00 (UTC+3) and decreasing to 1 $stdl^{-1}$ by 14:00 (UTC +3). The next measurement at 21:00 (UTC+3) showed no major change in the INP concentrations. A temperature scan during the afternoon revealed an increase in INP concentrations at high temperatures during this time, INP concentrations at 257 K increased from around 3×10^{-1} to 10^{1} $stdl^{-1}$ (see fig. 4.21). The INSEKT measurements of this day revealed an increase by almost 10^{2} in the concentrations at 257 K (from around2×10^{-3} to roughly 1×10^{-1} $stdl^{-1}$) comparing the day before and this day, while INP concentrations at 254 K increased by about 10^{1} (from around 8×10^{-2} to roughly 1 $stdl^{-1}$). This coincides with the increased INP concentrations measured with PINE. Measurements of particle concentrations with the APS (fig. 4.48) showed increases over the day, but these were apparently not strongly correlated with the changes in INPs. WIBS measurements (fig. 4.49) showed an increase in fluorescing particles along with the increase in the INP concentration. In particular, the particles categorized as ABC particles (fig. 4.50) showed an increase (by a factor of 10^{1}) and decrease with the decrease in measured INP concentrations. The shown concentrations of fluorescing particles are by a factor of 10^{1} lower than the observed INP concentrations. The INP concentration was observed to decrease during the evening, while WIBS measurements showed no change. The pictures in figure 4.51 show the presence of snow on the tree crowns during measurements on 24th April. The snow on the crowns reduced over the day.

April 25th (fig. 4.52): The INP concentrations at 251 K on this day was observed to stay close to the level reached during the night (around 0.7 $stdl^{-1}$). In the evening, a decrease of the INP concentration by a factor of 10^{1} was observed. On this day, the changes in temperature seem to not strongly affect the INP concentration. Measurements of particle concentrations (fig. 4.53) show constant concentration of particles larger than 2.5 µm during the time of constant INP concentrations, then also decrease at the same time as the INP concentrations. Measurements of fluorescing particles (fig. 4.54) reveal constant concentration of particles of category ABC during the time of level INP concentrations, which decrease at the same time as INP concentrations.

Figure 4.55 includes trajectories calculated with the HYSPLIT (Hybrid Single-Particle Lagrangian Integrated Trajectory) model (Stein et al. 2015). The trajectories show no major

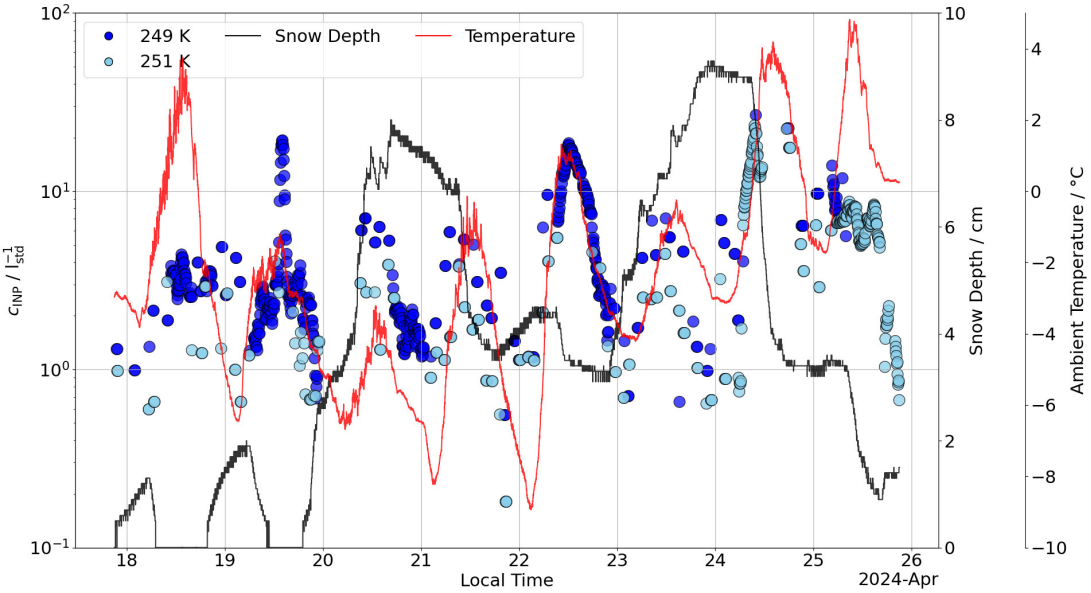

Figure 4.28.: Data time series for the 8-day period April 8th to 25th, 2024. Shown are the INP concentrations measured with PINE at temperatures of 249 K (blue circles) and 251 K (skyblue circles), the air temperature measured at 1.5 m above ground (red line) and the snow depth (black line).

change in air mass origin during the measurements until 24th April, a change of air mass origin happens on 25th.

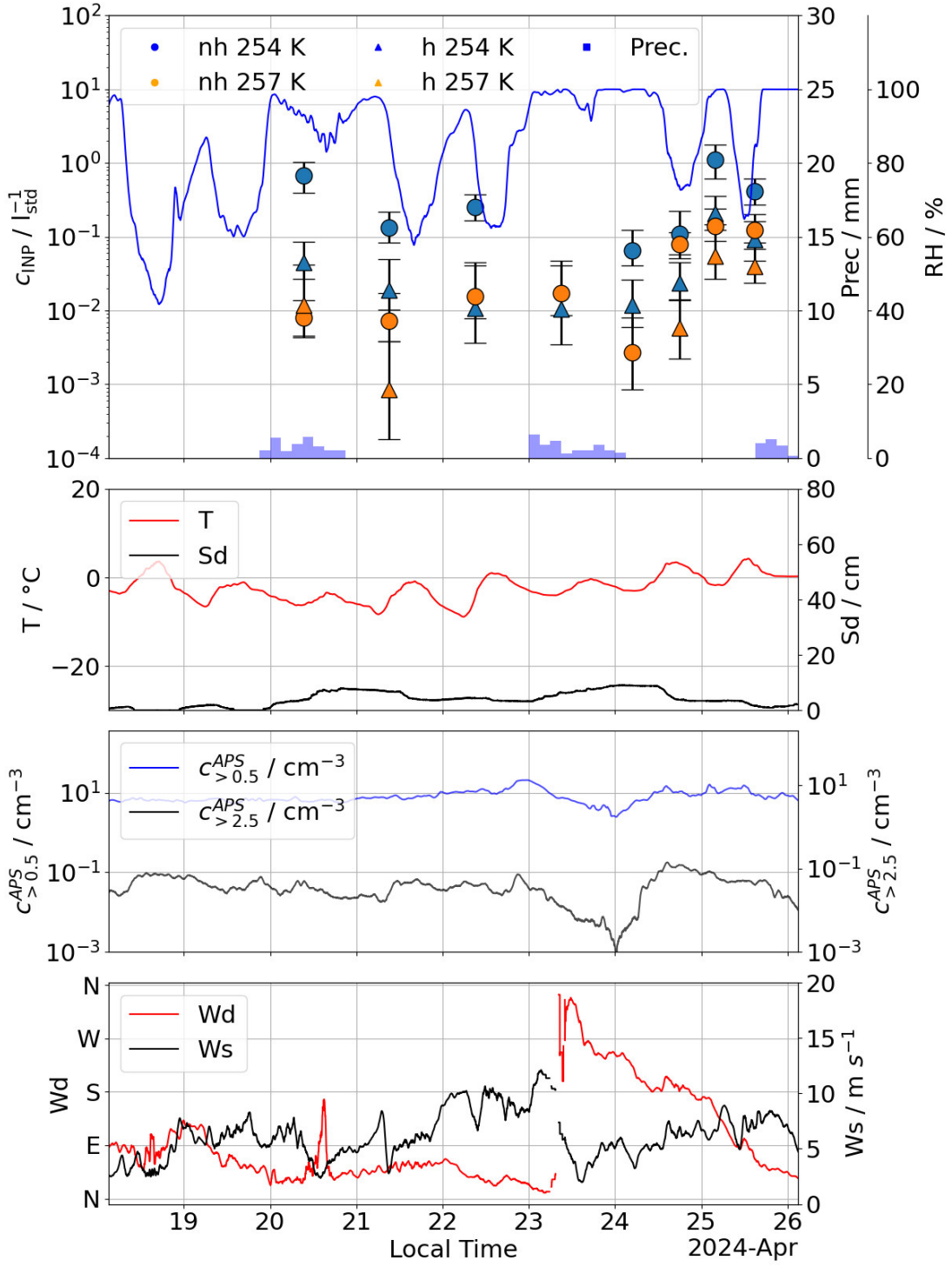

Figure 4.29.: Data time series for the 8-day period April 8th to 25th, 2024. The top panel shows INP concentrations measured with INSEKT in the PINE container and analyzed without heat treatment (nh, circles) and with heat treatment (h, triangles), and for temperatures of 254 K (blue) and 257 K (orange). The top panel also shows the 6 h accumulative precipitation (light blue areas) and the ambient relative humidity (blue line). The second panel shows the one-day running mean of the air temperature (red line) and snow depth (black line). The third panel shows the number concentrations for particles with diameters larger than 0.5 µm (blue line) and larger than 2.5 µm (black line) measured by the APS in the PINE container. The bottom panel shows the direction (Wd, red line) and speed (Ws, black line) of the horizontal wind.

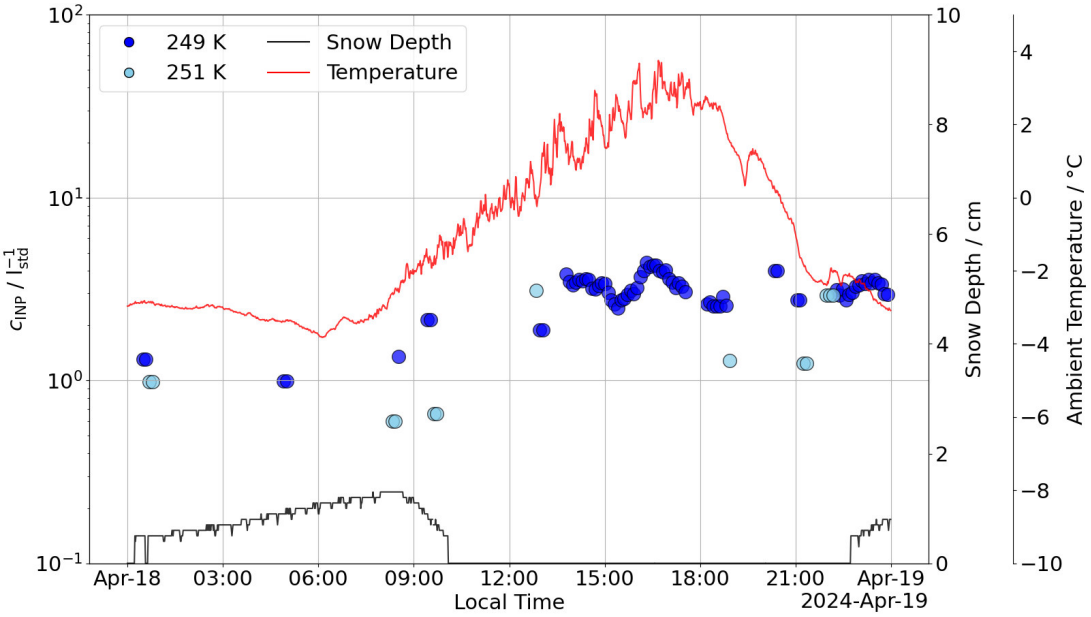

Figure 4.30.: Data time series for April 18th, 2024. The graph shows the 1 h running mean of INP concentrations measured with PINE at temperatures of 249 K (blue circles) and 251 K (skyblue circles), the ambient air temperature measured at 1.5 m above ground (red line) and the snow depth (black line).

(a)

(b)

Figure 4.31.: Change of the snow coverage in the forest on April 18th, 2024. The left picture (a) shows the snow cover on 10:01 (UTC +3). The right picture (b) shows the same location on 14:31 (UTC +3).

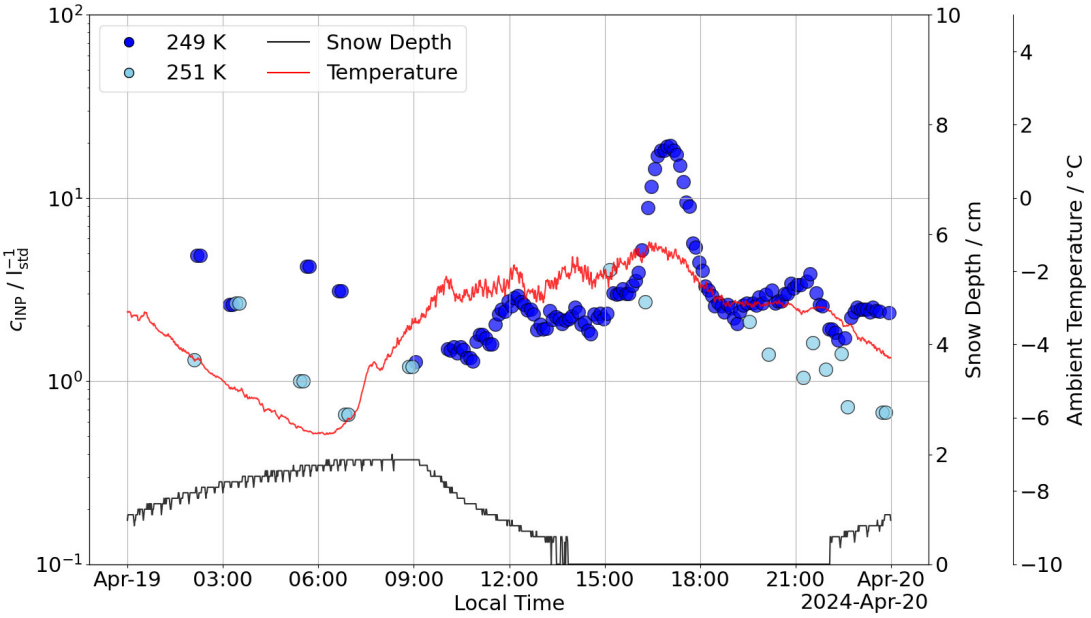

Figure 4.32.: Data time series for April 19th, 2024. The graph shows the 1 h running mean of INP concentrations measured with PINE at temperatures of 249 K (blue circles) and 251 K (skyblue circles), the ambient air temperature measured at 1.5 m above ground (red line) and the snow depth (black line).

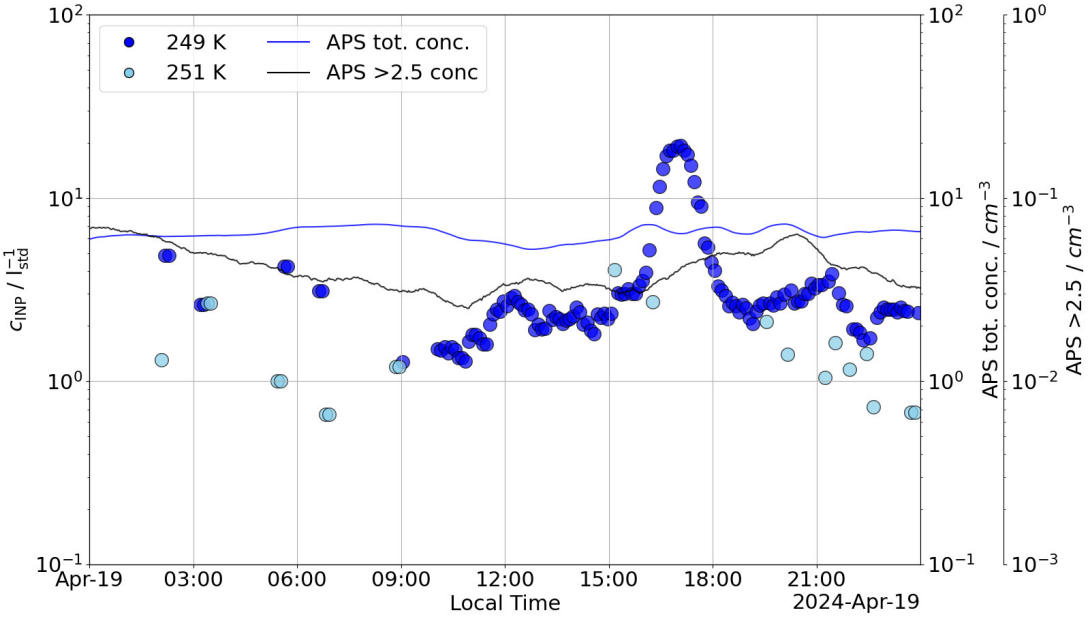

Figure 4.33.: Data time series for April 19th, 2024. The graph shows the 1 h running mean of INP concentrations measured with PINE at temperatures of 249 K (blue circles) and 251 K (skyblue circles), and the number concentrations for particles with diameters larger than 0.5 µm (blue line) and larger than 2.5 µm (black line) measured by the APS in the PINE container. The APS measurements are averaged with a 1 h running mean.

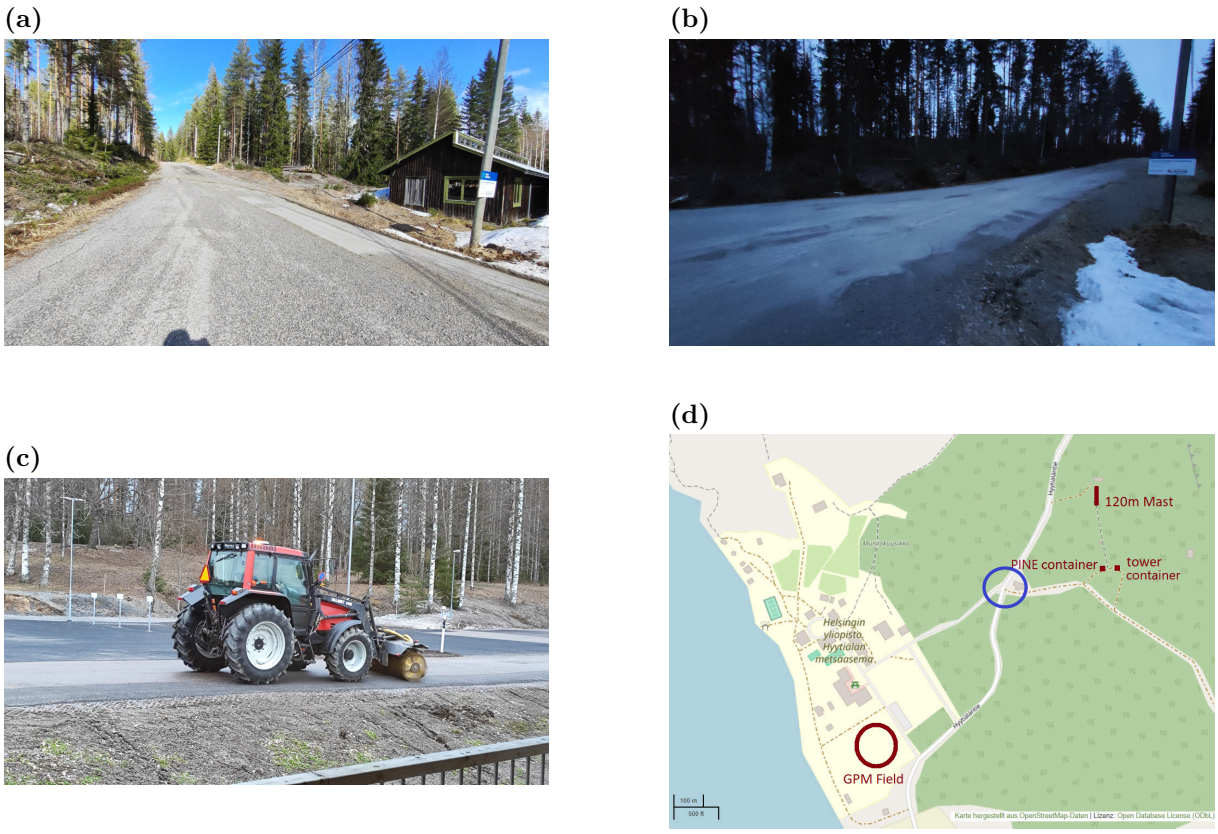

Figure 4.34.: Photos from road construction work causing a local dust source during April 19th, 2024. The picture in panel (a) shows the road covered with grit on April 13th. The picture in panel (b) shows the same road after grid removal in the evening of April 19th. The picture in panel (c) shows the machinery used for the removal of grit. The map (OpenStreetMap contributors 2017) in panel (d) shows the location of the street in (a) and (b) relative to the measurement locations.

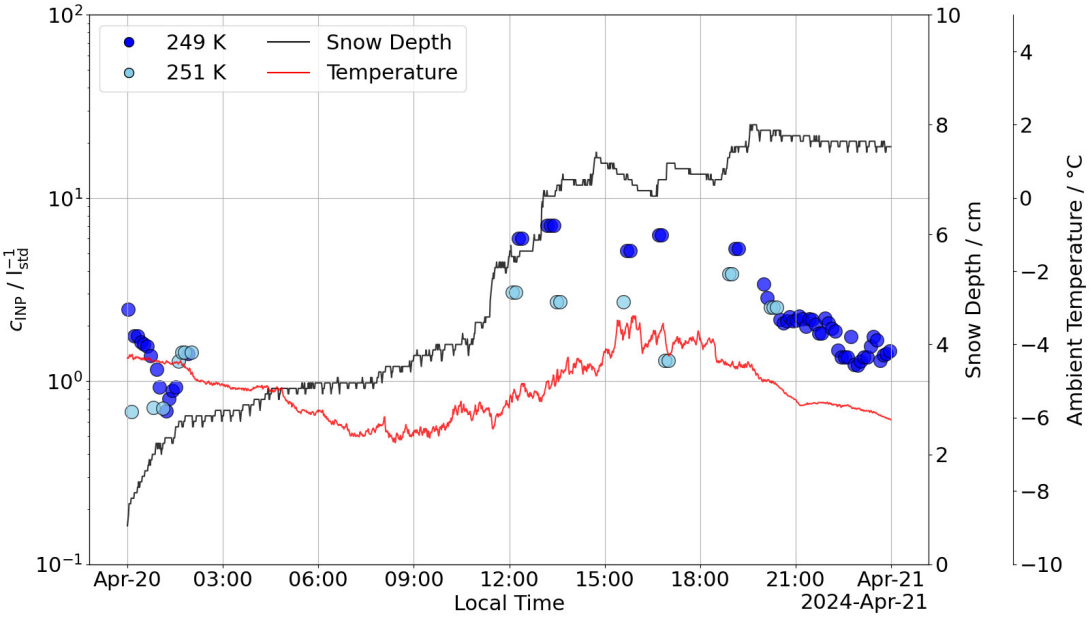

Figure 4.35.: Data time series for April 20th, 2024. The graph shows the 1 h running mean of INP concentrations measured with PINE at temperatures of 249 K (blue circles) and 251 K (skyblue circles), the ambient air temperature measured at 1.5 m above ground (red line) and the snow depth (black line).

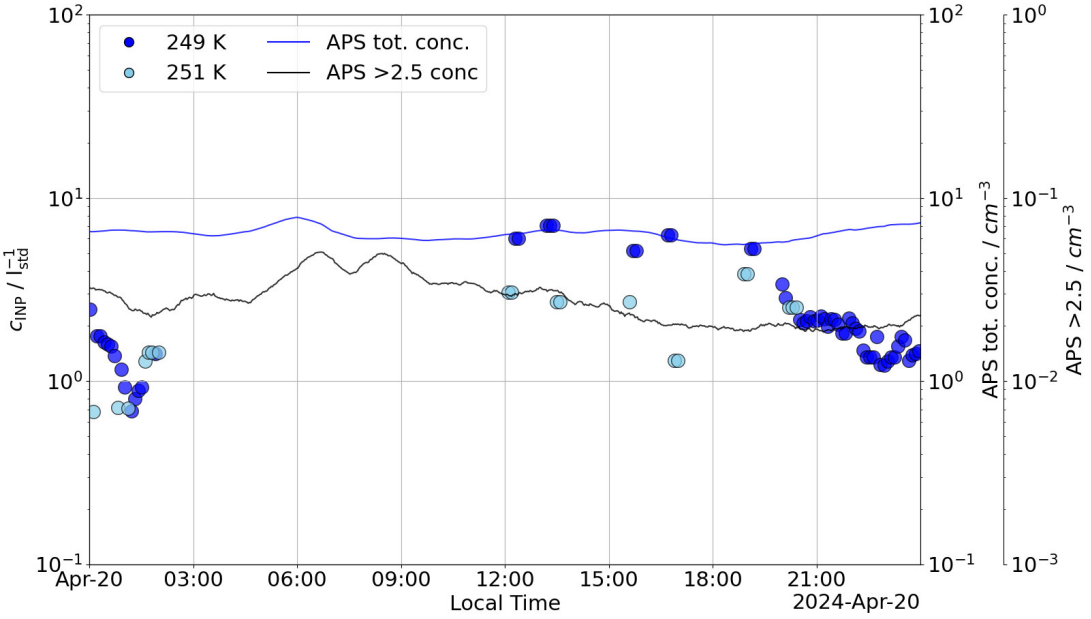

Figure 4.36.: Data time series for April 20th, 2024. The graph shows the 1 h running mean of INP concentrations measured with PINE at temperatures of 249 K (blue circles) and 251 K (skyblue circles), and the number concentrations for particles with diameters larger than 0.5 µm (blue line) and larger than 2.5 µm (black line) measured by the APS in the PINE container. The APS measurements are averaged with a 1 h running mean.

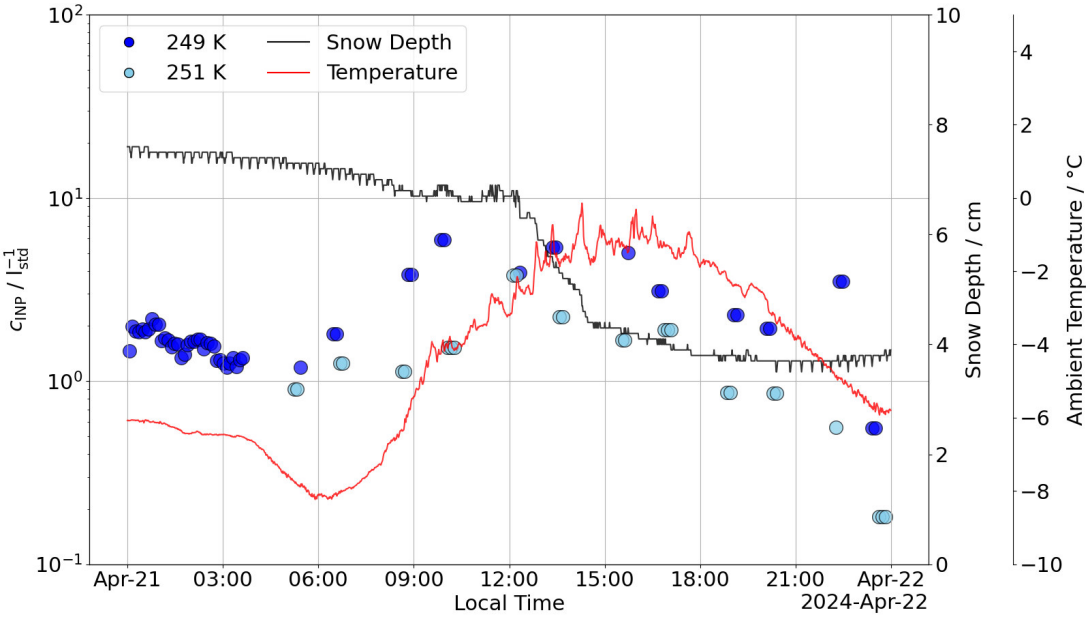

Figure 4.37.: Data time series for April 21st, 2024. The graph shows the 1 h running mean of INP concentrations measured with PINE at temperatures of 249 K (blue circles) and 251 K (skyblue circles), the ambient air temperature measured at 1.5 m above ground (red line) and the snow depth (black line).

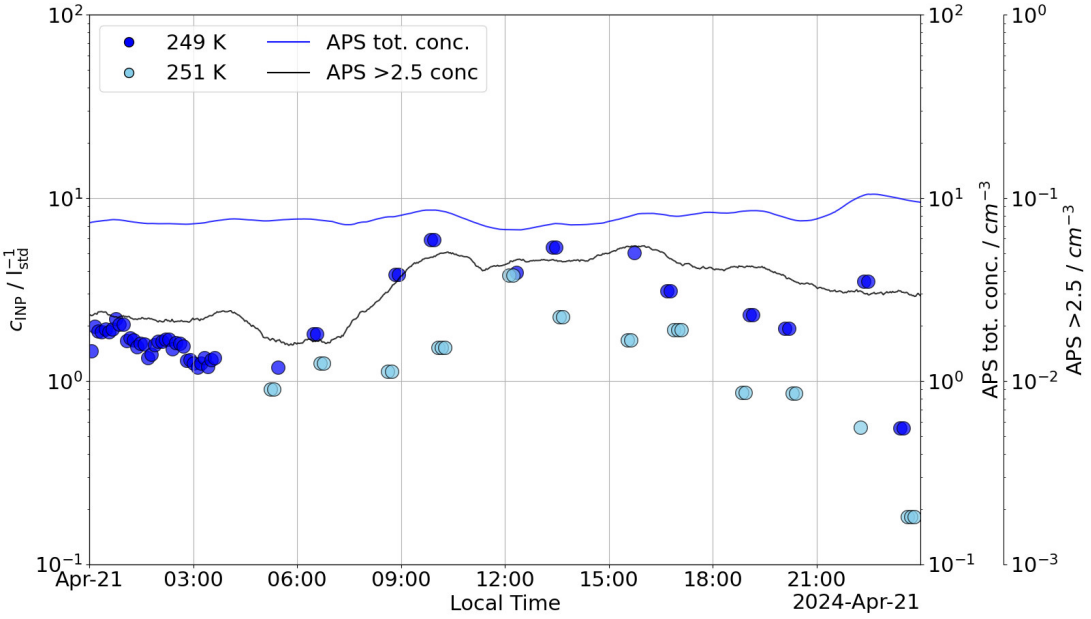

Figure 4.38.: Data time series for April 21st, 2024. The graph shows the 1 h running mean of INP concentrations measured with PINE at temperatures of 249 K (blue circles) and 251 K (skyblue circles), and the number concentrations for particles with diameters larger than 0.5 µm (blue line) and larger than 2.5 µm (black line) measured by the APS in the PINE container. The APS measurements are averaged with a 1 h running mean.

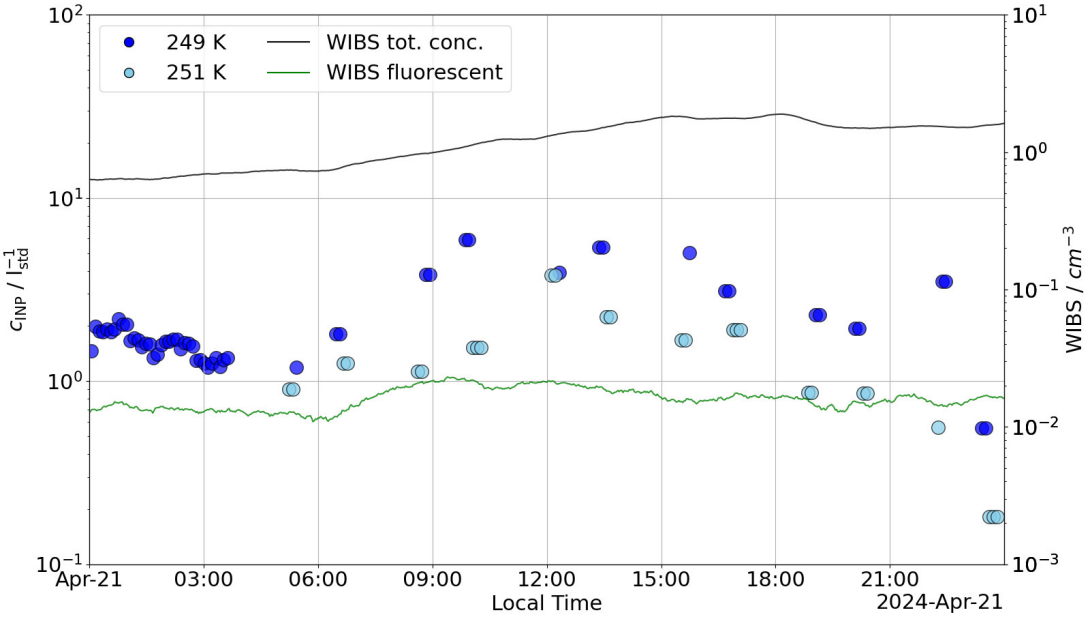

Figure 4.39.: Comparison of INP measurements with WIBS data on April 21st, 2024. The graph shows the 1 h running mean of INP concentrations measured with PINE at temperatures of 249 K (blue circles) and 251 K (skyblue circles), as well as the number concentration of all particles (back line) and fluorescing particles (green line) measured with the WIBS in the PINE container. The WIBS measurements are averaged with a 1 h running mean.

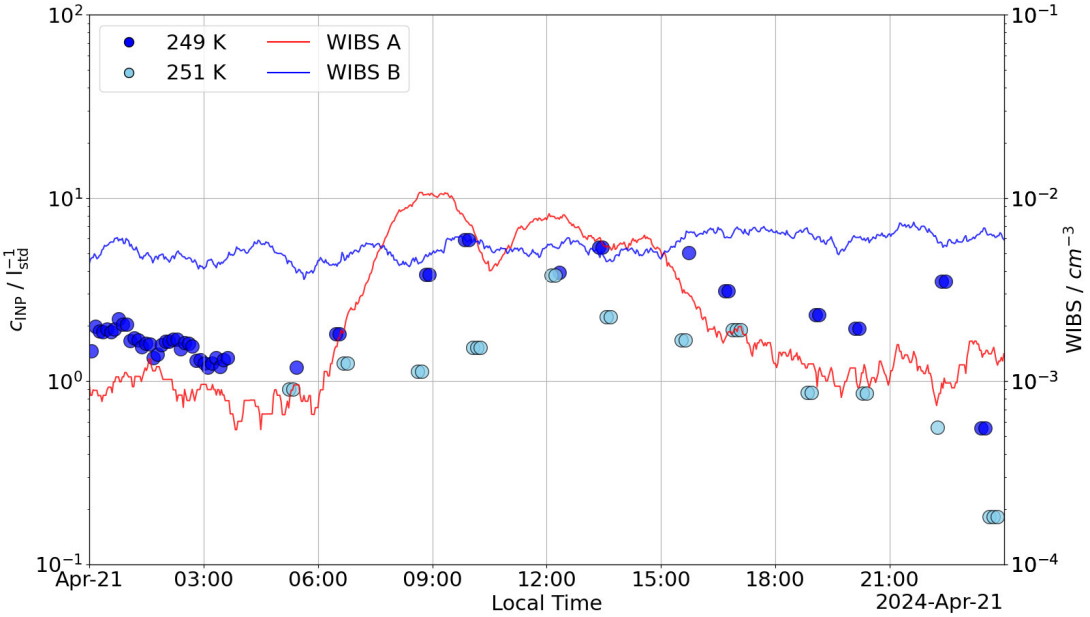

Figure 4.40.: Comparison of INP measurements to WIBS data on April 21st, 2024. The graph shows the 1 h running mean of INP concentrations measured with PINE at temperatures of 249 K (blue circles) and 251 K (skyblue circles), as well as number concentrations of fluorescent particles in categories A (red line) and B (blue line) measured with the WIBS in the PINE container. The WIBS measurements are calculated as 1 h running mean.

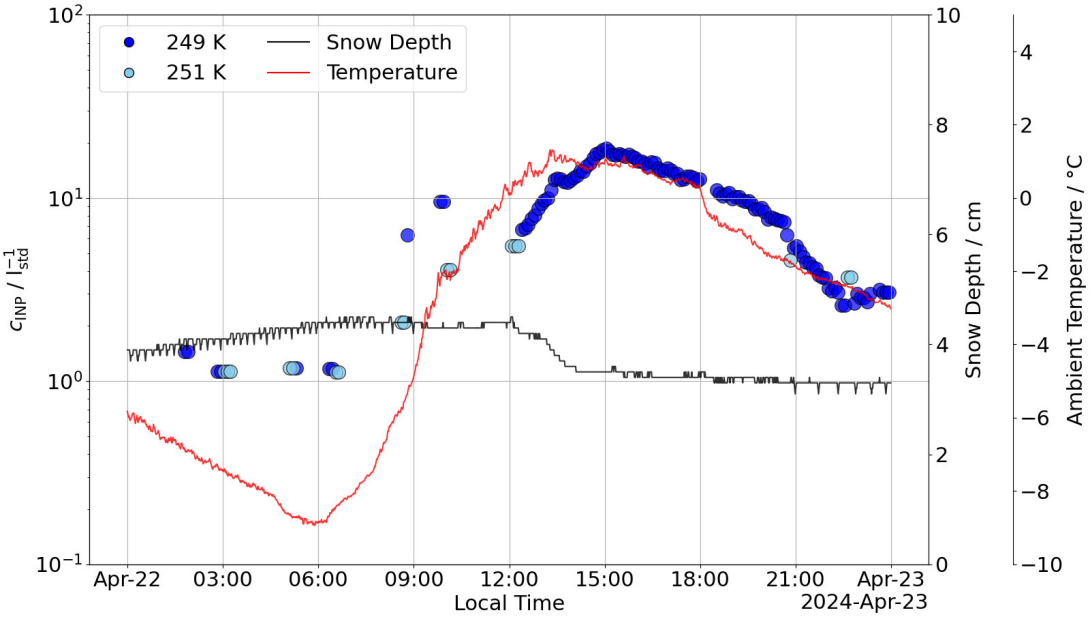

Figure 4.41.: Data time series for April 22nd, 2024. The graph shows the 1 h running mean of INP concentrations measured with PINE at temperatures of 249 K (blue circles) and 251 K (skyblue circles), the ambient air temperature measured at 1.5 m above ground (red line) and the snow depth (black line).

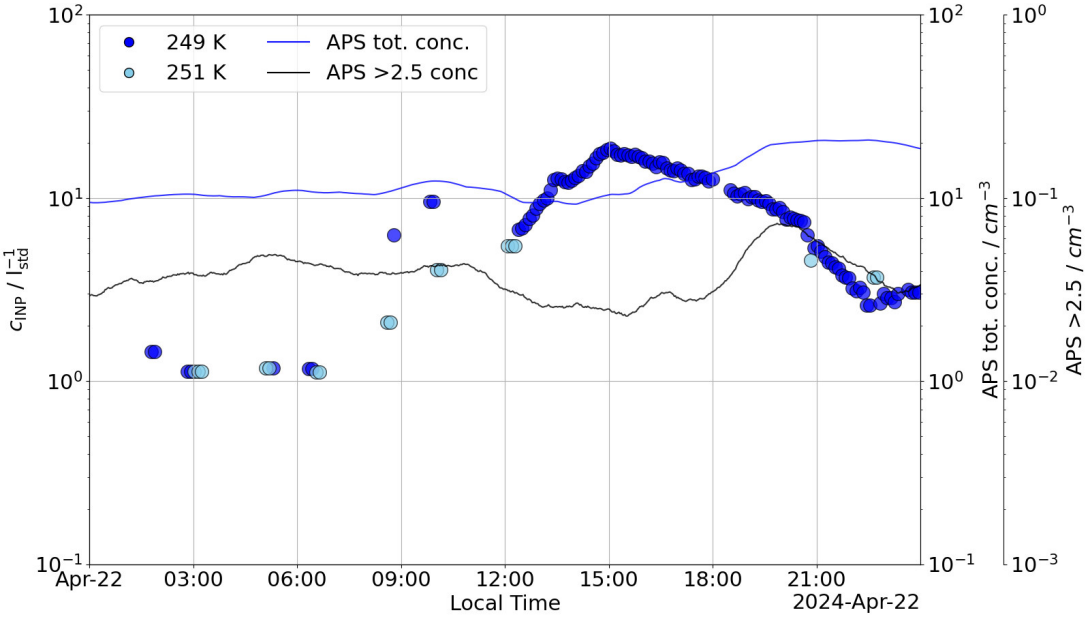

Figure 4.42.: Data time series for April 22nd, 2024. The graph shows the 1 h running mean of INP concentrations measured with PINE at temperatures of 249 K (blue circles) and 251 K (skyblue circles), and the number concentrations for particles with diameters larger than 0.5 µm (blue line) and larger than 2.5 µm (black line) measured by the APS in the PINE container. The APS measurements are averaged with a 1 h running mean.

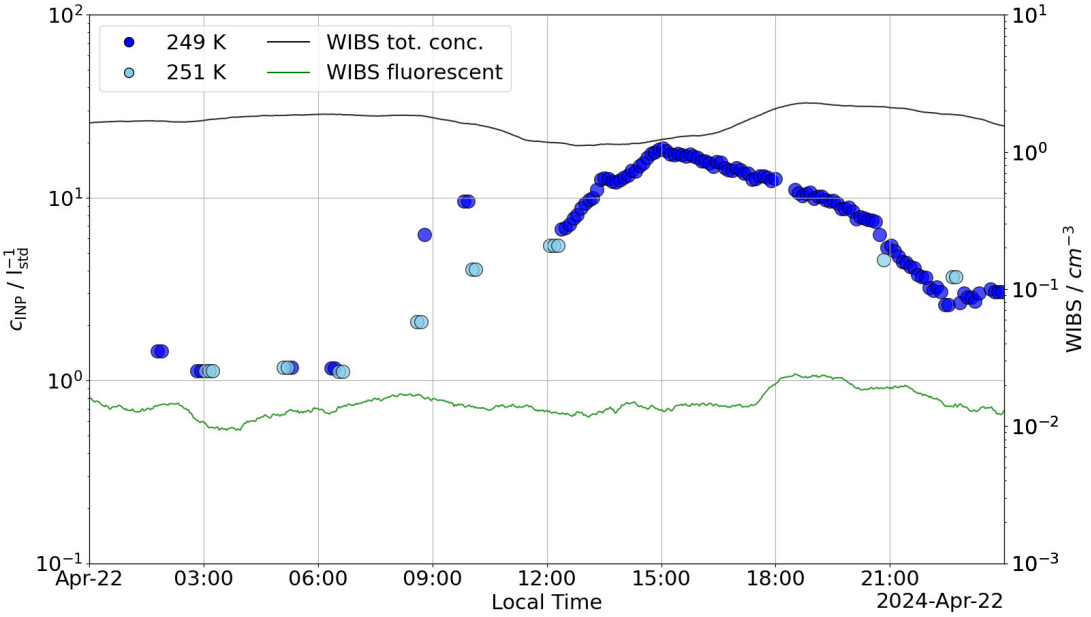

Figure 4.43.: Comparison of INP measurements with WIBS data on April 22nd, 2024. The graph shows the 1 h running mean of INP concentrations measured with PINE at temperatures of 249 K (blue circles) and 251 K (skyblue circles), as well as the number concentration of all particles (back line) and fluorescing particles (green line) measured with the WIBS in the PINE container. The WIBS measurements are averaged with a 1 h running mean.

(a)

(b)

Figure 4.44.: Development of snow coverage on tree crowns from April 21st to 22nd, 2024. The left picture (a) shows the tree crowns at 15:31 (UTC +3) on April 21st. The right picture (b) shows the tree crowns at 10:01 (UTC +3) on April 22nd.

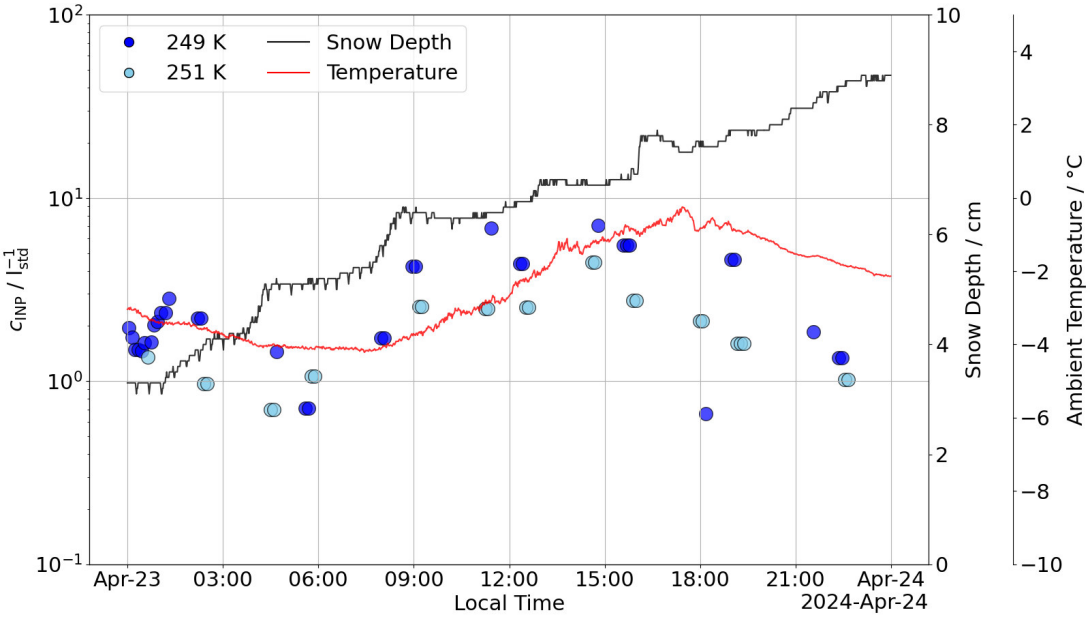

Figure 4.45.: Data time series for April 23rd, 2024. The graph shows the 1 h running mean of INP concentrations measured with PINE at temperatures of 249 K (blue circles) and 251 K (skyblue circles), the ambient air temperature measured at 1.5 m above ground (red line) and the snow depth (black line).

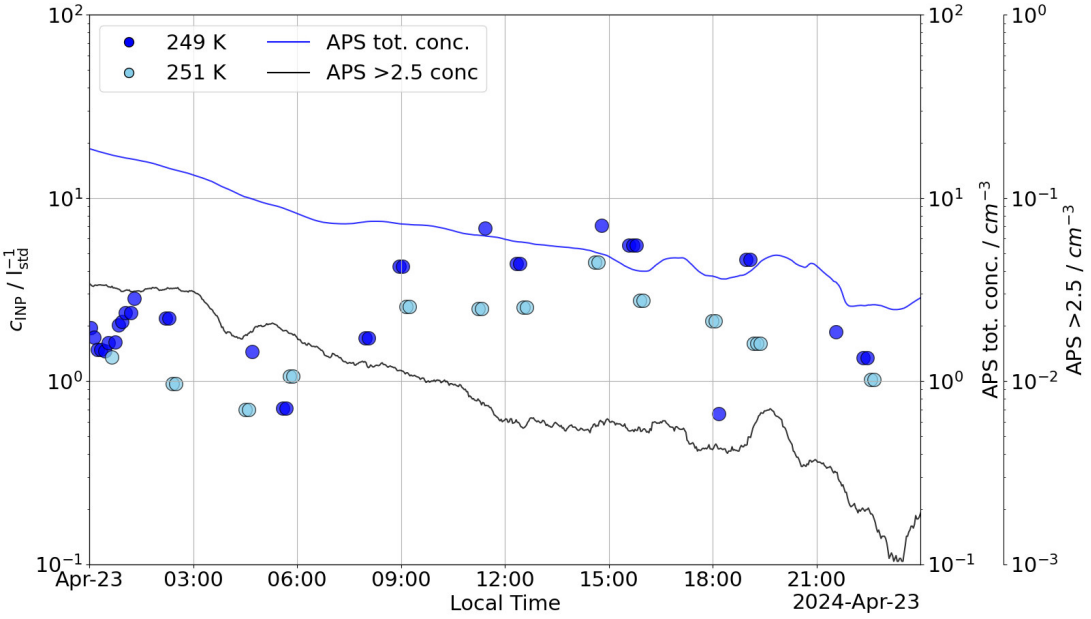

Figure 4.46.: Data time series for April 23rd, 2024. The graph shows the 1 h running mean of INP concentrations measured with PINE at temperatures of 249 K (blue circles) and 251 K (skyblue circles), and the number concentrations for particles with diameters larger than 0.5 µm (blue line) and larger than 2.5 µm (black line) measured by the APS in the PINE container. The APS measurements are averaged with a 1 h running mean.

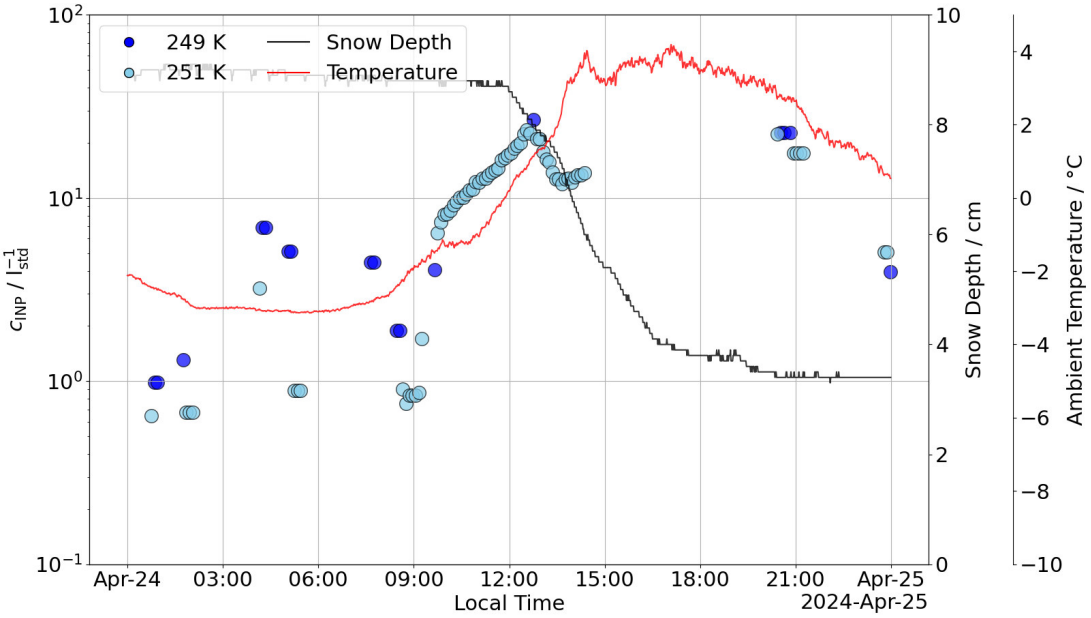

Figure 4.47.: Data time series for April 24th, 2024. The graph shows the 1 h running mean of INP concentrations measured with PINE at temperatures of 249 K (blue circles) and 251 K (skyblue circles), the ambient air temperature measured at 1.5 m above ground (red line) and the snow depth (black line).

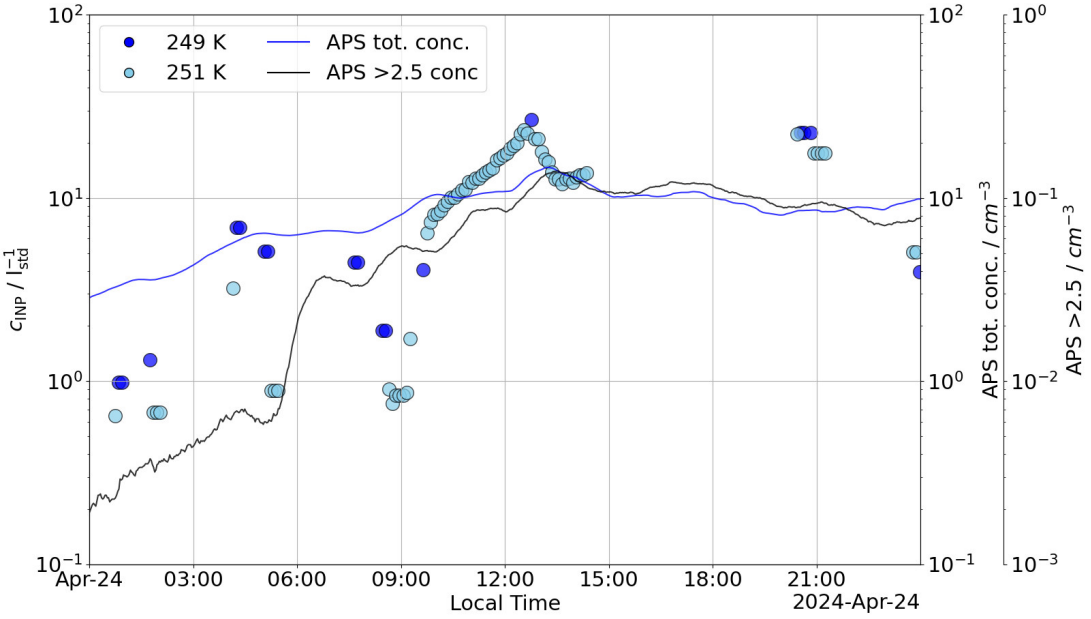

Figure 4.48.: Data time series for April 24th, 2024. The graph shows the 1 h running mean of INP concentrations measured with PINE at temperatures of 249 K (blue circles) and 251 K (skyblue circles), and the number concentrations for particles with diameters larger than 0.5 µm (blue line) and larger than 2.5 µm (black line) measured by the APS in the PINE container. The APS measurements are averaged with a 1 h running mean.

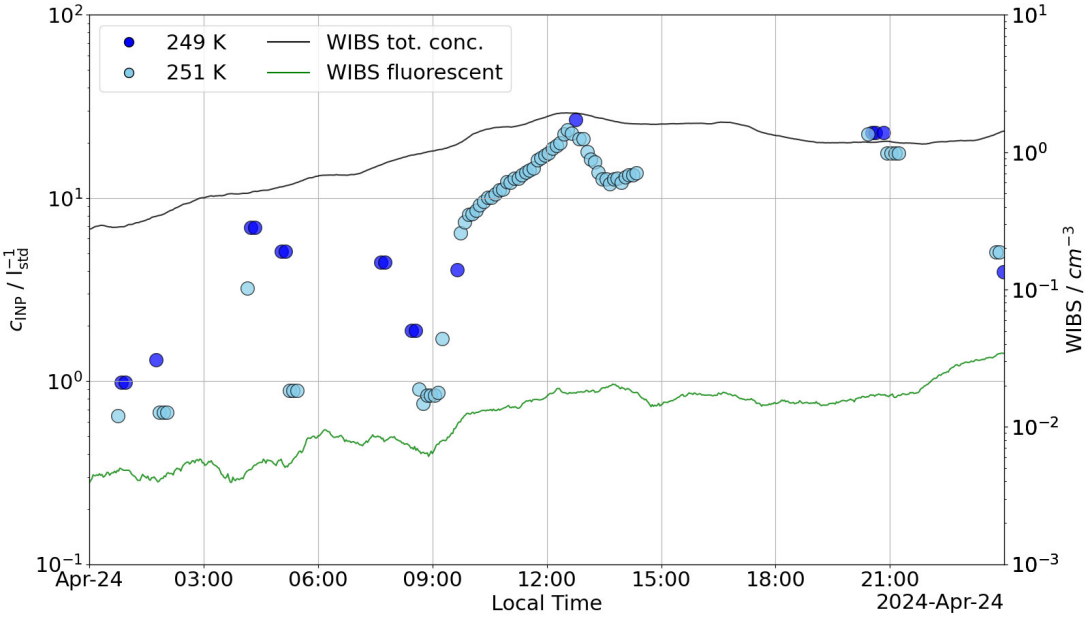

Figure 4.49.: Comparison of INP measurements with WIBS data on April 24th, 2024. The graph shows the 1 h running mean of INP concentrations measured with PINE at temperatures of 249 K (blue circles) and 251 K (skyblue circles), as well as the number concentration of all particles (back line) and fluorescing particles (green line) measured with the WIBS in the PINE container. The WIBS measurements are averaged with a 1 h running mean.

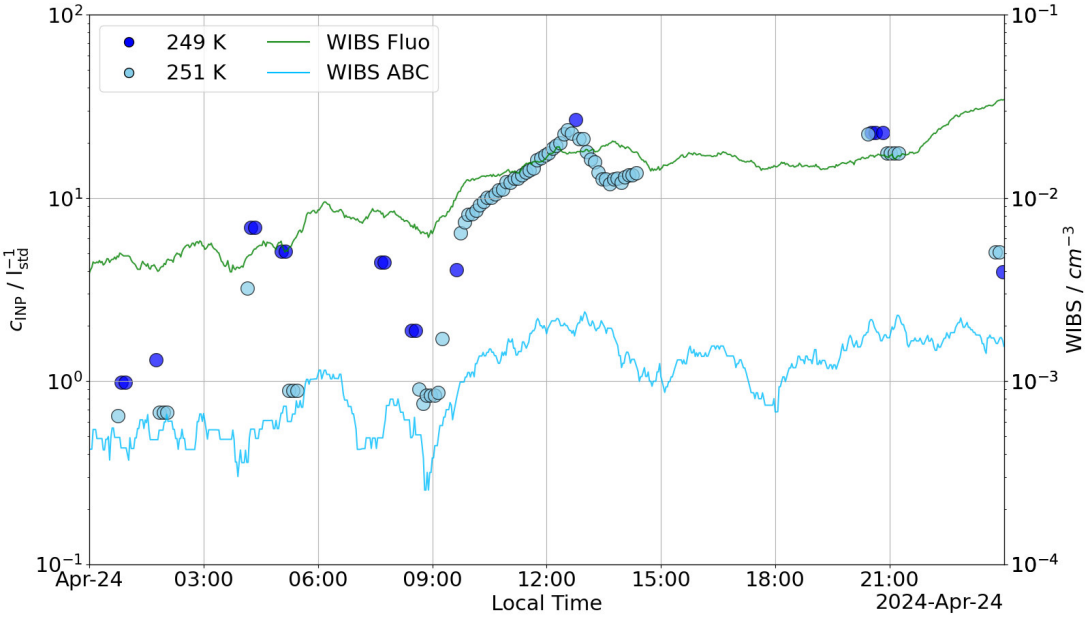

Figure 4.50.: Comparison of INP measurements to WIBS data on April 24th, 2024. The graph shows the 1 h running mean of INP concentrations measured with PINE at temperatures of 249 K (blue circles) and 251 K (skyblue circles), as well as number concentrations of fluorescent particles (green line) and particles in category ABC (sky blue line) measured with the WIBS in the PINE container. The WIBS measurements are calculated as 1 h running mean.

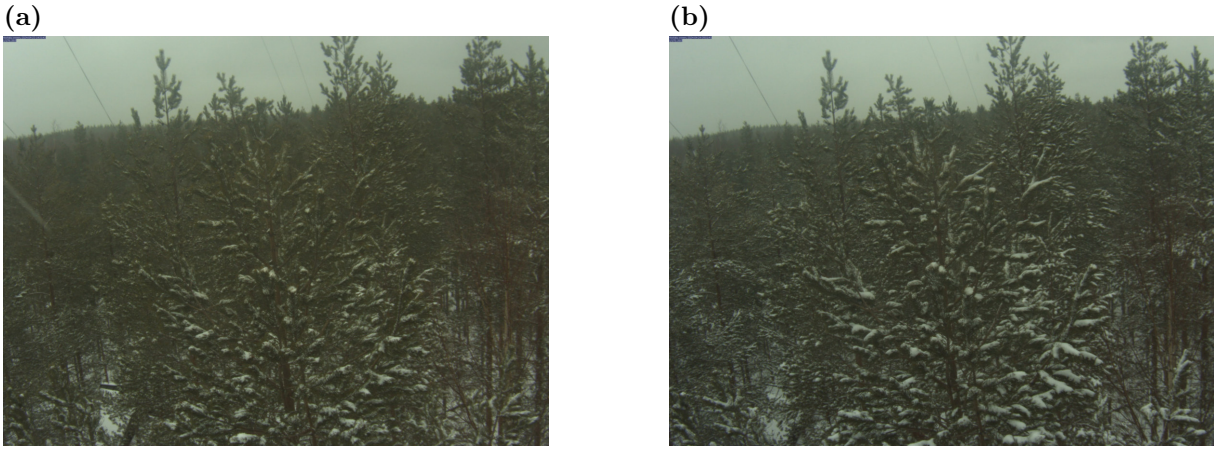

Figure 4.51.: Development of snow coverage on the tree crowns from April 23rd to 24th. The left picture (a) shows the tree crowns at 15:31 (UTC +3) on April 23rd. The right picture (b) shows the tree crowns at 10:01 (UTC +3) on April 24th.

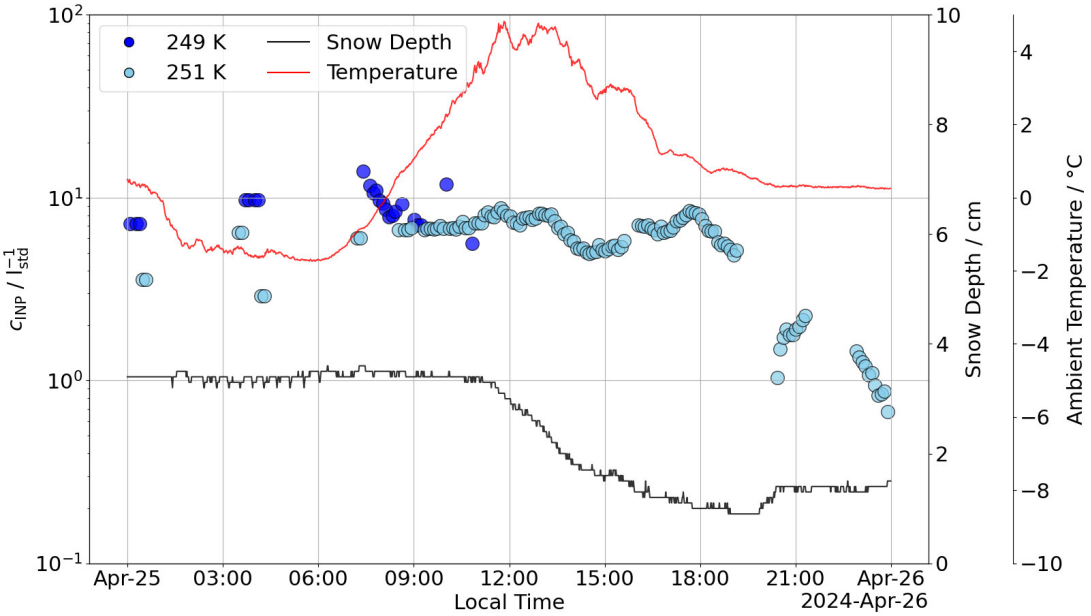

Figure 4.52.: Data time series for April 25th, 2024. The graph shows the 1 h running mean of INP concentrations measured with PINE at temperatures of 249 K (blue circles) and 251 K (skyblue circles), the ambient air temperature measured at 1.5 m above ground (red line) and the snow depth (black line).

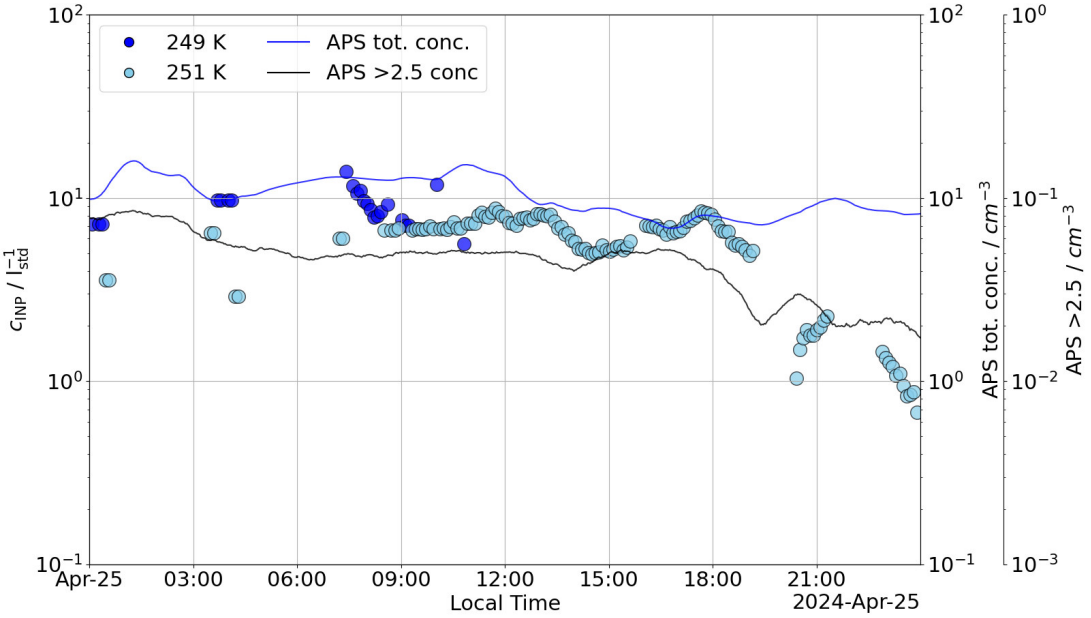

Figure 4.53.: Data time series for April 25th, 2024. The graph shows the 1 h running mean of INP concentrations measured with PINE at temperatures of 249 K (blue circles) and 251 K (skyblue circles), and the number concentrations for particles with diameters larger than 0.5 µm (blue line) and larger than 2.5 µm (black line) measured by the APS in the PINE container. The APS measurements are averaged with a 1 h running mean.

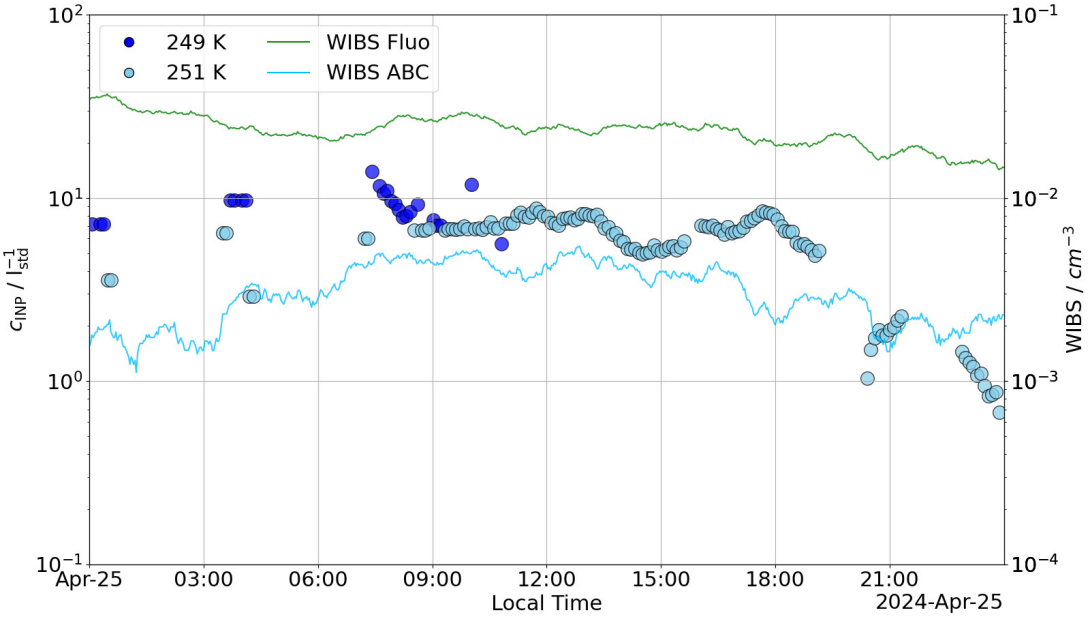

Figure 4.54.: Comparison of INP measurements to WIBS data on April 25th, 2024. The graph shows the 1 h running mean of INP concentrations measured with PINE at temperatures of 249 K (blue circles) and 251 K (skyblue circles), as well as number concentrations of fluorescent particles (green line) and particles in category ABC (sky blue line) measured with the WIBS in the PINE container. The WIBS measurements are calculated as 1 h running mean.

(a)

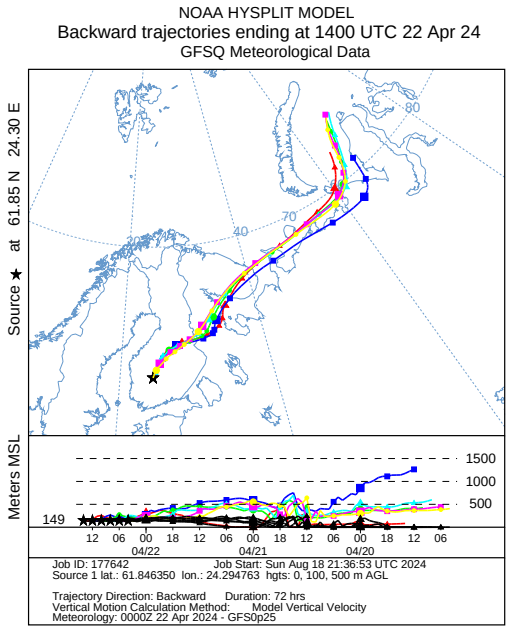

(b)

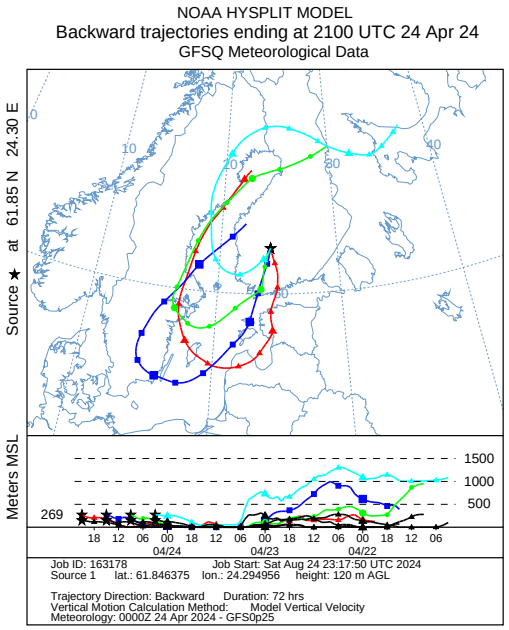

Figure 4.55.: Backwards trajectories calculated with the HYSPLIT (Hybrid Single-Particle Lagrangian Integrated Trajectory) model (Stein et al. 2015) for April 22nd and 24th, 2024. Every 6 h, one trajectory was calculated going 72 h back in time.

Chapter 5.

Summary and Outlook

5.1. Summary

The boreal forest is an important source of biogenic INPs (Schneider et al. 2021). Changes in both the INP emission rates, types and concentrations can vary depending on many different parameters. A seasonal cycle, especially for the INP concentrations at temperatures between 255 K and 259 K, linked to biogenic particles, was found during a year-long measurement in the HyICE-2018 campaign (Schneider et al. 2021). New parameterizations for this region were formulated, one of which is relating the INP concentrations to the ambient temperature (Schneider et al. 2021). INP measurements at lower temperatures suggested a dependence on biogenic aerosol sources as well (Vogel et al. 2024). Tree dwelling lichen, not covered in snow during winter, were found to be possible sources for INPs in this region (Proske et al. 2024). Further observations of the INP concentration, especially at high temporal resolution, were shown and discussed in this thesis.
The observations on INPs in the boreal forest of southern Finland were performed during the HyICE23 campaign (successor to HyICE-2018). The INP concentrations of INPs active between 242 K and 262 K were measured with the portable expansion chamber PINE at high temporal resolution (6 min). INPs active between above 248 K were measured by analyzing aerosol filter samples with INSEKT. The filter samples were taken in the PINE container and in a container on a 35 m high tower (Tower container) for time periods between 4 h and 4 days. The particle size distribution was measured using an APS in parallel to the PINE instrument and filter samples in the PINE container.
The PINE instrument was operated using different temperature settings at the begging of the campaign to get an overview of the ambient INP population. The instrument was operated alternatively for periods of constant temperature and a temperature ramps during winter time. The PINE instrument was then operated using different temperature settings, including more and longer periods of constant temperature and temperature ramps during spring, to observe the winter to spring transition in more detail.
During autumn 2023, the aerosol samples for INSEKT INP analysis were also taken for shorter time periods in order to observe the change in INP concentrations from night to day. They were analyzed for a comparison between the two sample locations over the whole campaign. Heat treatment was used on a set of samples, and compared to non-heated samples, in order to gain information on the contribution of biological particles to the ambient INP population.
Comparison of the two measurement methods PINE and INSEKT showed a good agreement for INP concentrations below about 255 K. The PINE instrument tends to measure higher concentrations than INSEKT above a temperature of about 255 K. In conclusion, the two methods

complement each other well and allow observation of the whole temperature range above 242 K. The INP measurements were compared to particle properties as well as meteorological data from the SMEAR II station. At low temperatures, the INP measurements with INSEKT showed a positive correlation to the concentration of particles larger than 2.5 µm measured with APS. The correlation increased for higher temperatures. The INP measurements with INSEKT showed close to no correlation to the concentrations of particles larger than 0.5 µm measured with APS, even slightly negative at higher temperatures. Both results differ to the findings in Kaufmann 2019. The INP measurements with INSEKT also showed a high correlation to the ambient temperature in both locations. The measurements on the tower showed a slightly lower correlation to the ambient temperature. It should also be mentioned that the INP concentrations were measured to be slightly higher at the tower container location than at the PINE container location. The correlations calculated for INSEKT INP measurements with the ambient temperature showed differences during the different phases of the campaign. The highest correlation was observed for measurements in phase 3 (spring). This coincides with the findings of the predecessor campaign HyICE-2018. Measurements during phase 1 (autumn) showed that samples taken during daytime and nighttime show no difference.
Comparison of the samples taken during the different seasons showed a decrease of the INP concentration at temperatures between 255 K and 260 K during winter, which agrees to the seasonal change found by Schneider et al. 2020 for the observed seasons. A comparison of heated aerosol samples to non-heated ones showed a decrease of the ice-active particles in the sample by a factor of 10^1 due to the heat treatment. The decrease of the INP concentrations by heat treatment was larger during winter compared to autumn or spring.
The samples taken during spring showed a large spread in the INP concentrations. The transition from winter (closed snow cover) to spring (no snow cover) was longer compared to the HyICE-2018 campaign, and less steady due to temperatures fluctuating above and below 0 °C from mid-February to late April, along with repeated periods of snow fall and snow melting. Therefore, an increase of the INP concentration with snow melting was still observed, but only for several shorter time periods. During periods above 0 °C, the INP measurements at 257 K with INSEKT showed 10^2fold higher concentrations compared to periods below 0 °C. The PINE instrument showed a 10^1fold change in INP during these occasions.
A seasonal change of the INP concentrations was also observed for the PINE measurements at a temperature of 255 K. This seasonality was clearly visible in a monthly mean analysis with the lowest values during January. The INP concentrations measured with PINE at 255 K showed no significant variation with the season. This indicated that the INPs at lower temperatures are of different type or come from different sources. This needs further measurements and investigation. The INP measurements of both PINE and INSEKT show a good agreement with the air temperature dependent parametrization proposed by Schneider et al. 2021.
The INP concentrations measured with PINE and INSEKT also showed changes during some precipitation events. The relation varied between a decrease of the INP concentration for all nucleation temperatures, a decrease at higher temperatures and an increase at lower temperatures, and occasionally no significant change at all. These may be due to various factors working at the same time, like changes in the air temperature, the snow coverage and the air mass origin related to the precipitation event.
Changes of the INP concentrations connected to meteorological events as well as short term local sources were observed in real time during the campaign. A dust cloud produced by local street maintenance increased INP concentrations by 10^1 for a duration of 1 h on 19th April. An increase of the INP concentrations in connection with decreasing snow depth as well as increasing temperature was observed during three of the days during a case study (18-25th April). The increase was more intense during periods where the temperature increased from below 0 °C to above. Pictures from a webcam showed presence and absence of snow on the tree branches for

two of the events (22nd, 24th). During an event on 21st April, an increase in fluorescent particles measured with WIBS was observed which coincided with an increase of the INP concentration at 249 K, in particular for fluorescence in category A. On 24th April, an increase of fluorescent particles was seen coinciding with the increase in INP at 251 K, in particular for fluorescence in category ABC. Measurements on 22nd April showed an increase of the INP concentrations at 249 K, which was not related to APS nor WIBS measurements. INSEKT INP measurements on this day also showed no strong relation to aerosol measurements. On the 25th April, changes of the INP concentration at 251 K was observed to be in related to changes in the concentration of aerosol particles larger than 2.5 µm, probably caused by an air mass origin change on this day.

5.2. Outlook

Further analysis of the data may bring an improved understanding of the links between the INP sources and concentrations in the Boreal forest with meteorological conditions, aerosol concentrations and types, as well as air mass origin. It should be noted that detailed measurements of the aerosol particle composition with a single particle mass spectrometer were planned for the HyICE-2023 campaign, but were not happening due to unforeseen circumstances. Simultaneous WIBS measurements at the PINE container and the tower container will provide further information on biological aerosols and their relation to the INP abundance. The data analysis and evaluation is still on going. Another experimental improvement as part of this thesis was the simultaneous measurement of the aerosol size distribution with high sensitivity and time resolution directly in the sampling line of the PINE instrument. The data analysis and evaluation of these new measurements are still ongoing and will allow a close and direct correlation of the PINE INP measurements with the aerosol concentration at high time resolution and accuracy. In future campaigns in the boreal forest, both the aerosol concentration and composition should be measured in more detail in order to gain a better understanding and more accurate parameterizations for predicting the INP sources and concentrations in this unique environment close to the polar region.

Appendix A.

First appendix

In the following, the comparison of the data acquired during the different phases of heating, cooling and constant temperature of the PINE instrument are shown in figure A.1 for all campaign measurements. Figure A.2 shows the temperature ramp, scanning temperatures between 257 K and 243 K within about 3.5 h.
As mentioned in the validation of the PINE temperature program (see section 2.1.1), the effect of possible residuals during the heating phase accounts to less than a 10% increase in measured INP concentrations during these compared to cooling phases, at low temperatures, the division between up and down ramp becomes hard, considering the cooling of the walls of the chamber happening slightly faster than then incoming air and reaching the point where up and down ramp change earlier.

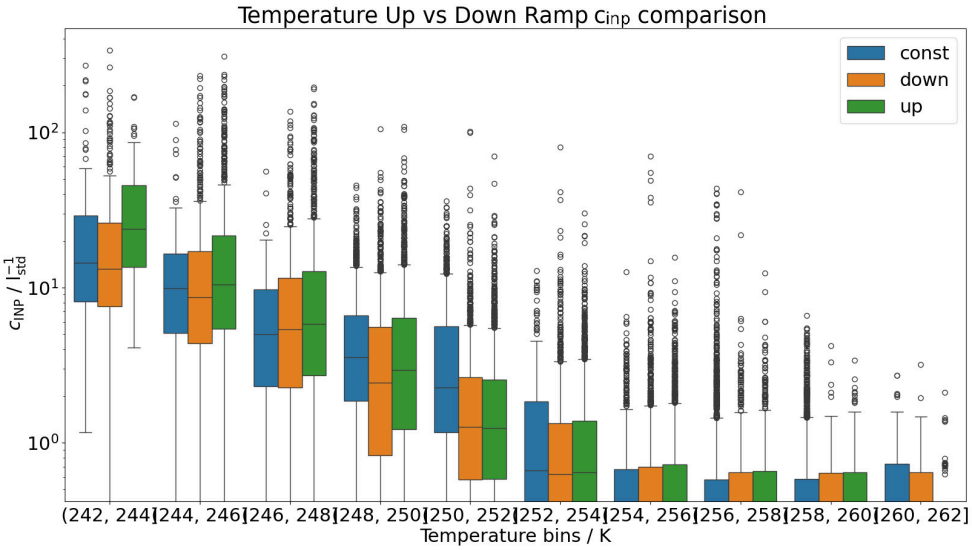

Figure A.1.: Comparison of PINE data created during the constant, cooling (down ramp) and heating (up ramp) phases. The graph shows a comparison of the over all PINE measurements of the HyICE23 campaign.

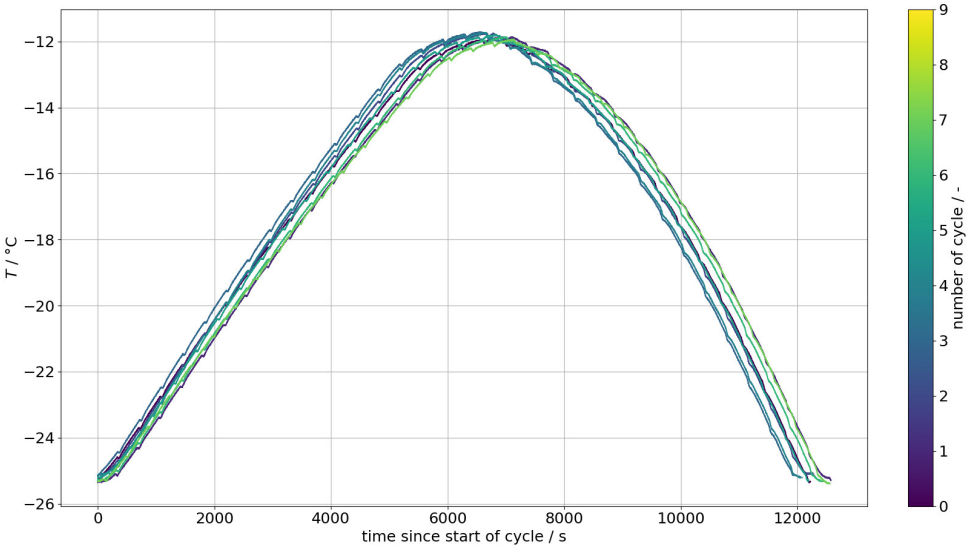

Figure A.2.: Temperature program cycle for short temperature scan. Shown is the temperature measured at the wall at middle height of the chamber. The graph shows cycles scanning the same temperatures between 243 K and 257 K over 3.5 h.

Bibliography

Armstrong, R. (1991). „The influence of climate on the dispersal of lichen soredia“. In: *Environmental and Experimental Botany* 31.2, pp. 239–245. ISSN: 0098-8472. DOI: https://doi.org/10.1016/0098-8472(91)90076-Z.

Augustin, S. et al. (2013). „Immersion freezing of birch pollen washing water“. In: *Atmos. Chem. Phys.* 13.21, pp. 10989–11003. DOI: 10.5194/acp-13-10989-2013.

Barry, K. R. et al. (2021). „Pragmatic protocols for working cleanly when measuring ice nucleating particles“. In: *Atmospheric Research* 250, p. 105419. DOI: 10.1016/j.atmosres.2020.105419.

Bergeron, T. (1935). „On the physics of clouds and precipitation“. In: *Proc. 5th Assembly UGGI, Lisbon, Portugal, 1935*, pp. 156–180.

Böhmländer, A. J. et al. (2024). „A novel aerosol filter sampler for measuring the vertical distribution of ice-nucleating particles via fixed-wing uncrewed aerial vehicles“. In: *Atmospheric Measurement Techniques Discussions* 2024, pp. 1–22. DOI: 10.5194/amt-2024-120.

Boucher, O. (2015). „Atmospheric Aerosols: Properties and Climate Impacts“. In: *Atmospheric aerosols*. Dordrecht: Springer Netherlands. ISBN: 978-94-017-9648-4. DOI: 10.1007/978-94-017-9649-1.

Boucher, O. et al. (2013). „Clouds and Aerosols“. In: *Climate Change 2013: The Physical Science Basis. Contribution of Working Group I to the Fifth Assessment Report of the Intergovernmental Panel on Climate Change*. Ed. by T. Stocker et al. Cambridge, United Kingdom and New York, NY, USA: Cambridge University Press. Chap. 7, pp. 571–658. ISBN: 978-1-107-66182-0. DOI: 10.1017/CBO9781107415324.016.

Brasseur, Z. et al. (2022). „Measurement report: Introduction to the HyICE-2018 campaign for measurements of ice-nucleating particles and instrument inter-comparison in the Hyytiälä boreal forest“. In: *Atmospheric Chemistry and Physics* 22.8, pp. 5117–5145. DOI: 10.5194/acp-22-5117-2022.

Burrows, S. M. et al. (2022). „Ice-Nucleating Particles That Impact Clouds and Climate: Observational and Modeling Research Needs“. In: *Reviews of Geophysics* 60.2. e2021RG000745 2021RG000745, e2021RG000745. DOI: https://doi.org/10.1029/2021RG000745. eprint: https://agupubs.onlinelibrary.wiley.com/doi/pdf/10.1029/2021RG000745.

C.E. Morris, D.G. Georgakopoulos, and D.C. Sands (2004). „Ice nucleation active bacteria and their potential role in precipitation“. In: *J. Phys. IV France* 121, pp. 87–103. DOI: 10.1051/jp4:2004121004.

Christner, B. C., C. E. Morris, C. M. Foreman, R. Cai, and D. C. Sands (2008). „Ubiquity of Biological Ice Nucleators in Snowfall“. In: *Science* 319.5867, pp. 1214–1214. DOI: 10.1126/

science . 1149757. eprint: https : / / www . science . org / doi / pdf / 10 . 1126 / science . 1149757.

Climate Change (IPCC), I. P. on (2023). *Climate Change 2021 – The Physical Science Basis: Working Group I Contribution to the Sixth Assessment Report of the Intergovernmental Panel on Climate Change*. Cambridge University Press.

Creamean, J. M. et al. (2013). „Dust and Biological Aerosols from the Sahara and Asia Influence Precipitation in the Western U.S“. In: *Science* 339.6127, pp. 1572–1578. DOI: 10.1126/science.1227279.

Cziczo, D. J. et al. (2013). „Clarifying the Dominant Sources and Mechanisms of Cirrus Cloud Formation“. In: *Science* 340, pp. 1320–1324. DOI: 10.1126/science.1234145.

DeMott, P. J. et al. (2010). „Predicting global atmospheric ice nuclei distributions and their impacts on climate“. In: *Proceedings of the National Academy of Sciences* 107.25, pp. 11217–11222. DOI: 10.1073/pnas.0910818107.

Engström, A., F. A.-M. Bender, R. J. Charlson, and R. Wood (2015). „The nonlinear relationship between albedo and cloud fraction on near-global, monthly mean scale in observations and in the CMIP5 model ensemble“. In: *Geophysical Research Letters* 42.21, pp. 9571–9578. DOI: 10.1002/2015gl066275.

Field, P. R. et al. (2017). „Secondary Ice Production: Current State of the Science and Recommendations for the Future“. In: *Meteorological Monographs* 58, pp. 71–720. DOI: 10.1175/amsmonographs-d-16-0014.1.

Findeisen, W. (1938). „Kolloid-meteorologische Vorgänge bei Niederschlagsbildung“. In: *(No Title)* 55, p. 121.

Gratzl, J., T. M. Seifried, D. Stolzenburg, and H. Grothe (2023). *A fluorescence approach for an online measurement technique of atmospheric microplastics*. DOI: 10.26434/chemrxiv-2023-qzhr8.

Hader, J. D., T. P. Wright, and M. D. Petters (2014). „Contribution of pollen to atmospheric ice nuclei concentrations“. In: *Atmospheric Chemistry and Physics* 14.11, pp. 5433–5449. DOI: 10.5194/acp-14-5433-2014.

Hari, P. and M. Kulmala (2005). „Station for Measuring Ecosystem-Atmosphere Relations (SMEAR II)“. English. In: *Boreal Environment Research* 10.5, pp. 315–322. ISSN: 1239-6095.

Harrison, A. D. et al. (2018). „An instrument for quantifying heterogeneous ice nucleation in multiwell plates using infrared emissions to detect freezing“. In: *Atmospheric Measurement Techniques* 11.10, pp. 5629–5641. DOI: 10.5194/amt-11-5629-2018.

Hill, T. C. J. et al. (2016). „Sources of organic ice nucleating particles in soils“. In: DOI: 10.5194/acp-2016-1.

Hill, T. C. J. et al. (2013). „Measurement of Ice Nucleation-Active Bacteria on Plants and in Precipitation by Quantitative PCR“. In: *Applied and Environmental Microbiology* 80.4, pp. 1256–1267. DOI: 10.1128/aem.02967-13.

Hinds, W. (1999). *Aerosol technology : properties, behavior, and measurement of airborne particles*. New York: Wiley. ISBN: 9780471194101.

Junninen, H. et al. (2009). „Smart-SMEAR: on-line data exploration and visualization tool for SMEAR stations“. English. In: *Boreal Environment Research* 14, pp. 447–457. ISSN: 1239-6095.

Kanji, Z. A. et al. (2017). „Overview of Ice Nucleating Particles“. In: *Meteorological Monograophs* 58, pp. 11–133. DOI: 10.1175/amsmonographs-d-16-0006.1.

Kaufmann, J. (2019). „Long-term Measurements of Ice Nucleating Particles in a Boreal Forest during the Winter to Spring Transition“. MA thesis. Karlsruhe Institute of Technology.

Keinert, A., D. Spannagel, T. Leisner, and A. Kiselev (2020). „Secondary Ice Production upon Freezing of Freely Falling Drizzle Droplets“. In: *Journal of the Atmospheric Sciences* 77.8, pp. 2959–2967. DOI: 10.1175/JAS-D-20-0081.1.

Knopf, D. A., P. A. Alpert, and B. Wang (2018). „The Role of Organic Aerosol in Atmospheric Ice Nucleation: A Review“. In: *ACS Earth and Space Chemistry* 2.3, pp. 168–202. DOI: 10.1021/acsearthspacechem.7b00120. eprint: https://doi.org/10.1021/acsearthspacechem.7b00120.

Koop, T., B. Luo, A. Tsias, and T. Peter (2000). „Water activity as the determinant for homogeneous ice nucleation in aqueous solutions“. In: *Nature* 406.6796, pp. 611–614. ISSN: 0028-0836. DOI: 10.1038/35020537.

Leonhard, T. (2024). *Measurements of Ice-Nucleating Particle Concentrations during the Snow Melting Season in the Boreal Forest in Finland*. BachelorThesis.

Lohmann, U., F. Lüönd, and F. Mahrt (2016). *An Introduction to Clouds: From the Microscale to Climate*. Cambridge: Cambridge University Press. ISBN: 9781139087513.

Lynch, D. et al. (2002). „Cirrus: The Future“. In: Oxford Univ. Press, pp. 449–455. ISBN: 0-19-513072-3. DOI: 10.1093/oso/9780195130720.003.0025.

Marshall, W. A. (1996). „Aerial dispersal of lichen soredia in the maritime Antarctic“. In: *New Phytologist* 134.3, pp. 523–530. DOI: https://doi.org/10.1111/j.1469-8137.1996.tb04370.x. eprint: https://nph.onlinelibrary.wiley.com/doi/pdf/10.1111/j.1469-8137.1996.tb04370.x.

McCoy, D. T., D. L. Hartmann, and M. D. Zelinka (2018). „Mixed-Phase Cloud Feedbacks“. In: *Mixed-Phase Clouds*. Elsevier, pp. 215–236. DOI: 10.1016/b978-0-12-810549-8.00009-x.

Moffett, B., G. Getti, S. Henderson-Begg, and T. Hill (2015). „Ubiquity of ice nucleation in lichen ' possible atmospheric implications“. In: *Lindbergia* 38, pp. 39–43. DOI: 10.25227/linbg.01070.

Möhler, O., P. J. DeMott, G. Vali, and Z. Levin (2007). „Microbiology and atmospheric processes: the role of biological particles in cloud physics“. In: *Biogeosciences* 4.6, pp. 1059–1071. DOI: 10.5194/bg-4-1059-2007.

Möhler, O. et al. (2021). „The Portable Ice Nucleation Experiment (PINE): a new online instrument for laboratory studies and automated long-term field observations of ice-nucleating particles“. In: *Atmospheric Measurement Techniques* 14.2, pp. 1143–1166. DOI: 10.5194/amt-14-1143-2021.

Mueller, R., J. Trentmann, C. Träger-Chatterjee, R. Posselt, and R. Stöckli (2011). „The Role of the Effective Cloud Albedo for Climate Monitoring and Analysis“. In: *Remote Sensing* 3.11, pp. 2305–2320. DOI: 10.3390/rs3112305.

Mülmenstädt, J., O. Sourdeval, J. Delanoë, and J. Quaas (2015). „Frequency of occurrence of rain from liquid-, mixed-, and ice-phase clouds derived from A-Train satellite retrievals“. In: *Geophys. Res. Lett.* 42.15, pp. 6502–6509. ISSN: 1944-8007. DOI: 10.1002/2015GL064604.

Murray, B. J., K. S. Carslaw, and P. R. Field (2021). „Opinion: Cloud-phase climate feedback and the importance of ice-nucleating particles“. In: *Atmospheric Chemistry and Physics* 21.2, pp. 665–679. DOI: 10.5194/acp-21-665-2021.

Murray, B. J., D. O'Sullivan, J. D. Atkinson, and M. E. Webb (2012). „Ice nucleation by particles immersed in supercooled cloud droplets“. In: *Chemical Society Reviews* 41.19, p. 6519. ISSN: 0306-0012. DOI: 10.1039/c2cs35200a.

O'Sullivan, D. et al. (2015). „The relevance of nanoscale biological fragments for ice nucleation in clouds“. In: *Sci. Rep.* 5, p. 8082. ISSN: 2045-2322. DOI: 10.1038/srep08082.

O'Sullivan, D. et al. (2018). „Contributions of biogenic material to the atmospheric ice-nucleating particle population in North Western Europe“. In: *Scientific Reports* 8.1, p. 13821. ISSN: 2045-2322. DOI: 10.1038/s41598-018-31981-7.

OpenStreetMap contributors (2017). *Planet dump retrieved from https://planet.osm.org*. https://www.openstreetmap.org.

Perlwitz, J., D. Knopf, and R. Miller (2020). „Comparison of INP Parameterizations for Dust Minerals in Climatological Simulations With a Global Model“. In: DOI: 10.5194/egusphere-egu2020-13437.

Perring, A. E. et al. (2015). „Airborne observations of regional variation in fluorescent aerosol across the United States“. In: *Journal of Geophysical Research: Atmospheres* 120.3, pp. 1153–1170. DOI: https://doi.org/10.1002/2014JD022495. eprint: https://agupubs.onlinelibrary.wiley.com/doi/pdf/10.1002/2014JD022495.

Pratt, K. A. et al. (2009). „In situ detection of biological particles in cloud ice-crystals“. In: *Nature Geoscience* 2, p. 398. DOI: 10.1038/ngeo521.

Proske, U. et al. (2024). „Measurement report: The ice-nucleating activity of lichen sampled in a northern European boreal forest“. In: *EGUsphere* 2024, pp. 1–22. DOI: 10.5194/egusphere-2023-2780.

Pruppacher, H. and J. Klett (2010). „Microstructure of Atmospheric Clouds and Precipitation“. In: *Microphysics of Clouds and Precipitation*. Dordrecht: Springer Netherlands, pp. 10–73. ISBN: 978-0-306-48100-0. DOI: 10.1007/978-0-306-48100-0_2.

Rosenfeld, D. and W. L. Woodley (2000). „Deep convective clouds with sustained supercooled liquid water down to -37.5 °C“. In: *Nature* 405.6785, pp. 440–442. ISSN: 1476-4687. DOI: 10.1038/35013030.

Savage, N. J. et al. (2017). „Systematic characterization and fluorescence threshold strategies for the wideband integrated bioaerosol sensor (WIBS) using size-resolved biological and interfering particles“. In: *Atmospheric Measurement Techniques* 10.11, pp. 4279–4302. DOI: 10.5194/amt-10-4279-2017.

Schaefer, V. J. (1946). „The Production of Ice Crystals in a Cloud of Supercooled Water Droplets“. In: *Science* 104.2707, pp. 457–459. DOI: 10.1126/science.104.2707.457.

Schiebel, T. (2017). „Ice Nucleation Activity of Soil Dust Aerosols“. en. Ph.D. thesis. Karlsruhe Institute of Technology. DOI: 10.5445/ir/1000076327.

Schneider, J. et al. (2021). „The seasonal cycle of ice-nucleating particles linked to the abundance of biogenic aerosol in boreal forests“. In: *Atmospheric Chemistry and Physics* 21.5, pp. 3899–3918. DOI: 10.5194/acp-21-3899-2021.

Schneider, J. et al. (2020). „The seasonal cycle of ice-nucleating particles linked to the abundance of biogenic aerosol in boreal forests“. In: DOI: 10.5194/acp-2020-683.

Schnell, R. C. and G. Vali (1973). „World-wide Source of Leaf-derived Freezing Nuclei“. In: *Nature* 246.5430, pp. 212–213. ISSN: 1476-4687. DOI: 10.1038/246212a0.

Seinfeld, J. H. and S. N. Pandis (2016). *Atmospheric chemistry and physics: from air pollution to climate change*. John Wiley & Sons. ISBN: 1118947401.

Sogacheva, L. et al. (2008). „New aerosol particle formation in different synoptic situations at Hyytiala, Southern Finland“. English. In: *Tellus Series B: Chemical and Physical Meteorology* 60.4. Contribution: organisation=fys,FACT1=1
Publisher name: Wiley-Blackwell Publishing, Inc.; Svenska Geofysiska Foerening, pp. 485–494. ISSN: 0280-6509. DOI: 10.1111/j.1600-0889.2008.00364.x.

Stein, A. F. et al. (2015). „NOAA's HYSPLIT Atmospheric Transport and Dispersion Modeling System“. In: *Bull. Am. Meteorol. Soc.* 96.12, pp. 2059–2077. DOI: 10.1175/bams-d-14-00110.1.

Storelvmo, T., C. Hoose, and P. Eriksson (2011). „Global modeling of mixed-phase clouds: The albedo and lifetime effects of aerosols“. In: *Journal of Geophysical Research* 116.D5. DOI: 10.1029/2010jd014724.

Sun, Z. and K. P. Shine (1994). „Studies of the radiative properties of ice and mixed-phase clouds“. In: *Quarterly Journal of the Royal Meteorological Society* 120.515, pp. 111–137. DOI: 10.1002/qj.49712051508.

Trueblood, J. V. et al. (2020). „A Two-Component Parameterization of Marine Ice Nucleating Particles Based on Seawater Biology and Sea Spray Aerosol Measurements in the Mediterranean Sea“. In: DOI: 10.5194/acp-2020-487.

Tucker, K. R. et al. (2018). „Ice Nucleation Measurements and Parameterizations“. In: *AGU Fall Meeting Abstracts*. Vol. 2018, A11L-2418, A11L–2418.

Tunved, P. et al. (2003). „One year boundary layer aerosol size distribution data from five nordic background stations“. In: *Atmos. Chem. Phys.* 3.6, pp. 2183–2205. ISSN: 1680-7324. DOI: 10.5194/acp-3-2183-2003.

Vali, G., P. J. DeMott, O. Möhler, and T. F. Whale (2015). „Technical Note: A proposal for ice nucleation terminology“. In: *Atmos. Chem. Phys.* 15.18, pp. 10263–10270. DOI: 10.5194/acp-15-10263-2015.

Vali, G. (1971). „Quantitative Evaluation of Experimental Results an the Heterogeneous Freezing Nucleation of Supercooled Liquids“. In: *Journal of Atmospheric Sciences* 28.3, pp. 402–409. DOI: 10.1175/1520-0469(1971)028<0402:QEOERA>2.0.CO;2.

Vogel, F. et al. (2024). „Ice-nucleating particles active below −24 C in a Finnish boreal forest and their relationship to bioaerosols“. In: *EGUsphere* 2024, pp. 1–25. DOI: 10.5194/egusphere-2024-853.

Wegener, A. (1911). *Thermodynamik der atmosphäre*. JA Barth.

Acknowledgements

At first, I would like to thank Prof. Dr. Thomas Leisner for being the first referent of this thesis and for giving me the opportunity to do my Master's thesis at IMK-AAF. He is also responsible for the LabView software of the INSEKT analysis.
I would also like to thank Prof. Dr. Corinna Hoose for taking over the part of the second referent, and for the helpful discussion we had accompanied with her great interest in the topic.
I thank my supervisor Dr. Ottmar Möhler for giving me the opportunity to work on such an exciting topic and for giving me the chance to take part in the HyICE23 field campaign, he was always open for questions and scientific discussions, which have benefited this thesis. I learned a lot on scientific working thanks to many insights he gave me. He provided me with opportunities to get in contact with scientists on an international level which opened up my field of view by a lot.
Furthermore, I want to thank the whole IMK-AAF, especially the AG Möhler, for the nice working atmosphere and for including me in the team. Special thanks goes to the technical staff for helping me with every technical issue and with general handling and transport of the instruments. Thanks to Susanne Bolz for all the organisational stuff.
I would like to thank Franziska Vogel for introducing me to the PINE instrument and INSEKT. Special thanks to Alexander Böhmländer, who gave me helpful advice and for helping me greatly, also with issues revolving PINE and INSEKT over the duration of the campaign, as well as accompanying me at the start of the campaign to ensure proper setup. He also provided the python programs for INSEKT calculations. I would also like to thank Nicole Büttner for providing the python program used for the calculation of the PINE data.
Thanks to Olga Dombrowski for providing and preparing the material (including filters) used for INSEKT, as well as helping during and with the analysis of samples.
I would like to thank Tobias Leonhard, who took over a part of the filter sampling and analysis during phase 3 as part of his Bachelor's thesis.
I would like to thank Prof. Dr. Tuukka Petäjä and his team from Helsinki University for organizing the campaign, giving me the opportunity to perform measurements in Hyytiälä and for the financial support through the European project ATMO-ACCESS. Thanks to the technicians at the SMEAR II station for helping us with the set-up and shipping of our instruments and for the nice working atmosphere in Hyytiälä. Thanks to the SMEAR II staff for providing the meteorological and aerosol data from the station as well as taking over the filter sampling during phase 2, a special thanks to Matti Loponen and Sirpa Rantanen regarding this. Thanks to Lauri R. Ahonen and Pauliina Schiestl-Aalto for many helpful discussions, organisation, as well as help during the measurements and setup of the instruments. Thanks to Hanna-Mari Uusi-Piuhari for all the organisational stuff regarding our stay in Hyytiälä.
I would like to thank Hinrich Grothe and his team at University of Vienna for providing the WIBS in the PINE container during the campaign. A special thanks to Jürgen Gratzl for many interesting discussions, and providing the WIBS data used in this thesis. I would like to thank Jorma Keskinen for providing the WIBS used on the Tower container and Eetu Naukkarinen for providing the data, which will be used in future analysis of the campaign data.

I would also like to thank Daniel Cziczo and his team who unfortunately could not take part in the measurements with their PALMS-NG but still worked with us on planning and ideas on connections between INP and particle properties.
Lastly I would like to thank my family for supporting me for my whole studies as well as during the stay in Hyytiälä.